Finite-size scaling of ^{4}He at the superfluid transition

Francis M. Gasparini,* Mark O. Kimball,† Kevin P. Mooney, and Manuel Diaz-Avila‡

Department of Physics, University at Buffalo, The State University of New York, Buffalo, New York 14260-1500, USA

(Published 4 September 2008; corrected 15 September 2008)

Experimental results for confined ^{4}He are reviewed that are relevant to correlation-length scaling near the superfluid transition. Data are discussed for which the uniform confinement represents dimensionality crossover from three dimensions (3D) to 2D, 1D, and 0D. In addition, data for the onset of superfluidity are discussed representing 2D to 1D crossover. Collectively, these data for the specific heat, superfluid density, and thermal conductivity yield, in some cases, excellent agreement with expectations of correlation-length scaling and, in others, surprising disagreement. This is especially true in the case of 3D to 2D crossover where data are most plentiful. Here there is a clear distinction between scaling when the confined helium is normal and the lack of scaling when helium becomes superfluid. By far the most problematic result is the lack of scaling for the superfluid density for 3D to 2D crossover and, to some extent, for 3D to 1D crossover. Connectivity and proximity effects can be identified with some data. These might explain some experimental results and present opportunities for further studies of weakly coupled superfluid regions. Measurements to test the universality of finite-size effects along the superfluid transition lines as function of pressure and ^{3}He concentration are also discussed. In the case of the specific heat, data indicate that the nonuniversal behavior of the critical exponent α, obtained from bulk measurements, is responsible for the observation of a distinct scaling locus for confined pure ^{4}He versus that of the confined mixtures.

DOI: 10.1103/RevModPhys.80.1009 PACS number(s): 67.25.bh, 67.60.gj

CONTENTS

*fmg@buffalo.edu
†mok2@buffalo.edu
‡http://enthalpy.physics.buffalo.edu

PRELUDE

Over the last two decades there has been substantial experimental and theoretical progress in understanding the behavior of uniformly confined ^{4}He in the critical region near the superfluid transition. Examined from the point of view of correlation-length scaling, the picture emerging from these data is that, along with remarkable successes, there are also notable failures that remain unexplained. Experimental studies have been done for confined helium with crossover dimensions of 2, 1, and 0. Some data are also available for crossover of two-dimensional (2D) to 1D films. Studies have also been done in which the expected universal behavior of finite-size scaling has been investigated when the superfluid transition temperature is changed due to pressure or ^{3}He concentration. We preview the principal results of all these studies.

By far the most extensive data available are for the specific heat of helium confined in a film geometry. This represents crossover from three to two dimensions. Data spanning a factor of over 1000 in film thickness have been obtained. Above the bulk superfluid transition temperature T_λ, the specific heat of these planar films collapses as predicted onto a universal scaling locus

when scaled with the ratio L/ξ, the thickness divided by the correlation length. This scaling locus can be analyzed to obtain the value of the correlation-length critical exponent ν. This value agrees with determinations of ν from bulk experiments and theories. Further, these data yield the correct behavior in the temperature region of the scaling function where the surface specific heat dominates the deviation from bulk behavior. Data in this region also agree with a theoretical calculation for the magnitude of the surface specific heat. These sets of results are unique for a system at a continuous transition and represent strong evidence for correlation-length scaling. Below T_λ, these data also collapse onto a scaling locus until the temperature region reaches close to the maximum of their specific heat. Here the data do not scale and show a systematic deviation with confinement size. This behavior persists into the region where the film becomes superfluid. Single-point scaling of the shift in the temperature of the specific-heat maximum, the value of the specific heat at T_λ, and the onset temperature of superfluid behavior are all consistent with the expected power-law behaviors and expected exponents. What is not consistent is the behavior of the *magnitude* of the specific-heat maximum as a function of confinement size. This, however, agrees with and confirms the observation that the overall scaling fails in the region of the maximum.

Specific-heat data for helium confined in pores and channels, representing a 3D to 1D crossover, are not as extensive as for films. The older data for helium confined in pores of Nuclepore filters show features that indicate a uniqueness to this confinement which distinguishes them, and hence their scaling locus, from the more recent measurements. The three most recent sets of data utilize confinements with much improved uniformity. They cover a factor of about 30 in the small dimension and show good scaling for temperatures above T_λ, a lack of scaling near the maximum (but not systematic with size as seen in the planar film data), and reasonable scaling into the superfluid side. It does not seem likely that the lack of scaling near the maximum reflects the same physics as observed for the 2D crossover.

There are two sets of specific-heat data for helium confined in all three dimensions, representing crossover to zero dimensions. With the addition of these data, one can make a comparison of the specific-heat crossover behavior for all three lower dimensions at the same small confinement. One finds an evolution of behavior as fluctuations are quenched in one, two, or all three dimensions. A plot of the shift in the temperature of the specific-heat maximum with size for all three dimensionality crossovers is consistent with scaling and shows a greater shift with decreasing lower dimension. However, closer examination of the 0D data with respect to scaling over the full temperature range shows that there are effects that may be attributed to coupling among the regions of 0D confinement as realized experimentally. This effect—the coupling of regions of superfluids—is of interest as an analog of Josephson coupling in superconducting arrays, but is somewhat outside the main interest of correlation-length scaling.

The superfluid density is problematic for both 2D and 1D crossovers. It is observed that data for 2D films, which vary by a factor of about 80 in the confining dimension, do not scale. It is also observed that data that cannot be scaled with size due to the uniqueness of their confinement also do not behave as expected in the *surface region*, where a simple power law is expected. This failure of scaling for the superfluid density is the counterpart of the failure of the specific heat for 2D crossover in the region of the maximum and below. Thus, at least experimentally, these two observations are consistent. Data for the shift of superfluid onset—which is always at a lower temperature than the specific-heat maximum—are consistent with correlation-length scaling. This agrees with the specific-heat results, where the shift of the temperature of the maximum is also consistent with scaling. This reaffirms the observations from the specific heat whereby, for the same data, there are features that scale properly and other features that do not.

Data for the superfluid density for 1D crossover are not as plentiful as for 2D crossover. However, these also indicate a lack of scaling. The single-point determination of the temperature shift of superfluid onset with size for 1D crossover, from a variety of experiments, is found to be consistent with the exponent of the correlation length. Thus, as for the specific heat, it is found that single-point features behave as expected, but there is failure of overall scaling.

Data for thermal conductivity have been obtained in a planar geometry where surface effects can be extracted; and, in a cylindrical geometry, for two different size pores, where scaling with size can be checked. It is found that the surface effects from the planar geometries do not scale. For the cylindrical geometry—with a factor of 2 variation in size—it is found that the thermal conductivity scales for temperatures greater than T_λ, but there is evidence of a lack of scaling below T_λ.

It is expected that films of helium with a free surface will change thickness near the superfluid transition. This is a manifestation of the Casimir effect in a thermodynamic system. Measurements of film thickness over a factor of 1.3 in size show good collapse on a universal locus as expected from correlation-length scaling. The location of the minimum in the film thickness falls on the same locus as the location of the maximum in the specific heat. One might have expected this on the basis that, for both measurements, this point represents the maximum in the thermodynamic fluctuations. We also note that there is a structure in the thinning of the film that coincides with, and scales on the same locus as, the onset of superfluidity.

Universality of finite-size effects has been studied for the specific heat as a function of ^{3}He concentration and, in the case of the thermal conductivity, as a function of pressure. For the specific heat it is found, most clearly for temperatures above T_λ, that all mixtures by themselves collapse on a universal locus. This, however, is

different from the locus for pure ^{4}He. This is true for both 2D and 1D crossovers. The striking difference in scaling loci is a reflection of the variation of the specific-heat critical exponent as one moves away from the thermodynamic point of saturated vapor pressure and zero ^{3}He concentration. It is thus a problem more with the bulk behavior concerning universality rather than with the confined system. It is interesting that the scaling of the confined specific heat is more sensitive to variations in the specific-heat critical exponent than for the bulk system.

Finally, the thermal conductivity for 1D crossover, when measured as a function of pressure, shows universal behavior for temperatures greater than T_λ, but demonstrates a lack of universality for temperatures below. This is quite different from the specific heat, where the lack of universality is not principally an issue of being above or below the bulk transition, but rather a behavior issue of the bulk exponent describing the specific heat in the critical region.

I. INTRODUCTION

A. Background and general remarks

The concept of the thermodynamic limit plays an important role in thermodynamics and statistical mechanics. It allows one to consider properties of a system which, when taken per particle or per unit volume, are independent of the sample size. Formally, one can say that it is the limit in which both the number of particles N and the volume V become very large (strictly infinite) but the ratio N/V remains finite. In practice this means that the dimensions of the sample are much larger than any length scale relevant to a thermodynamic response. In this limit, for what one might call a bulk sample, the detailed shape of the sample is irrelevant and need not be specified unless one performs a surface-specific type of measurement. In most circumstances the relevant length scale might be quite small, of the order of the interatomic dimensions. However, it is not uncommon that the phase diagram of a substance will have a special point or locus of points—a line or a surface—at which the system undergoes a continuous phase transition. This type of transition is one where the first derivatives of the free energy are continuous, but the second derivative has a singularity. Such a transition is marked by the appearance, below the transition temperature T_c, of a new lower symmetry phase than the high-temperature phase, and the appearance of an order parameter which might be a scalar or a vector quantity. The transition temperature is also marked by singularities in some thermodynamic responses near T_c, and by the divergence at T_c of the correlation length ξ. This length is associated with the spatial extent of correlated fluctuations in the relevant density. This might be, for instance, the mass density at a liquid-gas critical point, or the magnetization per unit volume in the case of magnetic ordering. In the case of exponentially decaying correlations, ξ may be defined as the second moment of the correlation function (see, for instance, Baker, 1990). In the case of helium, where the ordered state is characterized by a wave function and is hence analogous to a two-component (XY) magnetic system, one can define two correlation lengths, transverse and longitudinal (see, for instance, Privman *et al.*, 1991). This designation refers to correlations along the direction of a vector order parameter or in directions transverse to it. For superfluid helium, the transverse correlation length is relevant below the transition and is related to the superfluid density. Both transverse and longitudinal correlation lengths diverge at T_λ with the same critical exponent. This is a requirement of scaling (see, for instance, Privman *et al.*, 1991). It is evident now that with such a divergent length scale one might be concerned about achieving a true thermodynamic limit. Put another way, even for normally large systems, if one has the temperature resolution to make measurements close to T_c, one should see a modification of behavior from that expected in the thermodynamic limit.

There are several manifestations of finite-size behavior. Any response that is singular in the bulk limit will no longer be so, but will exhibit a finite maximum with a pronounced rounding as the transition region is approached. No true critical behavior is expected, unless, as in the case of a film of thickness L, the system displays critical behavior in two dimensions. In this case a crossover from three to two dimensions can be expected as one approaches the transition from either the high- or low-temperature side and $\xi \simeq L$. While a finite system will typically have no true criticality, there will be a marker, such as the maximum in the specific heat, or the temperature of onset of the ordered phase, that can be thought of as a shifted transition temperature $T_c(L)$. This temperature should approach the bulk T_c and the thermodynamic response to its bulk behavior, in the limit that, in the temperature range accessible experimentally, one has $\xi \ll L \sim \infty$.

One might try to understand the modification of behavior from the bulk limit by considering a hierarchy of corrections stemming from the topology of the sample, i.e., corners, edges, surfaces—features that are irrelevant in the thermodynamic limit. In this spirit, one may write for the singular part of the free energy

$$F \simeq Nf_\infty + N_s f_s + N_e f_e + N_c f_c + \cdots, \tag{1}$$

where the subscripts ∞, s, e, and c refer, respectively, in either the number of particles N or the free energy per particle f, to the infinite system (the bulk sample), and to surfaces, edges, and corners of the finite system. This might be confined to a small spatial dimension L, such as a film of thickness L, a long channel of cross section $L \times L$, or a box $L \times L \times L$. The earliest sources that we are aware of that use this formulation to include a surface contribution are Fisher and Ferdinand (1967) and Ferdinand and Fisher (1969). The review by Privman (1990) expands this to include edges and corners, and qualifies these terms as having been shown to apply to systems with no soft modes. This might then be prob-

lematic in the case for helium on the superfluid side of the transition.

Some of the terms in F might well be zero, such as in a sphere where there are no edges or corners. While such an expression might well be a reasonable "perturbative" expansion of the free energy, it should be clear that it cannot hold over the full range of the thermodynamic response. Specifically, the function F will have no singularity at the transition—except the case where critical behavior persists into the lower dimension. Thus, since f_∞ is singular at T_c and F is not, the additional terms cannot correct f_∞ to yield a nonsingular result. Hence such an expression for f would be applicable only away from T_c in the region where the ratio of ξ/L is small. Further, if one considers a finite system in which periodic boundary conditions exist, one would expect the leading deviation from bulk behavior to become exponentially small as $\sim e^{-L/\xi}$ [this was first suggested by Ferdinand and Fisher (1969), and later by Barber (1973, 1977) and Barber and Fisher (1973)]. It has been found recently that in the region for $T > T_c$, and $L/\xi \gg 1$, and for periodic boundary conditions on a lattice system of finite size L, scaling fails when the correlation length ξ, defined as the second moment of the order-parameter correlation function, is used. It was suggested that finite-size scaling is restored if the correlation length ξ_1, the so-called exponential correlation length introduced by Fisher and Burford (1967) is used (Chen and Dohm, 1999, 2000). However, this has turned out not to be so (Dohm, 2008).

A description of a finite system that is not limited to small values of ξ/L was suggested by Fisher (1971) and Fisher and Barber (1972). This is based on the ansatz that the finite system should be describable by the same critical exponents as the bulk. This finite-size scaling ansatz has subsequently been shown to be derivable from renormalization-group considerations (Nightingale, 1976; Suzuki, 1977; Brézin, 1982; see also Barber, 1983). One may also view finite-size scaling as an application of renormalization-group theory (Blöte and Nightingale, 1982). Implicit in the renormalization group approach is the fact that the same universality which appears in the bulk system will also be manifest in the finite system (Barber, 1983). Privman and Fisher (1984) have argued that within a given geometry of confinement one needs only two metric factors for the singular part of the free energy of the confined system: one associated with the temperature, the other with the ordering field. They argued that there is no additional system-dependent multiplicative factor necessary.

The finite-size scaling ansatz states that, under suitable conditions (barring, for instance, ordering fields associated with boundaries), the finite system will be described by scaling functions which depend only on the ratio L/ξ. In this theory of correlation-length finite-size scaling, data for samples of different L will collapse on a universal locus which depends on the crossover dimension, i.e., on how many spatial dimensions are made small, and will differ for each universality class. This class, for a continuous transition, is determined by the dimensionality of the bulk system and the vector character, or number of components, of the order parameter. The latter is the quantity that is zero above T_c and nonzero below. One may think, for example, of the magnetization in a magnetic system, the difference in the density from the critical density in a liquid-gas system, or, in the case of a superfluid like ^{4}He, a wave function which has two degrees of freedom: magnitude and phase. Last, the scaling functions also differ for different boundary conditions on the order parameter, and, if relevant, sample anisotropy (Chen and Dohm, 2004; Selke and Shchur, 2005). The scaling of the finite system with the bulk correlation length ξ implies that no new critical scale is introduced when the system is confined to a small dimension L. This makes the predicted scaling a powerful tool in extrapolating theoretical calculations of finite systems to the thermodynamic limit [see, for instance, Nightingale (1976) and also various references in Cardy (1988)].

Experimental verification of finite-size scaling presents several difficulties. One must deal with samples that are small: the correlation length might be of the order of micrometers at $t \equiv |1 - T/T_c| \sim 10^{-6}$. The ability to distinguish finite-size effects in any sample depends on the temperature resolution, the accuracy of the measurement itself, and the accuracy with which the corresponding bulk property is known. Strictly speaking, any sample one measures is finite, but this is typically not reflected in a measured property because of limited resolution. To verify finite-size effects and scaling, one must study samples in which one or more small dimensions are varied systematically over a range of L. High-resolution measurements of such small samples represent a challenge unless one can realize an ensemble of such systems. In this case, each replica in the ensemble must be made identical to all others. Further, for finite systems one must be aware that boundary conditions are important. Thus, the method of confinement of the small system is relevant. The boundaries should not influence the order parameter other than in providing a termination. A trivial example is that it would be inappropriate to study finite-size effects on a magnetic film if it were formed on a magnetic substrate. In the case of a critical liquid-gas system, the van der Waals influence at the walls will affect the density directly. More subtle effects are also possible. The substrate for a solid film might provide a volume constraint on the film formed on it which would modify the thermodynamic path toward criticality (Lutz *et al.*, 1978). Having said this, one notes that finite-size effects can be seen in many realizations of small systems, even when the confinement is not homogeneous. However, it is nearly impossible with such systems to verify scaling because they involve multiple length scales. Such samples order locally over a range of temperatures which reflect the spread in confinement characteristics. Thus, a given thermodynamic response cannot be uniquely ascribed to a single small dimension L.

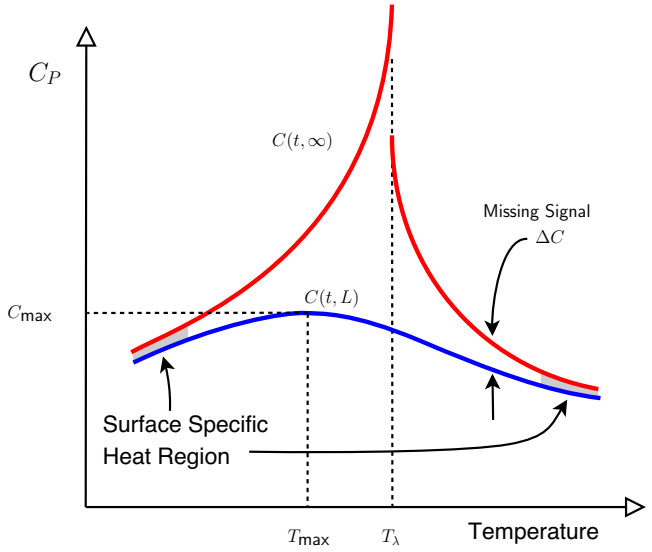

FIG. 1. (Color online) Sketch showing the qualitative difference between the specific heat at constant pressure of bulk $C(t,\infty)$ and confined helium $C(t,L)$.

Liquid helium at the superfluid transition, $T_\lambda = 2.1768$ K (Magnum and Furukawa, 1990), has a number of advantages for the study of finite-size effects. The most important of these is the fact that the order parameter is a wave function. Thus the walls of a container do not influence the order parameter in a critical way. To be sure, the walls do provide more than just a termination, since the van der Waals attraction will influence the transition due to the local variation of the pressure P, and T_λ is a function of P. However, this effect is not large; in some cases it can be estimated, and, if not, it can become negligible relative to the total sample as L becomes large. The realization of small samples is easy for helium because it wets, with some exceptions (Cheng *et al.*, 1991; Nacher and Dupont-Roc, 1991), almost all surfaces and will fill small regions designed to study finite-size effects. Another advantage of helium is the fact that the critical behavior in the bulk limit is well known. Thus, deviations from this limit can be obtained with good confidence. The major disadvantage with helium is the fact that only a limited range of thermodynamic quantities can be measured. The susceptibility to the ordering field cannot be measured since the latter is not physically accessible.

To focus on the effects of confinement, one may look at the specific heat of helium as sketched in Fig. 1. Here the top curve $C(t,\infty)$ indicates the behavior in the thermodynamic limit. The curve labeled $C(t,L)$ is the specific heat of a sample where one or more of the spatial dimensions are made small; i.e., a film of thickness L. The difference between these two curves is a missing signal, $\Delta C(t,L)$, which can be attributed to the quenching of critical fluctuations in one or more dimensions. Points of interest in $C(t,L)$ are the location of the specific-heat maximum T_{max}, the magnitude of the specific heat at this point, C_{max}, and the value of the specific heat at T_λ, $C(0,L)$. However, more generally, one is interested in the temperature dependence over the full range of the critical region, and the evolution of $C(t,L)$ into $C(t,\infty)$. For small deviations from bulk behavior, the shaded regions in Fig. 1, one expects that features embodied in Eq. (1) will be appropriate. Thus, for a film, a surface specific-heat description is appropriate. For this particular example, as one proceeds from high temperatures toward T_λ, one expects bulklike behavior far from T_λ [here $C(t,L)$ and $C(t,\infty)$ would merge], a deviation from $C(t,\infty)$ dominated by surface effects closer to T_λ, full finite-size effects near T_λ, and finally a crossover to two dimensions near the maximum. This blending of behaviors is also manifested on the low-temperature side. There are no sharp features that will distinguish one region from another. It is tempting to identify T_{max} as a shifted critical temperature for the confined system. This is not correct, or is at least ambiguous. For a finite system the temperature T_{max} and other characteristic temperatures, such as the point where the order parameter vanishes T_c, need not be the same. These temperatures merge only in the thermodynamic limit.

B. Scaling relations

We consider, for simplicity, a confined helium system that, in one or more dimensions, is confined to the same small dimension L. This might be a film with dimensions $L\times\infty\times\infty$, a channel of $L\times L\times\infty$ (or for a circular cross section with diameter L), or a box of $L\times L\times L$ (or, equivalently, a sphere of diameter L). We refer to these confinements as having two-, one-, or zero-dimensionality crossover, respectively. We assume in the spirit of correlation-length scaling that the bulk correlation length ξ is the only critical relevant length scale for the confined system. One may then write the following expression for the critical part of the Gibbs free energy per particle (Privman and Fisher, 1984):

$$f(t,L) = t^{2-\alpha}Y(L/\xi). \tag{2}$$

Here $t=|1-T/T_\lambda|$, $\xi=\xi_0 t^{-\nu}$, and α is the critical exponent of the specific heat. The prefactor ξ_0 can be taken as the value for $T>T_\lambda$ or $T<T_\lambda$. The critical exponent ν can be obtained from the superfluid density (Josephson, 1966) or from α itself via the hyperscaling relation $\alpha = 2-3\nu$ (Widom, 1965). The function Y does not contain the ordering field for helium since this is not accessible experimentally. This function will differ for each of the confinements listed above, and will also differ for the same-dimensionality crossover such as, for example, channels of different geometrical cross sections. From the above expression for the free energy one can calculate the specific heat at constant pressure, valid for small t, as

$$C(t,l) = -T_\lambda \left.\frac{\partial^2 f}{\partial T^2}\right|_P = -\frac{1}{T_\lambda}\left.\frac{\partial^2 f}{\partial t^2}\right|_P = t^{-\alpha}g(lt^\nu). \tag{3}$$

The function g contains Y itself as well as its first and second derivatives and the variable $l=L/\xi_0$. This equation can be cast in a more useful form by considering the

limit that $l \to \infty$, in which case one must obtain the bulk specific heat,

$$C(t, \infty) = t^{-\alpha} g(\infty). \tag{4}$$

Note that in both Eqs. (3) and (4) one needs to add a constant to compare with the experimental specific heat. Combining these two equations, one has

$$[C(t, \infty) - C(t,l)]t^{\alpha} \equiv \Delta C t^{\alpha} = g(\infty) - g(lt^{\nu}) = g_1(lt^{\nu}). \tag{5}$$

Thus, a scaling prescription for the specific heat is that the difference between the bulk and the confined system ΔC times t^{α} is a scaling function of lt^{ν}, or equivalently, a function of the variable $tl^{1/\nu}$.

Another useful form for the specific heat can be obtained by considering a particular temperature for $C(t, \infty)$, say t_0, where $\xi(t_0, \infty) = L$. Note that for the confined system ξ is renormalized to $\xi(t, L)$, which never becomes equal to L (see, for instance, Brézin, 1982). However, there is no ambiguity since finite-size scaling makes use of only the bulk correlation length $\xi(t, \infty)$. At t_0 one has

$$C(t_0, \infty) = t_0^{-\alpha} g(\infty) = l^{\alpha/\nu} g(\infty). \tag{6}$$

By recasting the expression for $C(t,l)$ in the following form:

$$C(t,l) = t^{-\alpha} g(lt^{\nu}) = l^{\alpha/\nu}(lt^{\nu})^{-\alpha/\nu} g(lt^{\nu}) = l^{\alpha/\nu} g_2(lt^{\nu}), \tag{7}$$

and combining with the expression for $C(t_0,l)$ one has

$$[C(t,l) - C(t_0, \infty)]l^{-\alpha/\nu} = g_2(lt^{\nu}) - g(\infty) \equiv f_1(lt^{\nu}). \tag{8}$$

Both functions g_1 and f_1 are useful in analyzing data, and in comparing with theoretical predictions. Their form is such that different features of the data are emphasized in the analysis. These functions are also related (Kimball *et al.*, 2000).

From the scaling ansatz Eq. (2), one can get a number of predictions that test *single points* in the thermodynamic response as opposed to the overall response. For instance, the temperature of the specific-heat maximum, the so-called shift equation, can be obtained from the condition that $\partial^3 f/\partial T^3|_{\max} = 0$. This yields the condition that $lt^{\nu}|_{\max} = \text{const}$, or

$$1 - \frac{T_{\max}}{T_{\lambda}} = a l^{-1/\nu}, \tag{9}$$

where a is a constant that will depend on the crossover dimension. Similarly, one might define a region of rounding in the specific heat by identifying the temperature at which the specific heat changes curvature. This inflection point T_{infl} is given by $\partial^4 f/\partial T^4 = 0$. This condition also yields an equation identical to the shift equation in the dependence on l where only the constant a differs. The value of $C(t,l)$ at $t=0$ is also of interest. This follows most simply from Eq. (5) by replacing $t^{-\alpha}$ with $l^{\alpha/\nu}(lt^{\nu})^{-\alpha/\nu}$ and setting $t=0$. This yields

$$C(0,l) = B - g_2(0) l^{\alpha/\nu}, \tag{10}$$

where $B = C(0, \infty)$ is the maximum value of the bulk specific heat. Thus, the specific heat at $t=0$ grows to its maximum value with a weak power law as L/ξ_0 increases. For helium, $\alpha \simeq -0.013$ and $\nu \simeq 0.671$.

An expression for the value of the specific-heat maximum $C(t_m,l)$ follows from the scaling function f_1 at the maximum $f_1(lt_m^{\nu})$. One has

$$C(t_m,l) - C(t_0, \infty) = f_1(a^{\nu}) l^{\alpha/\nu}, \tag{11}$$

where a is the constant in the shift equation. The above equation indicates that the difference in specific heats between t_m and t_0 goes to zero as a weak power law in the same way as the difference in the specific heats at $t=0$, Eq. (10). Alternatively, one may cast the above equation as

$$C(t_m,l) = [f_1(a^{\nu}) + g(\infty)] l^{\alpha/\nu} + B. \tag{12}$$

Equations (10) and (12) indicate that both $C(0,l)$ and $C(t_m,l)$ grow to their common maximum value B with the same weak power law but with different prefactors.

One can make a connection now with the expression for the free energy involving the topology of confinement. We illustrate the procedure by retaining only the surface term in Eq. (1),

$$F \simeq N f_{\infty} + N_s f_s. \tag{13}$$

From this one obtains

$$f \equiv \frac{F}{N} \simeq f_{\infty} + \frac{N_s}{N} f_s = f_{\infty} + \frac{\sigma_s S}{\rho_v V} f_s$$
$$= f_{\infty} + \frac{g_{sv} a_0}{L} f_s = f_{\infty} + \frac{g_{sv}}{L} f_s^*, \tag{14}$$

where σ_s and ρ_v are the surface s and volume v particle densities, respectively, and a_0 is the interatomic spacing. The constant g_{sv} is the surface-to-volume ratio taken as a dimensionless number. For a film, cylinder, and sphere one has $g_{sv} = 2$, 2, and 3, respectively. For these cases the small dimension L is the film thickness and the radii, respectively. With the inclusion of a_0 in f_s the dimensions of f_s^* can be taken as J Å mol^{-1}. Differentiating f twice to obtain the specific heat, one has

$$C(t,L) \simeq C_{\infty}(t) + \frac{g_{sv}}{L} C_s(t). \tag{15}$$

If one now assumes a power-law behavior for $C_s(t)$,

$$C_s(t) = \frac{A_s}{\alpha_s} t^{-\alpha_s}, \tag{16}$$

one can recast Eq. (15) in the form of Eq. (5),

$$[C(t, \infty) - C(t,L)]t^{\alpha} \equiv \Delta C t^{\alpha} \simeq -\frac{g_{sv}}{L} \frac{A_s}{\alpha_s} t^{-(\alpha_s - \alpha)}. \tag{17}$$

Thus, this bulk-plus-surface approach leads to an explicit form for the scaling function: a power law. For this to agree with correlation-length scaling one must have

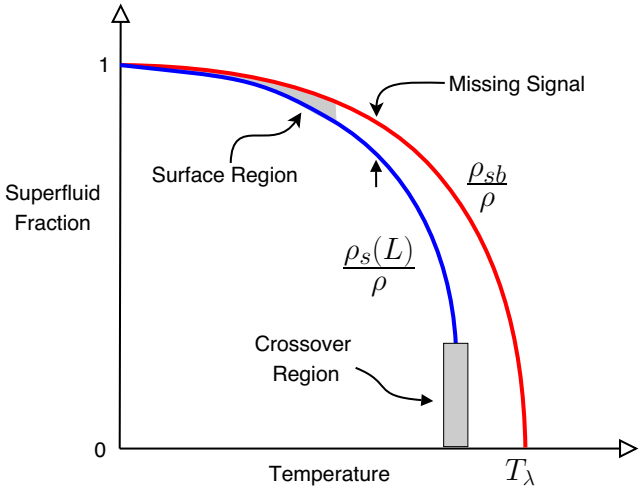

FIG. 2. (Color online) Sketch showing the qualitative difference between the superfluid density of bulk $\rho_{sb}(t)$ and confined helium $\rho_s(t,L)$.

$\alpha_s-\alpha=\nu$ so that the right-hand side is a function of Lt^ν (or lt^ν if ξ_0 is introduced). One should note that this approach has limited range of applicability and must give way to the full scaling function as lt^ν becomes small. Thus, there is no divergence implied in Eq. (17) as t becomes small. Note that the amplitude of the surface specific heat A_s must be negative if it is to reflect a decrease of the specific heat under the influence of confinement (at least for Dirichlet boundary conditions). A similar treatment for the edge term would lead to the following scaling function:

$$\Delta C t^\alpha \simeq -\frac{g_{ev}}{L^2}\frac{A_e}{\alpha_e}t^{-(\alpha_e-\alpha)}, \tag{18}$$

where, to satisfy correlation-length scaling, the edge exponent must be related to ν as $\alpha_e-\alpha=2\nu$. The last two relationships for ΔC are not expected to hold simultaneously. Indeed, on physical grounds, one would expect that, as t becomes small for a fixed L, the corner term would manifest itself first, then the edge, and then the surface. It is not clear *a priori* that, in a geometry where all these terms are expected to be present, they will be clearly identified as opposed to blending one into the other in a continuous way. Thus, in geometries with the same crossover dimension, say a box $L\times L\times L$ or a sphere of diameter L, the crossover to zero dimensions will take place along distinct loci.

The behavior of the superfluid fraction ρ_s/ρ for confined helium and ρ_{sb}/ρ for bulk helium is sketched in Fig. 2. As in the case of the specific heat, the confinement reduces the superfluid density so that there is a missing signal between the bulk and the confined helium. Also, ρ_s/ρ will vanish at a temperature below T_λ in a way that depends on the crossover dimension. Overall, the missing signal will be described by a scaling function $X(L/\xi)$. One may take this in the form

$$\frac{\rho_s(t,L)}{\rho}=\frac{\rho_{sb}(t)}{\rho}\left[1-X\left(\frac{L}{\xi}\right)\right]=\frac{\rho_{sb}(t)}{\rho}[1-X(lt^\nu)]. \tag{19}$$

For 1D and 0D crossovers one expects that

$$\lim_{T\to T_c} X(lt^\nu)=1. \tag{20}$$

This implies a shift equation for the vanishing of ρ_s,

$$1-\frac{T_c}{T_\lambda}=bl^{-1/\nu}. \tag{21}$$

This is in the same form as the shift equation for the specific-heat maximum, but T_c and $T_{\max}$ are not necessarily the same temperature, i.e., the constants a and b differ.

For crossover to two dimensions, the scaling function must reproduce the expected universal value for $L\rho_s(T_c)/T_c$ in the superfluid fraction (Nelson and Kosterlitz, 1977). Hence, one must have (Ambegaokar *et al.*, 1980)

$$\lim_{T\to T_c} X(lt^\nu)=1-\frac{1}{L\rho_{sb}(T_c)}\frac{2}{\pi}k_BT_c\left(\frac{m}{\hbar}\right)^2. \tag{22}$$

One can also approach the scaling of ρ_s from the point of view of confinement topology in a similar way as for the specific heat. This approach is meant to be applicable in the limit that ξ/L is small. We consider the contribution from a surface term, and write the total superfluid mass as (Gasparini and Rhee, 1992)

$$M_s(t,L)\simeq Nm_4\frac{\rho_{sb}(t)}{\rho}+N_sm_4\frac{\sigma_s(t)}{\sigma}, \tag{23}$$

where m_4 is the atomic mass and the σ's are areal densities. From the above equation one obtains

$$\frac{M_s}{Nm_4}=\frac{\rho_s(t,L)}{\rho}\simeq\frac{\rho_{sb}(t)}{\rho}+\frac{\sigma S}{\rho V}=\frac{\rho_{sb}(t)}{\rho}+\frac{g_{sv}a_0}{L}\frac{\sigma_s(t)}{\sigma}. \tag{24}$$

To obtain a specific form for the scaling function, one assumes power-law behaviors for ρ_{sb}/ρ and σ_s/σ,

$$\frac{\rho_{sb}}{\rho}=kt^\zeta, \tag{25}$$

$$\frac{\sigma_s}{\sigma}=k_st^{\zeta_s}. \tag{26}$$

Using these equations one obtains

$$\frac{\rho_s}{\rho}\simeq\frac{\rho_{sb}}{\rho}\left(1+\frac{g_{sv}a_0}{L}\frac{k_s}{k}t^{\zeta_s-\zeta}\right). \tag{27}$$

By comparing the above equations with the general scaling ansatz Eq. (19), one can see that k_s must be negative if $\rho_{sb}>\rho_s$; and, to agree with the scaling form, one must have $\zeta-\zeta_s=\nu$. Since for the bulk exponent one has $\zeta=\nu$ (Josephson, 1966), then one must have $\zeta_s=0$. Thus, the difference in superfluid fraction in the "surface" region is a constant for any given L,

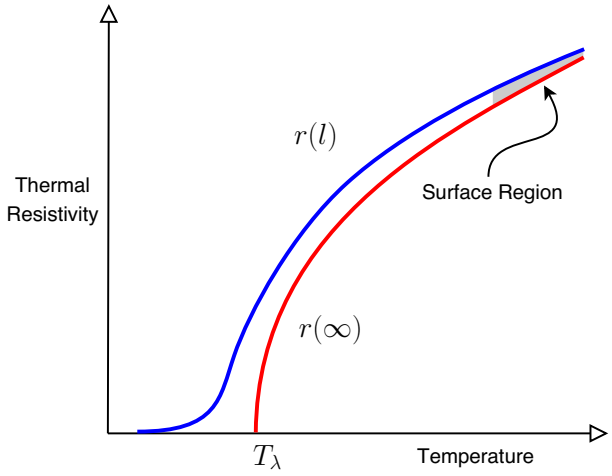

FIG. 3. (Color online) Sketch showing the qualitative difference in the thermal resistivity between bulk $r(t,\infty)$ and confined helium $r(t,L)$. Adapted from Frank and Dohm, 1990.

$$\left(\frac{\rho_s}{\rho}-\frac{\rho_{sb}}{\rho}\right)L \simeq g_{sv}a_0\frac{k_s}{k}. \tag{28}$$

Equivalently, the fractional difference $(\rho_{sb}-\rho_s)/\rho_{sb}\sim t^{-\nu}$. This result is supported by explicit calculations from ψ theory (Ginzburg and Pitaevskii, 1958; Mamaladze, 1967; Sobyanin, 1972; Ginzburg and Sobyanin, 1976, 1982, 1987). In this theory one has a differential equation for the order parameter. This can be solved for a film using Dirichlet boundary conditions to give an explicit form for the function X. One finds for the superfluid fraction

$$\frac{\rho_s(t,L)}{\rho}=\frac{\rho_{sb}(t)}{\rho}\left[1-2\sqrt{2}\frac{\xi_\psi}{L}\tanh\left(\frac{1}{2\sqrt{2}}\frac{L}{\xi_\psi}\right)\right], \tag{29}$$

where $\xi_\psi=\xi_{0\psi}t^{-\nu}$, a critical length scale that differs in magnitude from ξ; also, the critical exponent in this theory is $\nu=2/3$ (with $\alpha=0$). This is close, but not quite equal, to the experimental value of 0.6705 (Goldner and Ahlers, 1992; see below). In the surface region, where ξ_ψ/L is small, one has

$$\left(\frac{\rho_s}{\rho}-\frac{\rho_{sb}}{\rho}\right)L \simeq -2\sqrt{2}\xi_{0\psi}k. \tag{30}$$

This again shows that for fixed L the difference in the superfluid density is a constant. Putting numbers in the above equation, one finds that the surface contribution for a film of 100 nm at $t=10^{-2}$ reduces ρ_s/ρ by ~10%.

The thermal conductivity κ of helium above T_λ is the thermodynamic response that mirrors the superfluid density below T_λ. In bulk this quantity diverges. In a confined system its behavior is modified. The thermal resistivity $r\equiv 1/\kappa$ for bulk and confined helium is sketched in Fig. 3. The situation with κ is more complicated than for the specific heat and the superfluid density. If one considers the situation with a film of thickness L, one could think of conduction perpendicular to the surface area or along the direction parallel to it. For either case one may write $r(t,l)$ as

$$r(t,l)=r(t,\infty)[1+R(tl^{1/\nu})]. \tag{31}$$

Introducing a power-law behavior $r(t,\infty)=r_0t^\mu$, where $\mu\simeq 0.44$ is an effective exponent (Tam and Ahlers, 1985), one has the scaling form

$$[r(t,l)-r(t,\infty)]t^{-\mu}=r_0R(tl^{1/\nu}), \tag{32}$$

or equivalently the form

$$[r(t,l)-r(t,\infty)]l^{\mu/\nu}=r_0(tl^{1/\nu})^\mu R(tl^{1/\nu})\equiv r_0G(tl^{1/\nu}). \tag{33}$$

Equation (32) is analogous to Eq. (5) for the specific heat. From the above equation one can see that as $t\to 0$ for fixed l one must have $R(tl^{1/\nu})=R_0(tl^{1/\nu})^{-\mu}$; hence one finds

$$r(0,l)=r_0R_0l^{-\mu/\nu}. \tag{34}$$

Thus the value of the conductivity $\kappa(0,l)=1/r(0,l)$ at $t=0$ grows to infinity as $l^{\mu/\nu}\simeq l^{0.66}$, a much more rapid variation than the heat capacity, which tends toward a maximum with a power law $l^{\alpha/\nu}\simeq l^{-0.017}$. Note that the scaling function would differ for different arrangements of heat current relative to the small dimension L.

One can also proceed using a bulk-plus-surface approach. Consider first the situation where the heat flow is along L, i.e., perpendicular to the surface of area A. One measures a conductance $K^\perp$. It is easier in this case to consider instead the thermal resistance $R^\perp=1/K^\perp$ and write

$$R^\perp \simeq \frac{L}{A}r_\infty+2\frac{a_0}{A}r_s^\perp, \tag{35}$$

where the 2 comes from the two surfaces, a_0 is the interatomic spacing, and $r_s^\perp$ is the thermal resistivity attributed to the surface. Rearranging the above equation, one has

$$r^\perp \simeq r_\infty\left(1+2\frac{a_0}{L}\frac{r_s^\perp}{r_\infty}\right)=r_\infty\left(1+2\frac{a_0}{L}\frac{r_0^\perp}{r_0}t^{\mu_s^\perp-\mu}\right), \tag{36}$$

where we have introduced power laws for the resistivities $r_s^\perp=r_0^\perp t^{\mu_s^\perp}$ and $r_\infty=r_0t^\mu$. In order for $r^\perp$ to be in scaling form one must have $\mu_s^\perp=\mu-\nu$. Thus one can write that the fractional difference in the resistivity is a power law,

$$\frac{r^\perp-r_\infty}{r_\infty}=2\frac{a_0}{L}\frac{r_0^\perp}{r_0}t^{-\nu}, \tag{37}$$

or in the scaling form of Eq. (32) one has

$$(r^\perp-r_\infty)t^{-\mu}\simeq\frac{2a_0}{\xi_0}r_0^\perp(tl^{1/\nu})^{-\nu}. \tag{38}$$

Thus the scaling function for this perpendicular geometry is a simple power of the scaling variable with exponent ν. Note that in these expressions, unlike those for

the specific heat and superfluid density, the amplitude of the surface term $r_0^{\perp}$ is positive. Also, the fractional difference in the thermal resistivity obeys the same power law as the fractional difference of the superfluid fraction [see Eq. (28) and the text following it].

The situation when heat is propagating parallel to surface A separated at a distance L can be treated similarly. It is easier in this case to work with the conductivity directly and write

$$\kappa^{\parallel} \simeq \kappa_{\infty} + 2\frac{a_0}{L}\kappa_s^{\parallel}. \tag{39}$$

One can now introduce power laws in a similar way as for $\kappa^{\perp}$ and note that one now requires that $\mu_s^{\parallel}=\mu+\nu$ for correlation-length scaling to work. The final expression for this parallel geometry is

$$\frac{\kappa^{\parallel}-\kappa_{\infty}}{\kappa_{\infty}} \simeq 2\frac{a_0}{L}\frac{\kappa_0^{\parallel}}{\kappa_0}t^{-\nu}. \tag{40}$$

One can also cast this in terms of the resistivity,

$$r_{\infty} - r^{\parallel} \simeq r_{\infty} r^{\parallel}\frac{2a_0}{L}\kappa_s^{\parallel}. \tag{41}$$

Introducing power laws and following Eq. (31), one finds the following two equivalent scaling forms:

$$(r_{\infty} - r^{\parallel})t^{-\mu} \simeq \frac{2a_0 r_0^2}{\xi_0 r_0^{\parallel}}(tl^{1/\nu})^{-\nu}[1 + R(tl^{1/\nu})], \tag{42}$$

$$(r_{\infty} - r^{\parallel})l^{\mu/\nu} \simeq \frac{2a_0 r_0^2}{\xi_0 r_0^{\parallel}}(tl^{1/\nu})^{\mu-\nu}[1 + R(tl^{1/\nu})]. \tag{43}$$

In this geometry the amplitude of the surface term $\kappa_0^{\parallel}$ is negative. Note also that Eq. (40) does not apply in the limit that t becomes small since here κ_{∞} must diverge. In this limit the full scaling function R or G would apply. Also, for this parallel geometry, one has a power-law behavior in the surface region only to the extent that $R \ll 1$.

We note here that, although in all cases the scaling of the finite system is done with the bulk correlation length, the correlation length for the finite system $\xi(t,L)$ is itself modified to reflect the fact that fluctuations are limited to a maximum distance L in the direction of confinement. Thus it is not correct to state that the temperature at which ρ_s vanishes or where the specific heat has its maximum identifies the point at which $\xi \approx L$. The situation is actually more complicated than this in the case of a film geometry where the crossover is to two dimensions. Here the 2D correlation length should become relevant at a certain temperature. This might be a region where scaling with the 3D correlation length could fail. We also note in this context that it is quite possible to realize a situation in helium where one is dealing with a relatively thin film that is laterally confined. This would be a situation where finite-size effects governed only by the 2D correlation length would be manifest. Although some work has been done in this area (see Sec. VIII), much remains to be explored in detail (Diaz-Avila *et al.*, 2004; Diaz-Avila, 2006).

We have not emphasized in the above discussion the effect of boundary conditions on scaling functions. This is simply because Dirichlet conditions are the natural experimental situation. However, in helium, using suitable lithographic techniques, one should be able to realize confinements where, at least in one direction, periodic conditions apply. This work remains to be done.

Much work also remains to be done to extend existing data and explore the universality of finite-size scaling. We discuss this in Sec. IX. There are two ways to change the transition temperature in helium: one via pressure P, and the other via the introduction of ^{3}He at a concentration $x \equiv N_3/(N_3+N_4)$, where N_3 and N_4 are the molar quantities of ^{3}He and ^{4}He, respectively. Then the superfluid transition takes place across a surface $T_{\lambda}(P,x)$. Finite-size effects should be manifest for any of these thermodynamic coordinates and yield universal scaling functions.

II. HELIUM IN THE THERMODYNAMIC LIMIT

The behavior of helium in the thermodynamic limit is needed to analyze data for finite-size effects. As pointed out in Sec. I.B, one typically needs to calculate differences between the response of the confined system and that of the system in the thermodynamic limit. We discuss briefly in this section how the bulk behavior is represented.

A. Specific heat

In the case of the specific heat one needs to calculate $\Delta C t^{\alpha}$ [see Eq. (5)]. This could present a problem in the sense that the absolute magnitude of $C(t,\infty)$ is known to a much lower accuracy than the precision with which ΔC can be obtained. One can avoid this difficulty by normalizing $C(t,L)$ to $C(t,\infty)$ sufficiently far from the transition where the effect of confinement is too small to measure. This might well be outside the critical region where the exponent α is obtained. Thus a representation of $C(t,\infty)$ is required that is valid over a broad range of t. This representation was obtained by Mehta *et al.* (1999) by combining several sets of bulk data (Ahlers, 1971; Gasparini and Moldover, 1975; Chen, 1978; Lipa and Chui, 1983) that collectively covered the range $10^{-8} < t \lesssim 0.07$. The data for both sides of the transition were fitted separately to the function

$$C = \left(\frac{A}{\alpha}t^{-\alpha}(1 + Dt^{0.5}) + B\right)\left[1 + E\frac{t}{\ln t} + F\left(\frac{t}{\ln t}\right)^2\right]. \tag{44}$$

The parameters that provide the best fit are given by Mehta *et al.* (1999). A plot of these data and the deviation from Eq. (44) are shown in Figs. 4 and 5. One can see from these plots that Eq. (44) represents the full range of data with no residual systematic errors. More

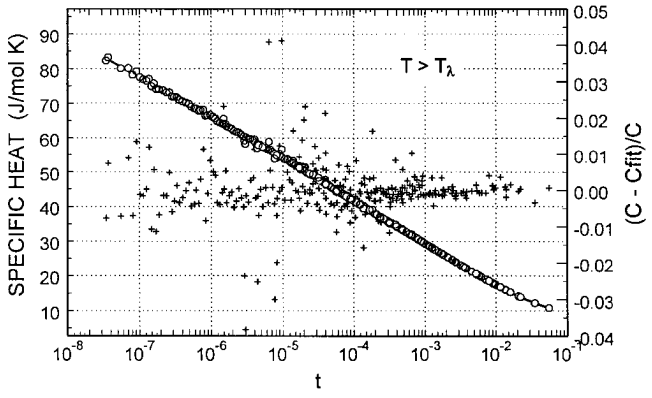

FIG. 4. Four independent measurements of bulk helium above the superfluid transition (Ahlers, 1971; Gasparini and Moldover, 1975; Chen, 1978; Lipa and Chui, 1983) combined into one data set (open circles). The solid line represents a fit of the combined data to Eq. (44). The pluses are the difference between individual points and the solid line. From Mehta *et al.*, 1999.

recent data (Lipa *et al.*, 2003) are in agreement with this representation (after an overall magnitude rescaling by a factor of 1.006). In particular, for $T<T_\lambda$ these data agree within 0.1% with the Mehta *et al.* (1998) representation in the range $t\simeq 10^{-2}$–10^{-3}, but have a slightly different temperature dependence that produces a 0.6% difference closer to the transition in the range of $t=10^{-7}$–10^{-8}. While one may choose any suitable function to represent $C(t,\infty)$, finite-size scaling also requires knowledge of the exponent α which can only be obtained by a careful analysis within the critical region. The precise value of α, however, is not crucial because the dominant temperature dependence in $\Delta C t^\alpha$, at least for large values of the scaling variable $tl^{1/\nu}$, comes from ΔC, which is in turn governed more strongly by the temperature dependence of the correlation length. Values of α in the range of −0.011 to −0.014 affect the locus of $\Delta C t^\alpha$ by a few percent. In practice, a value of α and ν should be chosen in a consistent way so that they satisfy the hyperscaling relation $\alpha=2-3\nu$. Given this, one may regard the exponent ν as a variable and see which value

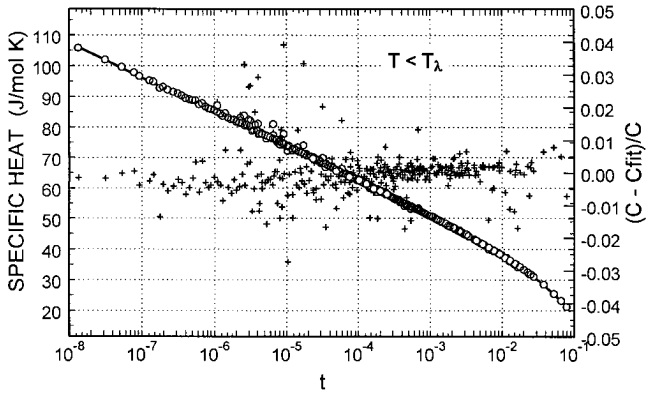

FIG. 5. The equivalent plot to Fig. 4 for data below the bulk transition temperature. From Mehta *et al.*, 1999.

best collapses the data according to Eq. (5) (this is shown in Sec. V.A). The most important aspect of scaling the specific heat and calculating $\Delta C t^\alpha$ is that $C(t,\infty)$ should be the same as the data to which $C(t,L)$ has been normalized. This effectively takes out, to first order, systematic errors in the magnitude of the specific heat.

B. Superfluid density

The superfluid fraction has been measured in a number of experiments (Clow and Reppy, 1966; Tyson and Douglass, 1966, 1968; Greywall and Ahlers, 1972, 1973; Goldner and Ahlers, 1992; Goldner *et al.*, 1993; Nissen *et al.*, 2000). Data near the transition can be described well by the following function:

$$\frac{\rho_s}{\rho} = k_0(1+k_1 t)t^\zeta(1+Dt^\Delta+Ot^{2\Delta}). \tag{45}$$

The term linear in t and the first term involving the confluent singularity, t^Δ with $\Delta\simeq 0.5$, allow a good representation of the superfluid fraction in the range $5\times 10^{-6}\lesssim t\lesssim 10^{-2}$. Data for ρ_s do not extend as close to the transition as in the case of the heat capacity, but the critical exponent is well established from these measurements; $\zeta=0.6710\pm 0.0005$ is a good representative value. Note that the absolute magnitude of ρ_s from various experiments varies much more substantially than the magnitude of the specific heat. This is reflected in k_0, which can differ by as much as 4% for different experiments. However, as in the case of the heat capacity, a measurement of the superfluid fraction for a confined system will be normalized to the bulk value far from the transition, where finite-size effects are negligible. Hence the absolute magnitude of ρ_s is not important in the analysis. The Josephson scaling relation (Josephson, 1966) is given by $3\zeta=2-\alpha$; hence, with the hyperscaling relation $3\nu=2-\alpha$ (Widom, 1965), one has $\zeta=\nu$. Finite-size scaling yields the exponent ν directly; thus it may be viewed as testing these relationships by providing an independent determination of ν (see Sec. V.A for this analysis).

C. Thermal conductivity

The thermal conductivity κ of helium above T_λ was expected, on the basis of dynamic scaling theory, to diverge asymptotically as $\kappa\sim t^{-\nu/2}$ (Ferrell *et al.* 1967; Halperin and Hohenberg, 1967; Halperin *et al.*, 1974; Hohenberg and Halperin, 1977). However, it was shown that this asymptotic behavior is not realized because of a weak-scaling fixed point whose presence influences the behavior of κ in the temperature region where static properties achieve their asymptotic temperature dependence (De Dominicis and Peliti, 1978; Dohm, 1978, 1985; Dohm and Folk, 1981). Thus the usual power-law correction to the scaling approach cannot be used for κ, and one needs a nonlinear dynamic renormalization analysis to compare theory and experiment (Dohm, 1991, 2006;

Folk and Moser, 2002). It is customary to examine an effective dimensionless amplitude (Dohm and Folk, 1981; Tam and Ahlers, 1986)

$$\hat{R}_\lambda(t) = \frac{\kappa}{k_B g_b (\xi C_p/k_B)^{1/2}}. \tag{46}$$

This effective amplitude is weakly temperature dependent, and asymptotically should become a constant when the specific heat per unit volume at constant pressure C_p reaches its maximum value. The coupling constant $g_b = k_B T_\lambda S_\lambda R^{-1}\hbar^{-1}$, with $S_\lambda R^{-1}$ being the dimensionless entropy at T_λ. In Eq. (46) k_B is the Boltzmann constant. If one examines κ directly, one finds that over a limited range in t it can be written as a power law $\kappa = \kappa_0 t^{-\mu}$, with $\mu \simeq 0.44$ as an effective exponent (Ahlers *et al.*, 1982; Tam and Ahlers, 1985, 1986; Dingus *et al.*, 1986; Lipa and Chui, 1987). For examining finite-size effects one can scale the thermal conductivity according to the equation developed in Sec. I.B. Alternatively, one notes that in Eq. (46) κ, ξ, and C_p should all scale with $tL^{1/\nu}$ for a finite system. Consequently, $\hat{R}_\lambda(t)$ can be scaled directly. This is done in Sec. V.C. As in the case of the specific heat and superfluid density, deviations from bulk behavior are obtained after normalization of $\kappa(t,L)$ to $\kappa(t,\infty)$ in a region of t where the difference in negligible.

D. Universality

One may also investigate the universal aspects of finite-size scaling. The concept of universality goes far back in the history of critical phenomena to the work of Landau [1937, see also Landau (1965) and Landau and Lifshitz (1959)] and later work by Griffiths (1970), and by Kadanoff (1971). The advent of the renormalization group (Wilson, 1971a, 1971b) provides a theoretical basis for the concept of universality and universality classes. A nice historical discussion of the concept of universality can be found in Domb (1996). As stated by Kadanoff (1971), critical systems can be divided into a set of classes distinguished by their dimensionality and the symmetries of the ordered state. These classes are characterized by the same values of the critical exponents and certain amplitude ratios of various thermodynamic responses. Thus quite different physical systems such as magnets and fluids can belong to the same universality class. In the case of the superfluid transition in ^{4}He, one can make use of the fact that $T_\lambda = T_\lambda(P,x)$, where P is the pressure and x is the molar concentration of ^{3}He. As these two variables increase, the transition temperature is lowered. This defines a surface in P,T,x space that may be crossed for any set of thermodynamic variables and defines response functions that are expected to have universal exponents and amplitude ratios. Note that, in the case of concentration, one must limit the range in x so as to avoid crossover effects near the tricritical point $x = 0.67$.

Various studies have been reported which probe the universality of the superfluid transition for both pressure and concentration variables (Gasparini and Moldover, 1969, 1975; Greywall and Ahlers, 1972, 1973; Terui and Ikushima, 1972; Ahlers, 1973; Ikushima and Terui, 1973; Ihas and Pobell, 1974; Mueller *et al.*, 1975; Gasparini and Gaeta, 1978; Okaji and Watanabe, 1978; Takada and Watanabe, 1980; Singsaas and Ahlers, 1984). It is found that this universal behavior holds in the thermodynamic limit away from $x = 0$ and $P = 0.05$ bar (saturated vapor pressure). At zero concentration and saturated vapor pressure, in the case of the specific heat, one finds slightly different results which seem at present to be just outside experimental uncertainty (Gasparini and Gaeta, 1978; Kimball and Gasparini, 2005, see also Sec. IX). For the confined system, for instance, one might be interested in the scaling of $C(t,l,x)$ or $\rho_s(t,l,x)$ for various values of l and x; or the scaling of $\kappa(t,l,P)$ for various values of l and P. Thus these studies combine finite-size scaling with universality. There are also some additional complications in extending this universality concept to finite-size effects. These have to do with the choice of the right thermodynamic path and taking proper account of the nonuniversal amplitudes of the thermodynamic response and of the bulk correlation length $\xi(P,x)$. Only if this is done can one expect universal collapse on the locus of the scaling function determined at saturated vapor pressure and zero concentration.

III. EXPERIMENTAL REALIZATIONS OF CONFINEMENT

A. Helium films

Since ^{4}He wets almost all solid surfaces, the simplest realization of confined helium is that of a film formed on a substrate and in equilibrium with its vapor at a pressure P less than the saturated vapor pressure P_0. Here the thickness of the film d can be determined by relating the change in the chemical potential (relative to the bulk) in the film $V(d)$, and in the vapor in equilibrium with it. If the latter is treated as an ideal gas, one has

$$V(d) = -kT \ln \frac{P}{P_0}, \tag{47}$$

where the potential $V(d)$ represents the helium-substrate potential energy, which for thin films varies as d^{-3} (Dzyaloshinskii *et al.*, 1961). Alternatively, one can keep track of the number of moles introduced in an experimental cell and deduce the film thickness from the known surface area and the equilibrium vapor pressure. In this case, one typically has to take into account the fact that the first few layers are not at the bulk density. Indeed, the first layer might be solid. The earliest work with films yielded a rounded specific heat, shifted specific-heat maximum, shifted superfluid onset temperature, and reduced superfluid fraction. These are all features of finite-size effects. However, in many cases, the interpretation of these experiments as it relates to finite-size scaling was ambiguous. There are problems with film homogeneity, mostly due to capillary condensation and surface roughness when films are formed on

surfaces of porous media or packed powders. This is especially true if thick films are formed, which is necessary for finite-size effects. When one tries to avoid this difficulty in more open experimental arrangements, films vary significantly in thickness as the temperature and hence the equilibrium pressure varies. This is especially troublesome in measurements of heat capacity, where the vapor and the process of evaporation can contribute a significant signal in addition to that of the liquid film itself. In light of this, measurements of the specific heat follow a unique thermodynamic path which depends on the ratio of surface to volume of a particular experimental cell. One can also measure films at saturated vapor pressure by examining the film in equilibrium at a given height H above the bulk liquid. Here the equilibrium thickness is determined by equating the gravitational potential energy m_4gH with $V(d)$, where d is the local thickness at the height H above the liquid surface. A limited range of thicknesses can be explored in this way because of the weak dependence of d on H.

B. Complete confinement

There is a long history of research in helium with samples completely filling the voids in packed powders and various porous media (for a review, see Reppy, 1992). In these cases, as observed for films, one finds shifted onset temperatures and a modified thermodynamic response, which can be attributed to confinement. However, for investigation of finite-size scaling, this type of system is not very useful because the confinement is over a distribution of spatial dimensions. One cannot use data for such systems for size scaling. However, one may extract the behavior in the surface region as discussed in the Introduction. Thus the temperature dependence of the initial deviation from bulk behavior can be examined to see if it has the expected power-law behavior in a region not too close to the transition. This will work provided all spatial dimensions in the sample are much larger than the correlation length, and, for the full spectrum of sizes, one is in the critical region of the thermodynamic response, typically in the range $t \leq 10^{-2}$–10^{-3}. We come back to this below.

The first experiments in which relatively homogeneous complete confinement was studied involved nearly cylindrical pores. Notarys (1969) determined the onset of superfluidity for helium in pores of mica. Other measurements, specific heat (Chen and Gasparini, 1978), superfluid density (Brooks *et al.*, 1979; Schubert and Zimmermann, 1981), and superfluid onset (Thomlinson *et al.*, 1973; Ihas and Pobell, 1974; Giordano, 1983), have been done with helium confined in pores of nuclepore filters. These are polycarbonate filters where different size pores are achieved by the etching of radiation tracks. The size distribution of the pores for nominally 200-nm diameter size was measured and it was found that ~80% of the pores were within 10% of the mean value (Chen *et al.*, 1980). This mean value was lower than the nominal value by about 10%. The pores had an asymmetric distribution, with a longer tail at smaller diameters. Other scanning electron microscope (SEM) measurements, as well as gas flow measurements, also indicate average sizes which tend to be smaller than nominal sizes (Giordano, 1983). Measurements of adsorption isotherms with helium and nitrogen yield surface areas that are larger than the geometric area (Chen *et al.*, 1980). These data indicate that the surface of the pores becomes rougher the smaller the diameter. Also, work with gases of various molecular size indicates that the surface might be fractal, at least over some limited range of sizes (Gasparini and Mhlanga, 1986).

More recently, confinement in multichannel plates (BURLE Electro-Optics Inc.) has been used by Lipa *et al.* (2001) and Genio *et al.* (2005). These are plates in which channels are formed in a process involving the drawing and bundling of glass fibers which have a sacrificial core surrounded by a stable glass. The etching of the cores leaves homogeneous cylindrical channels with presumably smooth surfaces. Measurements of thermal conductivity and heat capacity have been made with helium confined in these channels. Sizes as small as 1 μm in diameter have been used by Murphy *et al.* (2003). Measurements of heat capacity have also been done with Anopore filters, which have pores etched in an alumina matrix (Lipa *et al.*, 2001).

Silicon wafers with exceptional surface smoothness and overall flatness have been used to achieve confinements that can be controlled using a combination of lithographic techniques and the process of direct bonding of two wafers (Rhee *et al.*, 1990). This will be discussed below. Alternatively, one can use a stack of silicon wafers or any other flat wafers, separated by spacers. Helium between the wafers will be in a planar geometry. This is the arrangement used for the heat-capacity measurement by Lipa *et al.* (1998, 2000). A stack with substantial vertical height would result in serious gravitational rounding of the transition, which would mask finite-size effects. For this reason these measurements were done on the Space Shuttle (Lipa *et al.*, 2000). Silicon wafers have also been used as a substrate to study the Casimir force with saturated films (Ganshin *et al.*, 2006).

C. Confinement in bonded Si wafers

Silicon can be bonded directly to silicon dioxide to form silicon-on-insulator structures (Gösele and Tong, 1998, and references therein). For the purpose of studying finite-size effects, SiO_2 can be patterned lithographically to achieve a variety of open and uniform spaces in the bonded structure in which helium can be confined. Rhee *et al.* (1990) were the first to use such a process to achieve planar confinement. This was used for the determination of the superfluid density with the confined helium as part of the moment of inertia of a torsional pendulum. The patterning, bonding, and diagnostic process was improved and diversified in subsequent work (Mehta *et al.*, 1999; Diaz-Avila *et al.*, 2004; Kimball *et al.*, 2004; Kimball, 2005; Diaz-Avila, 2006). The preparation of the experimental cells starts with Si wafers of excep-

tional free-state flatness, about 1 μm over the full area of a 5-cm-diameter wafer, and local flatness better than or equal to 0.5 nm/μm^2 (Umicore). SiO_2 is grown on a wafer using a wet oxide process. This ensures the presence of OH ions in the oxide, which is important for the bonding process (Rhee *et al.*, 1990). Subsequently, the oxidized wafer is patterned using standard optical lithography. A second wafer is prepared, which at its simplest is a bare one, by drilling a hole in the center using diamond paste. This hole is later used to introduce helium into the cell. For the bonding process, the two wafers are chemically cleaned and staged about 1 mm apart on a spinner inside a clean chamber (Mehta, 1998). The wafers are rinsed and then spun dry before they are allowed to touch. The room-temperature bonding is started using a home-made press which starts the bonding at the center and propagates it to the edges. The quality of the bonded wafers is examined with an infrared imager and, if it is not adequate, as evidenced by interference fringes, the wafers can be pried apart and the process started again. Alternatively, one can wait about 24 h and the wafers will unbond as built-in stresses relax. An example of two bonded wafers is shown in Fig. 6. The bright areas in this figure represent bonded SiO_2, and the darker area is the open space where helium would reside. This cell is designed for planar confinement and the uniformity of the spacing is ensured by the bonded SiO_2 posts. The separation of the posts is chosen so that there is no appreciable bending of the silicon in the intervening area between the posts. The continuous ring in Fig. 6 forms a leak-tight seal. After room-temperature bonding, the wafers are staged on a quartz fixture which is used to evacuate the volume between the wafers, and to place them in a furnace where they are annealed at 1100 °C for a period of 3–4 h. Annealing can also be done for a longer time at lower temperatures (Tong *et al.*, 1994, 1998). After this process, the bonding is very strong, and typically one would shatter the silicon if the wafers were pried apart. Several diagnostic steps are used in this overall process. The thickness of the grown oxide is measured using ellipsometry. It can be further measured after patterning using a stylus instrument or an atomic force microscope. More complicated patterns are inspected using an electron microscope (Kimball, 2005). After bonding, the two wafers form a parallel structure in which the inner silicon surfaces can be used as a Fabry-Perot interferometer. The interferometer can be used to determine the local spacing and check the homogeneity of the bonded structure. Results for this spacing for three different cells used for 2D, 1D, and 0D confinement are shown in Fig. 7 (Kimball *et al.*, 2004). The continuous surfaces shown in this figure are constructed from a series of measurements over the full face of the bonded wafers using light in the infrared and a beam spot of about 1 mm^2. One can see that the separation is uniform to better than 1%. There are other details in the oxide patterns for these cells which are relevant to the eventual measurements with helium. These will be discussed in the context of these measurements.

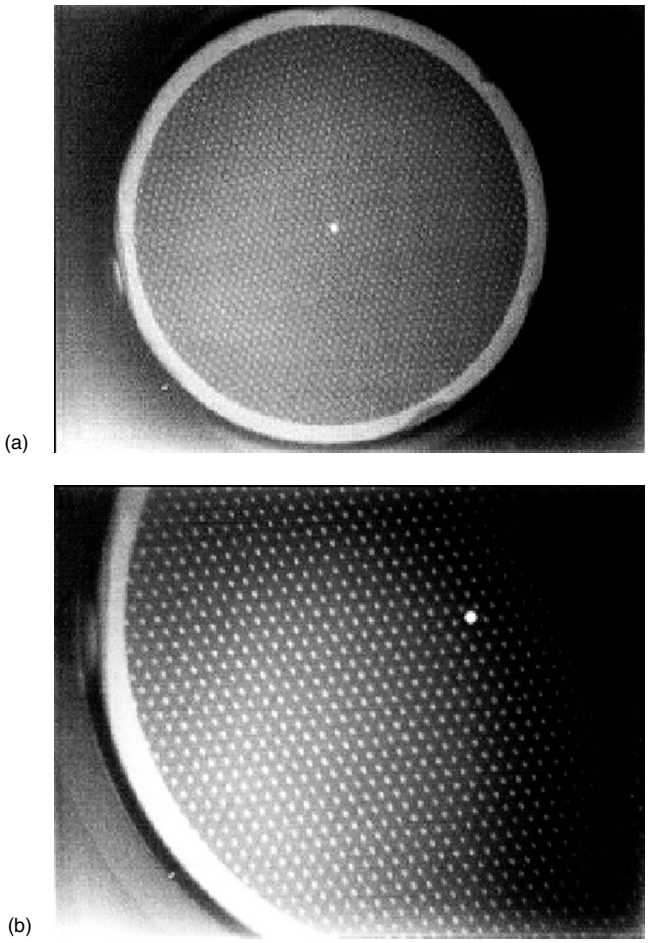

FIG. 6. An infrared transmission image of two 5-cm silicon wafers that are bonded together to form a closed structure used to confine liquid helium. These images are for a planar confinement where the light areas are bonded posts of silicon dioxide and the dark area is an open region to be filled with helium. The bright spot in the center of (a) is the hole in one of the wafers used to introduce helium into the cell. The only imperfections in the bonding occur in the outer border region and does not affect the area where helium will be confined.

IV. SCALING AND EARLY EXPERIMENTAL RESULTS

A comprehensive review of experimental and relevant theoretical results for helium was done by Gasparini and Rhee (1992). This review will be referred to as Paper I. We summarize here some of these earlier results with helium films. Some of these will be incorporated in the analysis of data obtained since Paper I appeared.

The specific heat of helium films has been measured by a number of researchers (Frederikse, 1949; Mastrangelo and Aston, 1951; Symonds, 1965; Brewer, 1970; Bretz, 1973; Chen and Gasparini, 1977; Yuyama and Watanabe, 1982). However, results relevant to finite-size scaling are not as plentiful as these studies might suggest. It is easy to ascertain that what is often characterized as a film of given thickness is actually not so, or, in some cases, the behavior is dominated by other effects which are not fully understood. Capillary condensation in packed powders and porous material is the most ob-

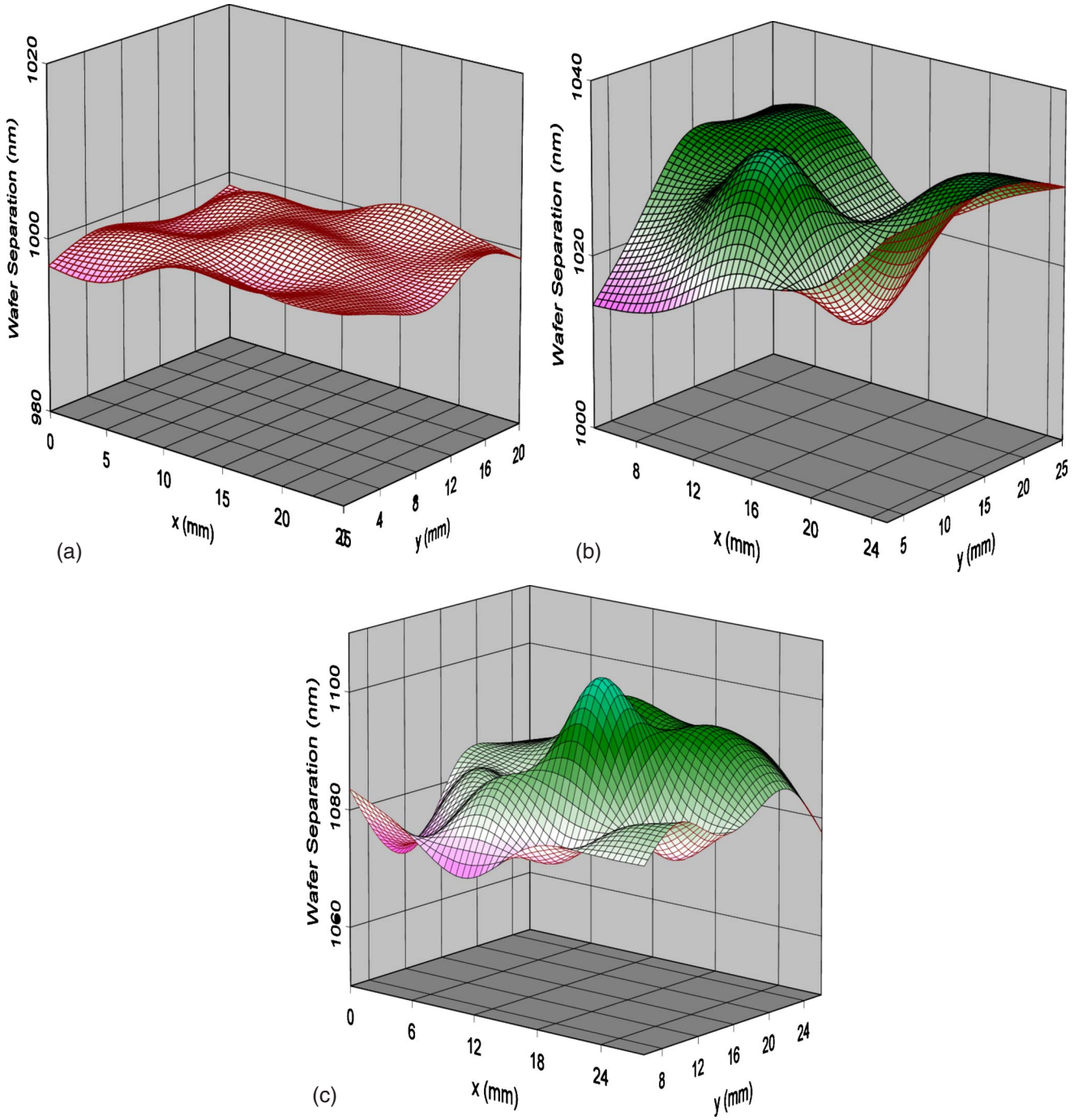

FIG. 7. (Color online) Measurement of the separation between two bonded wafers used for helium confinement as a function of position along the wafer surface. (a), (b), and (c) Cells designed for 2D, 1D, and 0D crossover, respectively. The wafers are separated with less than ~1% deviation from the average value.

vious difficulty. Other more subtle issues are associated with the finite lateral extent of films on grains or crystallites. Such films are not strictly $L \times \infty \times \infty$, as one would wish for size scaling of a planar film. Another effect, which has not been identified conclusively but is bound to be manifest at some level, is that films on powders or on surfaces of pores are first of all finite in at least one other dimension—i.e., along the perimeter of the powders or the pores—but also have presumably periodic boundary conditions as the film wraps around itself. Different boundary conditions are expected to affect the thermodynamic response (Fisher, 1971; Privman, 1990, and references therein).

Heat-capacity data for films on various substrates are reviewed in Paper I. For a variety of reasons, some of these data are not even in qualitative agreement with expectations of finite-size effects such as rounded specific-heat maxima. However, a subset of these data can be analyzed for the shift T_m in the specific-heat maximum. These results are shown in Fig. 8. Some of

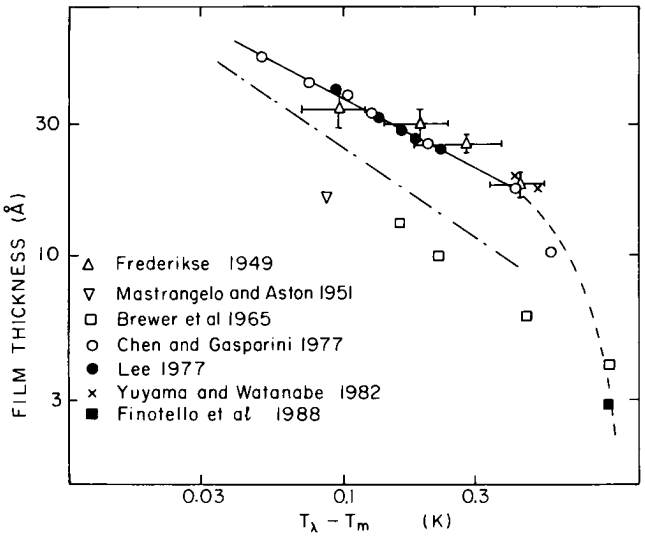

FIG. 8. The temperature shift of the specific-heat maximum of ^{4}He from T_λ for thin films. The shift is predicted to fall on a locus having a slope of $-\nu$. The dash dotted line is drawn with this slope. A fit to the open circles, the solid line, demonstrates a slope less than this. The dashed line is drawn as a guide to the eye and shows the behavior of the thinnest films. From Gasparini and Rhee, 1992.

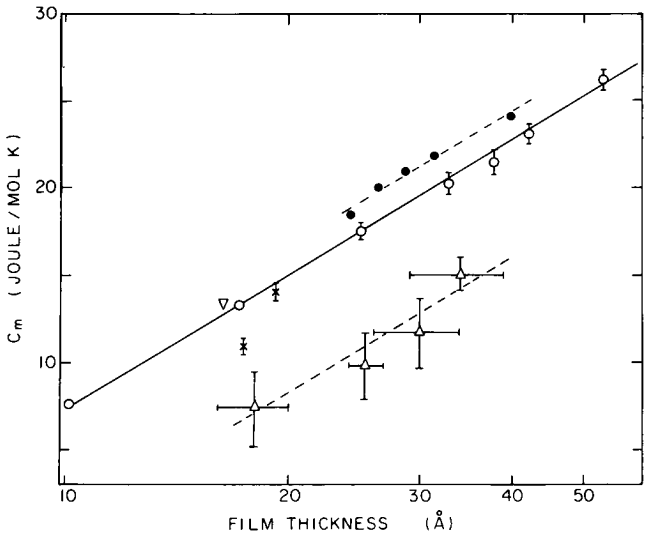

FIG. 9. Semilogarithmic plot of the specific-heat maximum vs film thickness. The symbols are the same as those in Fig. 8. The data determine a value of ν less than expected. The data which collapsed upon a single locus in Fig. 8 do not do so here. This demonstrates that one feature may scale while another may not for the same data. From Gasparini and Rhee, 1992.

these data fall on a straight line on this plot, indicating a power-law behavior over a very limited region between ~1.7 and 5.3 nm (Chen and Gasparini, 1977). The shift exponent over this limited region is $\sim 0.53 \pm 0.04$ when only the open circles are fitted, as shown by the solid line in Fig. 8. This is clearly less than $\nu = 0.671$, which would yield the slope indicated by the dash-dotted line. Data for other films are shown which do not fit along the locus of the solid line. These all suffer from capillary condensation, which biases the transition to a temperature closer to T_λ. This causes the shift in T_m to be smaller than expected.

If one plots the magnitude of the specific-heat maximum C_m vs the film thickness L, one obtains Fig. 9. Here even the data that had collapsed on a single curve for the shift in Fig. 8 fall on different loci. Note that this plot is log-linear; thus a straight line would indicate a logarithmic dependence on thickness. Strictly speaking, Eq. (12) indicates a power law. However, with α close to zero one might expect $C_m \sim (A/\nu) \ln L$ (Onsager, 1944). Using this relation, it was found that $\nu \sim 0.47 \pm 0.02$, again lower than 0.671 (Gasparini *et al.*, 1981). The other data seem consistent with this, only offset in the values of C_m. Setting aside the lower exponents obtained from T_m and C_m, we see that these "local fits" are not reliable because of the limited range in thickness, and because, in some cases, the films are not uniform in thickness.

There are other points to be made from Figs. 8 and 9. First, it should be clear that scaling, or data collapse, for one property does not imply the same for another. Thus data might well collapse on a T_m but not on a C_m plot. These two quantities are affected differently by various possible systematic errors in an experiment. Ideally, one would expect scaling of the thermodynamic response over the full range of the critical region. This would include, of course, T_m and C_m. Another point about the data in Fig. 9 is that the solid and open circles are for films formed on Nuclepore filters with 100- and 200-nm diameter pores, respectively. These films were demonstrably not affected by capillary condensation within the pores. Studies of the film formation in these pores agree with the maximum allowed film thickness limit on a cylindrical surface predicted theoretically (Cole and Saam, 1974; Saam and Cole, 1975). However, given the roughness of the pore surface, inhomogeneity in thickness is bound to be present even below the limit of capillary condensation. It is still interesting to note that the films on the smaller pores (100 nm, shown as solid circles in Fig. 9) have a slightly higher specific heat at the same thickness than do films on the 200-nm pores (open circles in Fig. 9). This might be a reflection of the fact that for smaller pores one has more of a realization of periodic boundary condition for the film along the perimeter than in larger pores, the latter a closer representation of a planar film. Periodic boundary conditions would tend to enhance the specific heat (Huhn and Dohm, 1988). This would be an interesting effect to identify conclusively in future experiments. One also notes that the specific heat of these films, and of helium films in general, must cross over ultimately to two dimensions. Hence one should expect some signature in the specific heat associated with the Berezinskii-Kosterlitz-Thouless transition (Berezinskii, 1971; Kosterlitz and Thouless, 1972, 1973). Enhancement due to the unbinding of vortex pairs has qualitatively a similar contribution to the specific heat as do finite-size effects. This contribution remains to be identified unambiguously in helium films (Yu *et al.*, 1989; Steele *et al.*, 1993).

There are much more data for the critical temperature T_c of the superfluid onset in films than for the specific heat. This temperature can be determined from the superfluid side via the vanishing of the superfluid density per unit area σ_s, and from the normal side via measurements of the heat conduction $\kappa_{\rm film}$. Both of these reflect the process of vortex pair unbinding near T_c. The heat conduction for a film in equilibrium with its vapor is a convective process involving the flow of the film and the reflux of the vapor (Ambegaokar *et al.*, 1980; Teitel, 1982). To locate T_c one can fit the expected thermal response with T_c as a free parameter. The behavior of the conductance is given by

$$\kappa_{\rm film} = f(T)\exp\left[\frac{4\pi}{b}\left(\frac{T}{T_c}-1\right)^{-1/2}\right], \tag{48}$$

where $f(T)$ is a function which involves the latent heat of evaporation, the geometry of the experimental cell, the vortex diffusion constant, and the vortex core diameter. The constant b is nonuniversal and depends on the thickness of the film. The superfluid density has a cusp near T_c given by (Nelson and Kosterlitz, 1977)

$$\sigma_s \simeq \sigma_s(T_c)(T/T_c)\left[1+\frac{b}{4}\left(1-\frac{T}{T_c}\right)^{1/2}\right], \tag{49}$$

where $\sigma_s(T_c)/T_c = 2m^2k_B/\pi\hbar^2$ is the universal jump of the superfluid density at T_c. Thus T_c for a film is a well-defined marker which, at least for sufficiently thick films, should obey a shift equation similar to T_m. However, T_c is the marker of the 2D transition and one might argue that it is the "onset" temperature $T_{\rm onset}$ of 2D behavior rather than T_c itself which should scale with the 3D correlation length. Fortunately, the difference between $T_{\rm onset}$ and T_c is not significant relative to $T_\lambda - T_c$, and this distinction is not made in many experiments. The onset temperature is not as well defined as T_c, and depends on how sensitively one can determine the deviation from a background behavior. Results from ~20 different experiments (Long and Meyer, 1955; Brewer and Mendelssohn, 1961; Henkel *et al.*, 1969; Kagiwada *et al.*, 1969; Henkel, 1971; Chester and Yang, 1973; Sabisky and Anderson, 1973; Scholtz *et al.*, 1974; Wang *et al.*, 1974; Adams, 1978; Bishop and Reppy, 1978, 1980; Roth *et al.*, 1980; Maps and Hallock, 1981; Hess and Muirhead, 1982; Maynard and Chan, 1982; Kotsubo and Williams, 1984; Finotello and Gasparini, 1985; Adams and Glaberson, 1987; Wang and Gasparini, 1988; Agnolet *et al.*, 1989; Yu *et al.*, 1989) which yield T_c or $T_{\rm onset}$ have been summarized in Paper I. A plot of the onset data is shown in Fig. 10. The symbols are defined in Paper I. There is substantial scatter in these data, not all of which can be attributed to experimental issues. There is an indication from these that a power-law behavior is obtained for films exceeding 2–3 nm. However, there is no shift exponent that can be obtained from these collective data.

Among the early experiments, several reported measurements over a range of film thickness useful to extract the shift exponent. Sabisky and Anderson (1973) find a shift exponent of 2/3. They determined the onset

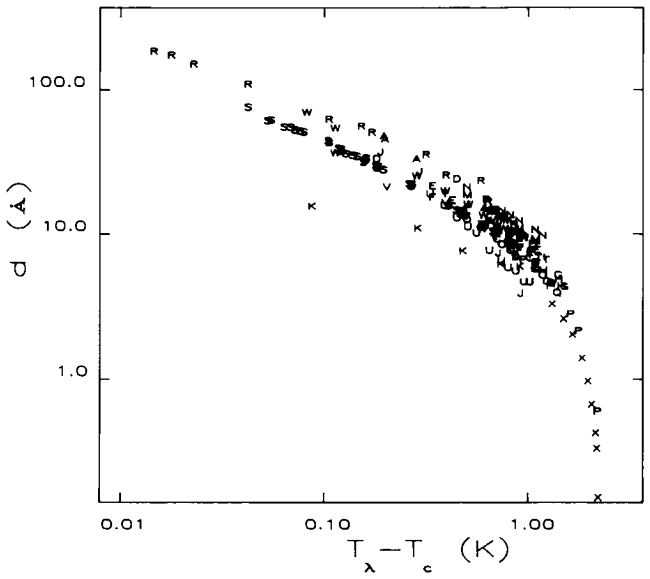

FIG. 10. The shift in the superfluid onset or critical temperature T_c for ^{4}He on various substrates. The symbols refer to data found in Table 1 of Gasparini and Rhee (1992). From Gasparini and Rhee, 1992.

temperature for films on CaF_2 in the range of 2–7.5 nm. Maps and Hallock (1981) find a shift exponent of 0.71 ± 0.05 for the onset thickness for films on Mylar. They find a power-law behavior over the full range of films studied ~1–6.1 nm. Yu *et al.* (1989) studied the convective conductance for both saturated and unsaturated films on Mylar and Kapton. They find power-law behavior for the critical temperature in the range of 2–15.6 nm. These data yield a shift exponent of 0.52 ± 0.01. A comparison of these data can be found in Yu *et al.* (1989). van de Laar (1994) and van de Laar *et al.* (1995) measured the onset thickness of films on glass. This yielded a shift exponent which is consistent with the behavior of the 3D correlation length. The range of these data is ~0.8–4.7 nm. It is found in this work that if ~0.43 atomic layer (~0.15 nm) are subtracted, the full range of shift data is then proportional to the 3D correlation length. There are several unsettling aspects of some of these results from the point of view of finite-size scaling. One would not expect power-law behavior to be applicable to the thinnest films that have been studied, as has been found in some experiments. Such films would be outside the critical region where Eq. (9), based on the 3D correlation length, would apply. Also, all these data should collapse on the same locus. The fact that they do not indicates residual substrate effects which are beyond finite-size scaling. It seems clear now that further work with yet thicker films, over a wider range of thickness, and with smoother substrates, is necessary in order to be in the critical region and avoid spurious effects.

V. FILMS: 3D-TO-2D CROSSOVER

In this section we consider more recent data for helium films. These data are typically with much thicker

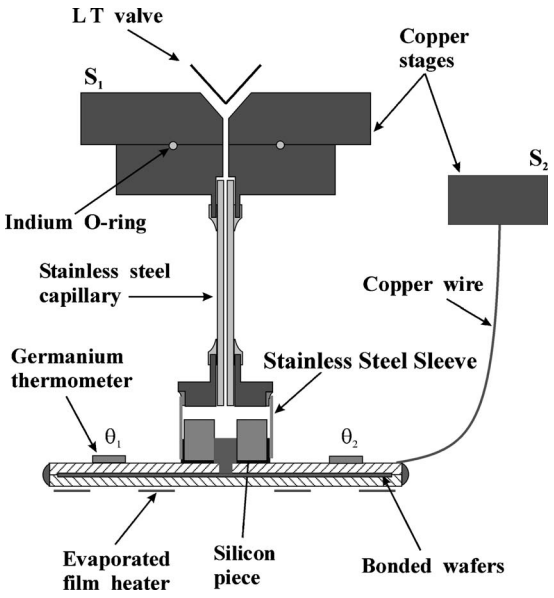

FIG. 11. Experimental setup for the ac measurement of small uniform samples of confined helium between two silicon wafers. Adapted from Mehta *et al.*, 1999.

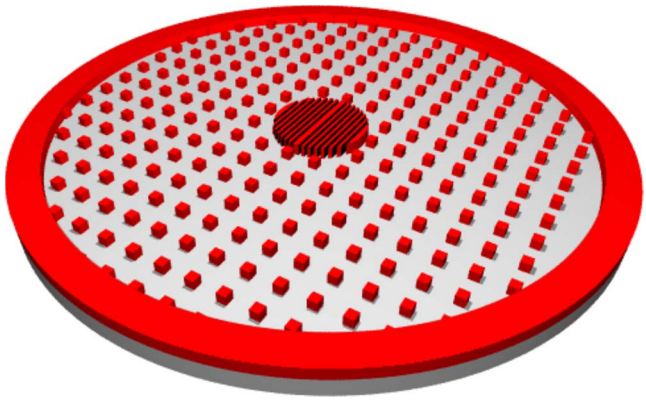

FIG. 12. (Color online) Oxide pattern used to confine helium to a planar geometry. This is achieved when a second silicon wafer is bonded to the structure. The outer border and posts provide a uniform separation between the two silicon wafers. The structure in the center minimizes the amount of liquid in this region and shifts the local superfluid onset well below the specific maximum.

films in better controlled geometries compared to earlier work. Comparisons, where possible, will be made with the results described in Sec. IV.

A. Specific heat

It should be clear that, to verify predictions of finite-size scaling, confinement to more uniform and larger sizes than that achieved with unsaturated and saturated films is desirable. The use of directly bonded silicon wafers satisfies these requirements. The measurement of heat capacity with such cells requires an ac technique (Sullivan and Seidel, 1968; Mehta and Gasparini, 1998). Basically, adiabatic calorimetry is not possible because one is dealing with small amounts of helium, ~2–50 μmol, which makes thermal isolation next to impossible. The arrangement for the ac measurement is shown in Fig. 11 (Mehta and Gasparini, 1997). The technique involves oscillating the temperature of the silicon cell—typically by a few microkelvins—and looking for the temperature response on one of the thermometers, θ_1, attached to the top of the cell. The cell is regulated using the other thermometer, θ_2, at an average temperature such that it is colder than stage S_1 and warmer than stage S_2 (see Fig. 11). This prevents distillation of the helium into the filling line anchored to S_1. The reservoir of helium in the filling line, ~1 mm^3 on top of the bonded wafers, plays an important role. It yields a marker for the bulk superfluid transition and provides a thermal ballast which helps in the stabilization of the cell's temperature. This bulk liquid, which can be several orders of magnitude larger than the amount of helium in the cell, does not respond to the ac oscillations (Mehta *et al.*, 1999). Thus effectively, by operating at a finite frequency, one is sensitive only to the helium confined in the cell.

There is one drawback with these cells which was realized after the first series of measurements and corrected in later designs. When the confined helium is normal, the portion of liquid between the two wafers, below what is labeled silicon piece in Fig. 11, does not contribute to the heat capacity. It is strongly coupled to the thermal mass of the bulk liquid in the filling line. Below the superfluid transition of the confined helium, which takes place at a temperature colder than T_λ and colder than the specific-heat maximum T_m, the liquid in this center region begins to contribute. Further, when the helium in the cell is superfluid, a resonance can be set up which distorts the heat-capacity signal (Gasparini and Mehta, 1998; Gasparini *et al.*, 2001). For these reasons, only data above the superfluid onset for the original cells are used in the scaling analysis. To avoid these difficulties, cells were designed subsequently so that most of the liquid was removed from the center region by patterning a series of fill channels. This is indicated in Fig. 12. In this figure the darker area is SiO_2. The region which contains the helium to be studied is punctuated by "pillars" that, upon bonding the top wafer, will constrain the two wafers at a separation dictated by the thickness of the oxide. The center region is a mesa of oxide with lithographically patterned channels. The size of the channels is designed such that the amount of helium in these channels is small, and also that it remains normal in the region of interest for the heat capacity. This design ensures that the same amount of helium contributes to the measured signal whether the helium in the cell is normal or superfluid. Contrary to the opinion expressed by Barmatz *et al.* (2007), the behavior of these cells is well understood. The heat capacity is obtained without any nonlinear dynamics and there are no issues associated with the helium in the filling line, as demonstrated in control measurements by Mehta *et al.* (1999).

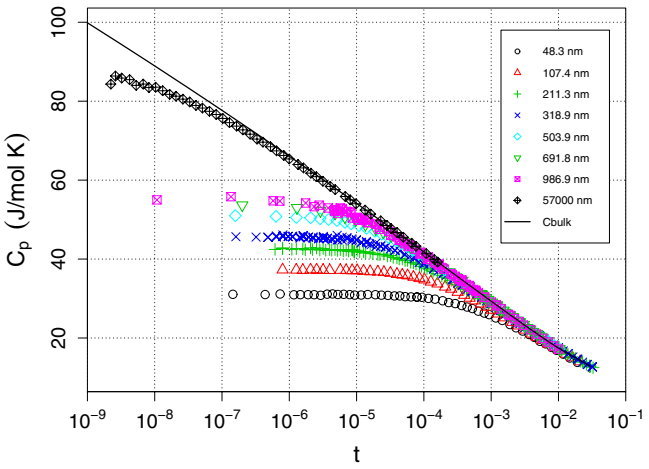

FIG. 13. (Color online) Data of specific heat for eight different planar confinements for temperatures above the bulk transition temperature T_λ.

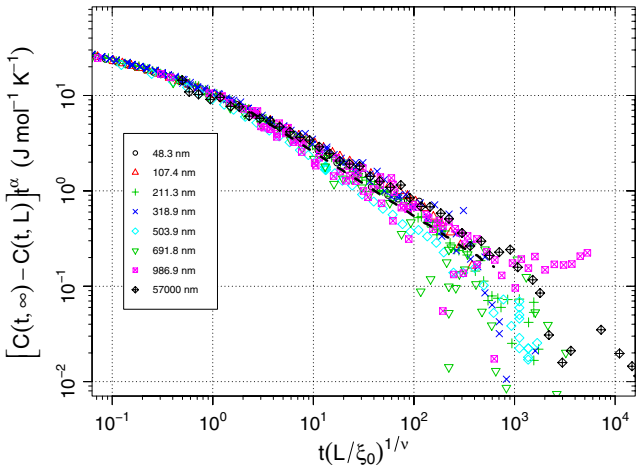

FIG. 15. (Color online) The data of Fig. 14 plotted on a log-log scale to emphasise the surface specific heat region. The dashed line is the calculation of the surface region by Mohr and Dohm (2000). This agrees with the data remarkably well.

Data taken with the above cells are shown in Fig. 13 (Mehta and Gasparini, 1997; Mehta *et al.*, 1999; Kimball and Gasparini, 2000; Diaz-Avila *et al.*, 2004). Shown here also are data for helium confined between silicon wafers spaced at 57 μm (Lipa *et al.*, 2000). These data are plotted on a semilogarithmic plot as a function of the reduced temperature measured relative to the bulk T_λ. The data have a common qualitative behavior: far from the transition they asymptote to the bulk specific heat, which is given by the solid line; and as T_λ is approached, the specific heat rolls off toward a constant. There are several ways to test these data to see if they support finite-size scaling. The simplest test is to plot the data after Eq. (5) according to which the quantity $[C(t,\infty)-C(t,l)]t^\alpha \equiv \Delta C t^\alpha$ should be a universal function of $tl^{1/\nu}$. For this plot one may choose $\nu=0.6705$ (Goldner and Ahlers, 1992) and the corresponding value of $\alpha=2-3\nu=-0.0115$. This plot is shown in Fig. 14, using $\xi_0=1.43$ Å. All the data, which in Fig. 13 define separate loci, clearly collapse on a universal locus, as expected from correlation-length scaling. This result for the specific heat of helium is unique, and there are no comparable experimental results for any other critical system. Note that the range of sizes tested in Fig. 14 spans a factor greater than 1000 in L. This result must be viewed as strong experimental evidence for finite-size correlation-length scaling for $T>T_\lambda$. Also plotted in Fig. 14, as a dashed line, is the theoretical prediction for the scaling locus by Schmolke *et al.* (1990, see also Dohm, 1993). One can see that the theory is close to the experimental locus, but it underestimates somewhat the effect of confinement. The calculation of Schmolke *et al.* (1990) involves a simulation of a film using Dirichlet boundary conditions in one direction of a cube and period boundary conditions in the other directions. This, although used in other calculations and simulations (see below), is not expected to give perfect agreement with experiments where the lateral dimensions are effectively infinite (relative to ξ) and not periodic. Another attempt to calculate the scaling locus was performed by Bhattacharjee and Ferrell (2003). They used an epsilon expansion technique with α fixed to 0. Good agreement is found for the critical region above T_λ. Their calculation also continues into the $T<T_\lambda$ region, up to the specific-heat maximum, where it overestimates the effects of confinement.

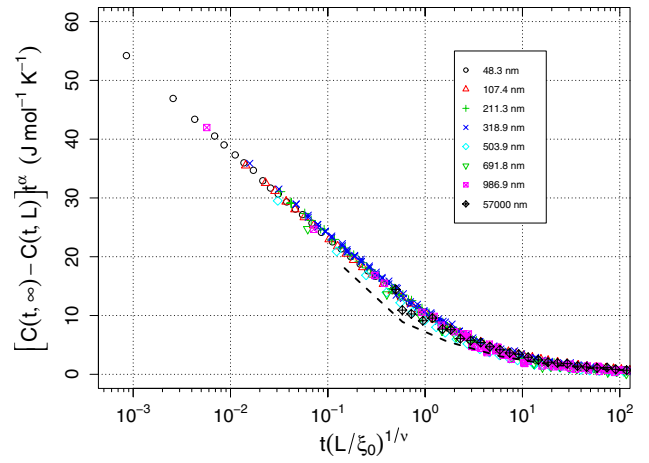

FIG. 14. (Color online) The data from Fig. 13 plotted in scaling form according to Eq. (5). The data show remarkable collapse onto a single locus. Also shown, as a dashed line, is the calculation of Schmolke *et al.* (1990).

There is a region in the scaling locus for which one expects a pure power law in the scaling function. This region reflects the behavior of the surface specific heat, Eq. (17). This behavior was first identified by Mehta and Gasparini (1997) for a subset of the data of Fig. 14 (see also Kimball and Gasparini, 2000, and Lipa *et al.*, 2000). This region is shown in Fig. 15 between 10^0 and 10^3 in the scaling variable. Also plotted on this figure, as a dashed line, is the theoretical prediction by Mohr and Dohm (2000) for the surface specific heat. The agreement between the data and theory is excellent. We note that the theoretical prediction is based solely on proper-

TABLE I. Values of the correlation-length critical exponent from various determinations.

Value of ν	How obtained	Reference
0.6704±0.0003	Variational perturbation (theory)	Kleinert (2000)
0.67155±0.00027	Improved high-temperature expansion (theory)	Campostrini *et al.* (2001)
0.6709±0.0001	Bulk specific heat and hyperscaling (experiment)	Lipa *et al.* (2003)
0.6705±0.0006	Superfluid density (experiment)	Goldner and Ahlers (1992)
0.669±0.004	Shift of C_{max} vs L for planar films (experiment)	This paper, Sec. V.A
0.6707±0.0002	Finite-size scaling of planar films, $T>T_\lambda$ (experiment)	This paper, Sec. V.A

ties of bulk helium and has no adjustable parameters. An analysis of a subset of these data has been given by Kimball and Gasparini (2000). There the data are averaged and a least-squares fit is done to extract the surface specific-heat exponent. It is found that if both α_s^+ and the amplitude of the surface specific heat A_s^+ are allowed to vary, one obtains $\alpha_s^+=0.65\pm0.01$ and $A_s^+=-5.7\pm0.2$ J mol^{-1} K^{-1}. This compares with $\alpha_s=\alpha+\nu=0.659$, and the theoretical value of $A_s^+=-5.7$ J mol^{-1} K^{-1} (Mohr and Dohm, 2000). Also, from the analysis of the 57 μm data by themselves, one obtains $\alpha_s^+=0.65\pm0.02$, which is consistent with the expected exponent (Lipa *et al.*, 2000).

One way of analyzing all the data of Fig. 13 is not to assume a particular value for the critical exponents but to allow the data to determine the exponents for optimum data collapse. This is difficult to do since there is no theoretical function which can be applied to all the data. However, Mehta *et al.* (1999) suggested the following empirical function:

$$\Delta Ct^\alpha = g_1(y) = \frac{A/\alpha}{1+ay^\nu} + \frac{by^\alpha}{1+cy^{\alpha+\nu}}. \tag{50}$$

This equation reflects the fact that, for large values of the scaling variable, one must obtain a pure power law of the surface specific heat; and, for small values of the scaling variable, one must have a behavior dominated by $C\sim t^{-\alpha}$. With the hyperscaling constraint $\alpha=2-3\nu$, one can vary the parameters a, b, c, and ν to obtain a least-squares fit to the function $t^{-(2-3\nu)}g_1(y)$. The value of A/α is fixed to the value found by Mehta *et al.* (1999). One finds that $\nu=0.6707\pm0.0002$ provides the best collapse. This agrees well with other values for ν listed in Table I. A log-log plot of the data in scaling form is shown in Fig. 16(a), and the solid line is the fit to the data using Eq. (50).

A plot of the deviation of the data from the fitted function is shown in Fig. 16(b). This is by far the most sensitive way to examine these data for scaling. It is interesting to note that data for almost all the individual values of L show systematic deviations which are greater than the precision of the data themselves. However, there are no systematic trends with size. This suggests that there are some residual systematic errors in all these data, but collectively, over eight different confinements, these systematic deviations tend to compensate. This also points to the danger of any conclusions about

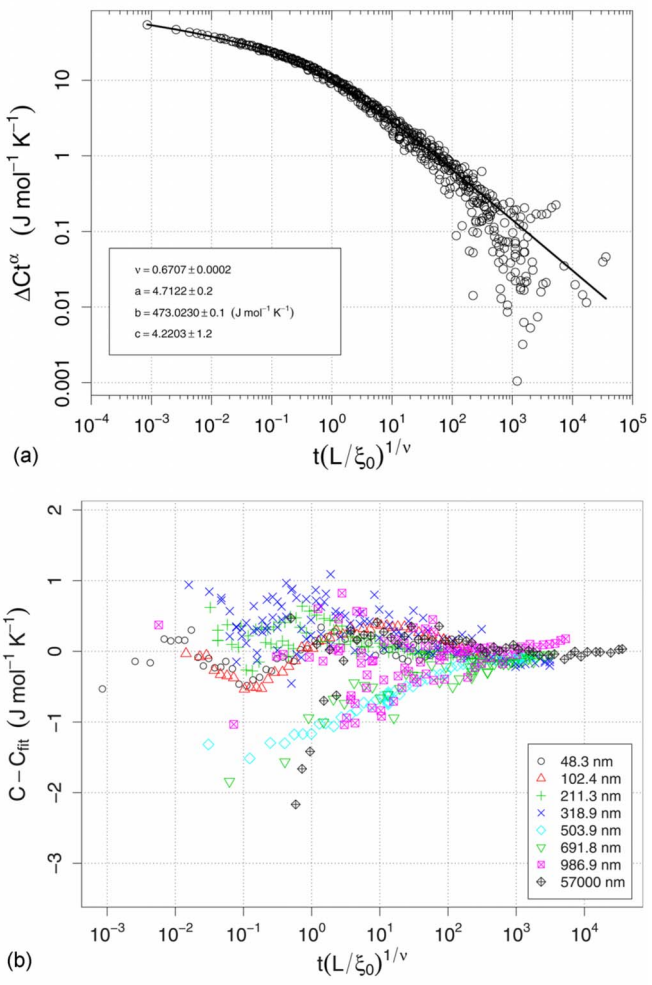

FIG. 16. (Color online) Data from helium confined in a planar geometry plotted according to Eq. (50). Here a least-squares fit to Eq. (50) is shown as the solid line. This is done by varying ν. (b) The deviation between the data and the best fit line shown in (a).

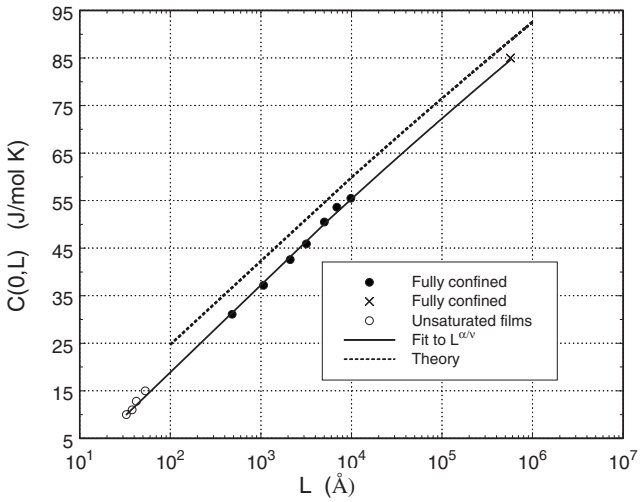

FIG. 17. The value of the specific heat at T_λ for helium confined to a planar geometry. Using Eq. (10) one can determine the critical exponents and the maximum value of the specific heat for bulk helium. The theoretical calculation of Sutter and Dohm (1994) is shown as the dashed line. This underestimates the effect of confinement but this is likely within the approximation used in the theory.

size scaling based on only a few measurements, as done by Ahlers (1999) and reproduced by Barmatz *et al.* (2007); see their Fig. 28.

The single-point scaling of the specific heat at $t=0$, $C(0,l)$, Eq. (10), can be tested with the data for $T>T_\lambda$ using the value at which the specific heat plateaus in Fig. 13. This is shown in Fig. 17. We have included in this plot data from Chen and Gasparini (1978) for films formed on 200 nm Nuclepore filters. In principle $C(0,l)$ can be fitted to Eq. (10) by varying the exponent α/ν, the prefactor $g_2(0)$, and the constant B. The latter is the maximum value of the bulk specific heat. Analyzed in this way, these data do not yield a precise value for the exponent. Another approach is to fix the exponent using the value of α from Lipa *et al.* (2003) and fit the data by varying only $g_2(0)$ and B. This is the solid line shown in Fig. 17 using the values of $\alpha=-0.012\,64$ and $\nu=0.6709$. The resulting values for the fitted parameters are $g_2(0)=-474.0\pm4.9$ J mol^{-1} K^{-1} and $B=453.8\pm4.3$ J mol^{-1} K^{-1}. The value of B obtained this way, from finite-size effects, agrees well with $B=460.2\pm7.3$ J mol^{-1} K^{-1} obtained by fitting the *bulk* specific heat (Lipa *et al.*, 2003). We note that the value of B is highly correlated with variations in α both in the analysis of the bulk data and in the case of Eq. (10). Thus a 10% increase in the magnitude of this exponent will result in a ~10% decrease in the value of B. The agreement for the asymptotic value of $C(t,\infty)$, coming from independent analyses of the bulk data and from $C(0,l)$, is evidence for the overall consistency of all these data. The dashed line shown in Fig. 17 is the theoretical calculation of Sutter and Dohm (1994) for $C(0,l)$. The line is close to, but lies above, the experimental values. This indicates, as in the case of the overall scaling function, that the theory underestimates the

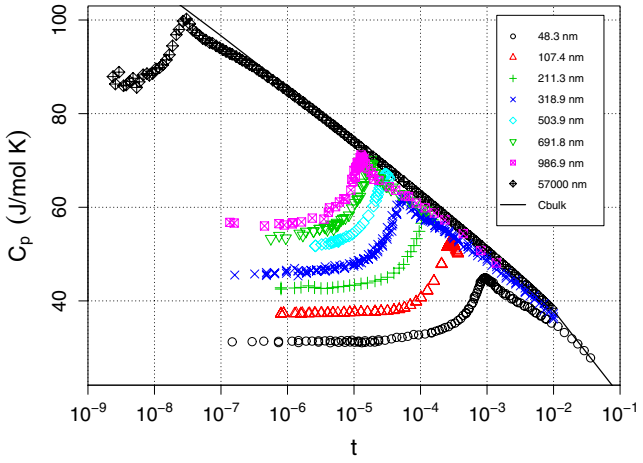

FIG. 18. (Color online) Specific-heat data below T_λ for helium confined to the same planar confinements, as shown in Fig. 13.

effect of confinement, but this is likely within the approximation used in the theory. Field theoretic results have also been obtained by Krech and Dietrich (1992). These yield an amplitude for $g_2(0)$ which is too small.

Data for $T<T_\lambda$ are shown in Fig. 18. The most striking feature of the branch below T_λ is the progressive shift of the heat-capacity maximum to lower temperatures (larger values of t in the plot). We note that for these data the confined helium remains normal until a temperature below the heat-capacity maximum. For some cells, using the setup shown in Fig. 11, one can establish the superfluid onset directly using adiabatic fountain resonance (Gasparini and Mehta, 1998; Gasparini *et al.*, 2001). This onset is always on the low-temperature side of the heat-capacity maximum. The scaling of these data according to Eq. (5) is shown in Fig. 19 for the region immediately below T_λ, but not quite up to the heat-capacity maximum. One can see that the collapse of the data in this region is as good as above T_λ with no systematic deviations associated with the different confinements. We note that the data for the bonded

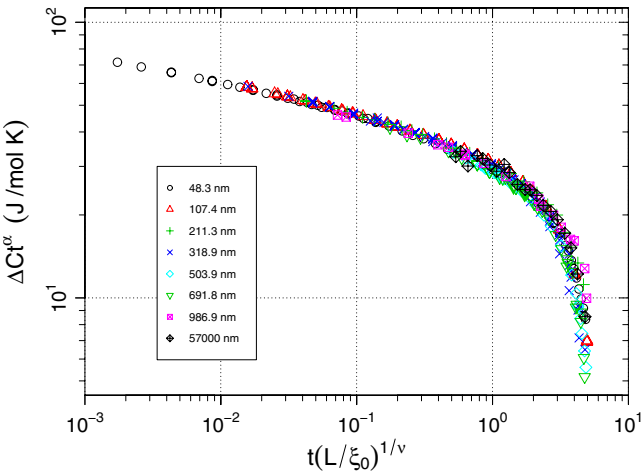

FIG. 19. (Color online) Scaling of the specific heat below T_λ according to Eq. (5) but above the maximum. Here the data scale as well as they do above T_λ; see Fig. 15.

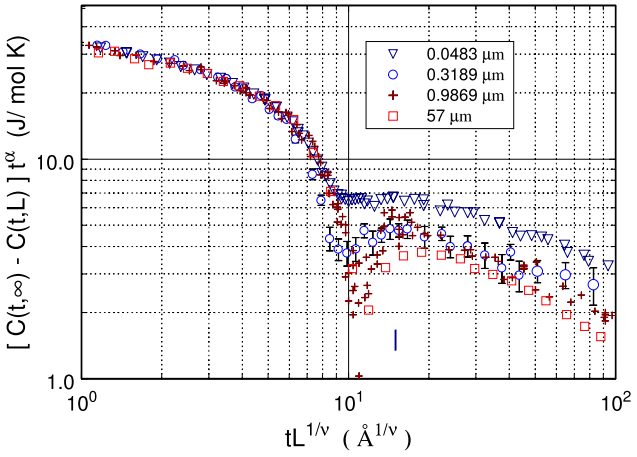

FIG. 20. (Color online) Same scaling plot as for Fig. 19 for the region near the maximum value of their specific heat (shown here as a minimum in the scaling function). The vertical line at 15 in the scaling variable is the position of the superfluid transition of the confined helium. The data do not collapse in this region as they do in Figs. 14 and 19.

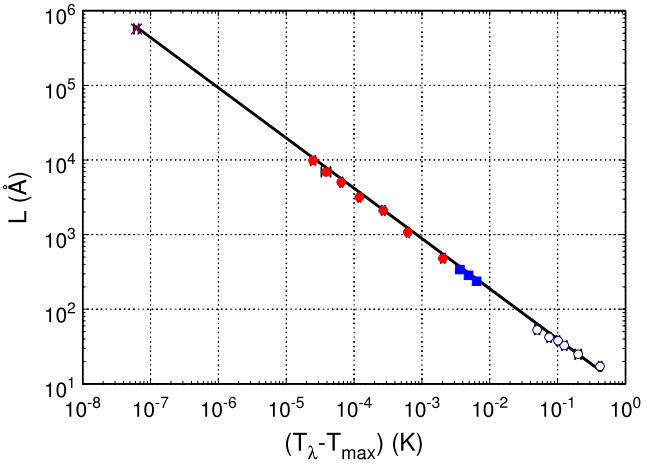

FIG. 21. (Color online) Data for ^{4}He confined to a planar geometry obeys the equation predicting the shift of the heat-capacity maximum from T_λ [see Eq. (9)]. This yields the expected correlation-length exponent ν.

silicon cells, seven of the eight data sets in Fig. 19, show no effects due to the presence of superfluid in the filling line. There is no correction, subtraction of signal, or averaging that has been applied to these data to achieve the collapse indicated in this figure.

The region near the heat-capacity maximum and below it is shown separately in Fig. 20 for a subset of the data (see also Fig. 11 in Kimball *et al.*, 2000). Here one sees that the data do not collapse but vary systematically from the smallest confinement to the largest. This indicates a failure of correlation-length scaling for 2D crossover. The location of the superfluid onset is indicated on this plot as a vertical line at a value of 15 $Å^{1/\nu}$. It is clear that the lack of scaling does not start at the point when the confined helium becomes superfluid, but is associated with the region of the specific-heat maximum where the fluctuations in the order parameter are the largest, and the crossover to two dimensions takes place. Note that this lack of scaling persists well below the specific-heat maximum. It is interesting to note that the position of the maximum (minimum in Fig. 20) takes place within the experimental uncertainty at the same value of the scaling variable. This is as expected from Eq. (9), and is shown more explicitly in Fig. 21, where L is plotted as a function of the shift in T_m. As for Fig. 17, the data from Chen and Gasparini (1978) for unsaturated films are also included in this plot. A least-squares fit of all these data yields $\nu=0.669\pm0.004$. This agrees well with the determination of ν from the overall scaling of the data above T_λ, and other values of ν (see Table I). Thus it would appear that the thin-film data, while by themselves they do not determine a correct shift exponent (see Fig. 8), are nonetheless at the right locus, as shown in Fig. 21, when compared with more recent results.

It is interesting that the shift of the specific-heat maximum scales well but the magnitude of the maximum, and the overall shape of the maximum, do not scale. This is brought out even more clearly in Fig. 22. Here we plot the data according to Eq. (11), whereby one expects that the quantity $[C(t_m,l)-C(t_0,l)]l^{-\alpha/\nu}=f_{1\,\max}(a^\nu)$ =const. One can see from this figure that there is a systematic trend in this "constant" which ranges from $\sim$1 J mol^{-1} K^{-1} for the thinnest films to $\sim$10–11 J mol^{-1} K^{-1} for the thickest. The dashed horizontal line on this plot is the value of $f_{1\,\max}(a^\nu)$ from the Monte Carlo calculation of Schultka and Manousakis (1995). It seems clear that, even if this calculation underestimates the effects of confinement and this is taken into account by lowering of the dashed line, one still

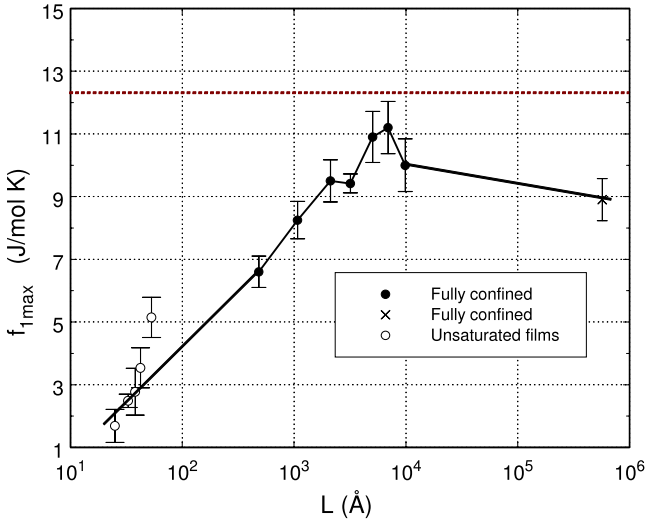

FIG. 22. (Color online) The maximum of the single-point scaling function $f_1(t,L)$ is expected to be a constant value regardless of film thickness [see Eq. (11)]. The prediction of this value from Schultka and Manousakis (1995) is shown by the dashed horizontal line. The uniform planar films measured do not support this result. This is the clearest indication of a problem with scaling at the heat-capacity maximum for planar films.

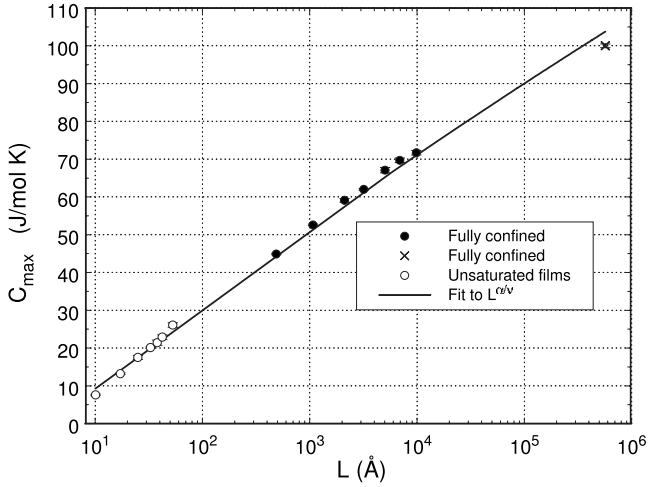

FIG. 23. The maximum value of the specific heat for planar films vs $L^{\alpha/\nu}$ and fit to Eq. (12) to yield the maximum value of the bulk specific heat. This analysis produces a value of 517.4 J mol^{-1} K^{-1} which is significantly larger than other determinations (see Table III). The deviation of the data from this fit is not as obvious as in the higher resolution plot, Fig. 22. See also Fig. 49.

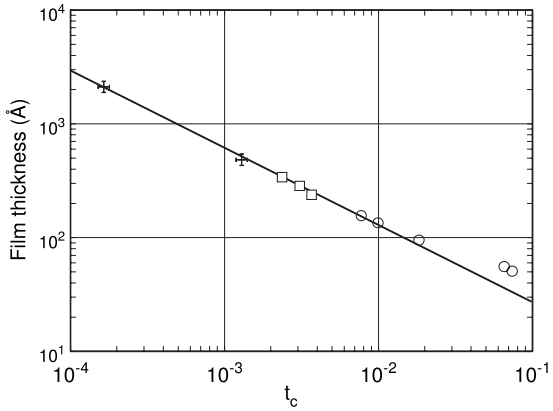

FIG. 24. Temperature shift of the onset of superfluidity for thin films of ^{4}He is consistent with a power law ν, except for the thinnest films. The crosses are from data taken with the AFR technique while the open circles are from thermal conductivity measurements. The boxes represent a feature seen in the critical thinning data of helium and fall on the same locus as the superfluid onset data.

cannot satisfy the trend displayed in these data.

A third way of showing the lack of scaling of $C_{\max}$ is to plot the latter as a function of $L^{\alpha/\nu}$ as given in Eq. (12). Such a plot, like Eq. (10) for $C(0,l)$, should yield the constant B, the maximum value of the bulk specific heat. The plot of $C_{\max}$ is shown in Fig. 23. The solid line in this figure is a fit to Eq. (12) with a fixed value of $\alpha/\nu = -0.018\,84$ (Lipa *et al.*, 2003). There are systematic deviations of the experimental data from the expected power-law dependence (see also Fig. 49). These are not as obvious as for Fig. 22, where one effectively looks at the data at a higher resolution by subtracting $C(t_0,\infty)$. The fit to $L^{\alpha/\nu}$ in Fig. 23 yields a value of $B = 517.4 \pm 6.9$ J mol^{-1} K^{-1}. This value is much higher than the expected value of 460.2 ± 7.3 J mol^{-1} K^{-1}obtained directly from bulk data. Thus one finds that $C_{\max}$ analyzed as in Figs. 20, 22, or 23 (see also Fig. 49) is not consistent with scaling. On the other hand, the shift of $C_{\max}$, i.e., $t_{\max}$ (Fig. 21), obeys Eq. (9) well and yields the correct exponent for the correlation length. These results for $C_{\max}$ are in strong contrast to the successful scaling of data at temperatures higher than $T_{\max}$ both above and below T_λ. Since it is near the specific-heat maximum that this difficulty arises, it is suggestive that the scaling fails, at least for 2D crossover, as fluctuations become largest. At temperatures below where the confined helium is superfluid, there is also strong evidence of lack of scaling from the superfluid density (Rhee *et al.*, 1989); see below.

Reliable data for the onset of superfluidity in thick planar films are not plentiful. We show a log-log plot of film thickness vs onset in Fig. 24. The crosses are adiabatic fountain resonance measurements (Gasparini and Mehta, 1998; Kimball and Gasparini, 2001). The circles are thick film T_c's from measurements of thermal conductivity (Yu *et al.*, 1989, see Sec. V.C). The boxes represent the kink in the scaling function for film thinning (Ganshin *et al.*, 2006; see also below). The solid line through the data is drawn with slope ν. The data are consistent with this except for the thinnest films from the thermal conductivity (open circles).

B. Superfluid density

The superfluid density of confined helium has been measured using a variety of techniques and a variety of confinements. Many of these measurements, which do show finite-size effects, cannot be used for scaling with size because the geometry is too complex to characterize the confinement by a single size L. However, if L or the average value $\langle L\rangle$ is large enough, even though not necessarily uniform, the initial deviation from bulk behavior can be characterized via the surface-plus-bulk analysis described in the Introduction. In particular, Eq. (27) can be cast in the following form:

$$k - \frac{\rho_s}{\rho} t^{-\zeta} \simeq \frac{g_{sv} a_0 |k_s|}{\langle L\rangle} t^{-\zeta} \sim t^{-\nu}, \tag{51}$$

where we have used $\zeta = \nu$, and $\langle L\rangle$ represents some average over the distribution of sizes in a given confinement. This approach is discussed in greater detail in Paper I, and applied there to several sets of data. Examples of this analysis are also found in Gasparini *et al.* (1984). Here data for the superfluid fraction were obtained using a confinement consisting of a roll made from a Mylar ribbon where the average spacing between layers, where the helium is confined, was estimated to be 0.46 μm. The technique for obtaining the superfluid fraction was to make the confined helium part of the inertial element of a torsional oscillator. As such, when the helium becomes superfluid it slips relative to the oscillating Mylar. The superfluid fraction can be deduced from the change

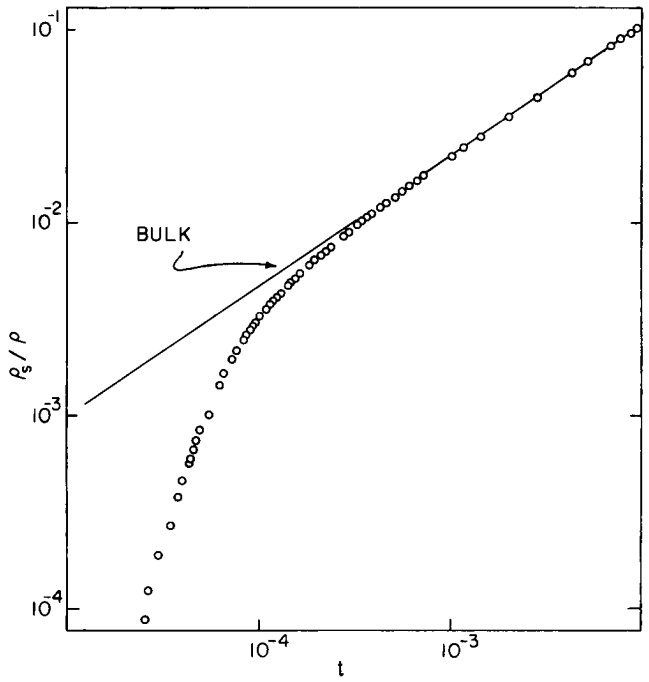

FIG. 25. Superfluid density of helium confined between Mylar surfaces spaced by alumina powder where the average separation is 0.46 μm. The data are measured using a torsional oscillator. From Gasparini and Rhee, 1992.

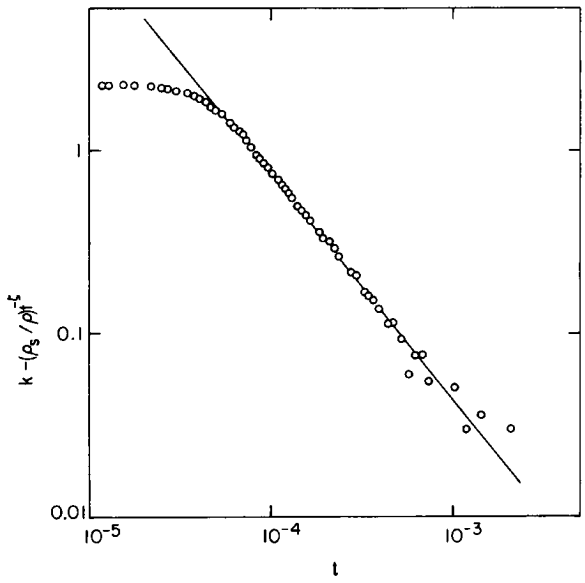

FIG. 26. Initial deviation from bulk behavior of the data shown in Fig. 25. Data in the region where Eq. (51) is valid should fall on a straight line and be described with an exponent of $\nu=0.671$. The data determine an exponent nearly double this expected value. From Gasparini and Rhee, 1992.

in the period of the oscillator. This is a technique first used by Andronikashvili (1946) and was applied to the measurements of the superfluid fraction near T_λ by Tyson and Douglass (1966). The measurements of Gasparini *et al.* (1984) follow this technique as developed by Bishop and Reppy (1978) in the study of near-monolayer films. The data from Gasparini *et al.* (1984) are shown in Fig. 25. The bulk behavior is shown as a solid line (Greywall and Ahlers, 1973). The deviation of the confined data from bulk behavior is obvious. However, it is only for small deviations from bulk behavior that Eqs. (27) and (51) apply. Closer to the transition, this system, as well as any other where there is no single unique small dimension, will yield a locus that is unique to that particular system. The analysis of these data according to Eq. (51) is shown in Fig. 26. One can see that there is a reasonable range where a power law applies, but this breaks down for t less than about 5.5×10^{-5}. Measurements of the dissipation associated with ρ_s indicate a maximum near $t=1.3\times10^{-5}$. Thus it would appear that the roll off is associated with 2D crossover. Note, however, that if the confinement had been completely uniform, the crossover to two dimensions would be indicated by the data rising above the straight line in Fig. 26. Thus there is both finite frequency (inherent in this type of measurement) and inhomogeneity rounding in these data. From the power-law region one obtains an exponent of 1.18 ± 0.06, substantially larger than the expected value of $\nu=0.671$. Similar analyses are reported in Paper I for data from Henkel *et al.* (1969), Smith (1971), and McQueeney (1988). The exponents from these experiments are tabulated in Paper I and average $\sim1.0\pm0.05$. These results are all substantially different from ν. However, none of these experiments lend themselves to scaling with size.

The first measurements of the superfluid fraction for planar confinement which could be scaled with size were reported by Rhee *et al.* (1989). Cells used for the confinement were similar in design to the cells used subsequently for the heat capacity. Two bonded silicon wafers were spaced uniformly apart using a pattern of SiO_2 posts (Rhee *et al.*, 1990). The technique for obtaining the superfluid fraction was a torsional oscillator (TO) as described above. Subsequent to these measurements, a different technique was used by Gasparini and Mehta (1998) and Kimball and Gasparini (2001), which made use of the adiabatic fountain resonance (AFR) between the confined helium and the helium in the filling line (see Fig. 11). This is a Helmholtz resonance which can be driven thermally, and involves the movement of the superfluid in and out of the cell with the compressibility of the helium providing the restoring force. A full analysis of this resonance has been given by Gasparini *et al.* (2001). Data for six different confinements using these two different techniques are shown in Fig. 27. On this plot the bulk behavior is shown as a dashed line (Greywall and Ahlers, 1973). The two cells for which AFR is used are for 0.0483 and 0.2113 μm. The horizontal lines on this plot represent the magnitude of the discontinuous jump in the value for the superfluid fraction which is expected on the basis of Kosterlitz-Thouless theory (Nelson and Kosterlitz, 1977). This is given by Eq. (22). Note that the AFR data, the crosses and circles, stop at this limit, i.e., there is no detectable resonance beyond this point. This is because of the severe dissipation due

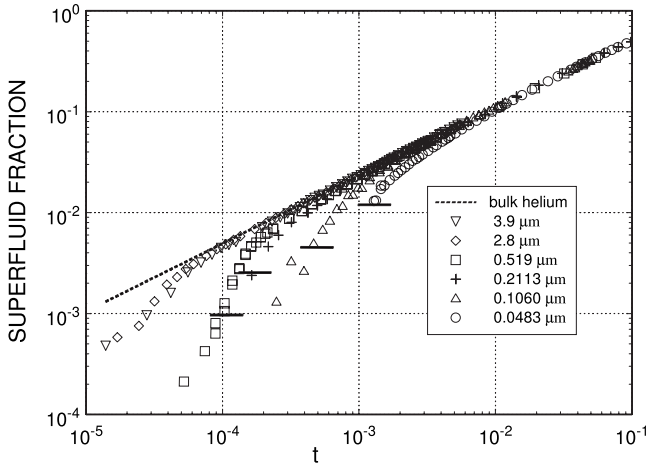

FIG. 27. Superfluid fraction of ^{4}He confined to a uniform planar geometry for six different confinements. The 0.0483- and 0.2113-μm data are obtained using the AFR technique while the others are measured using a torsional oscillator. The horizontal lines indicate the magnitude of the superfluid fraction where the discontinuous jump to zero is expected to occur (Nelson and Kosterlitz, 1977).

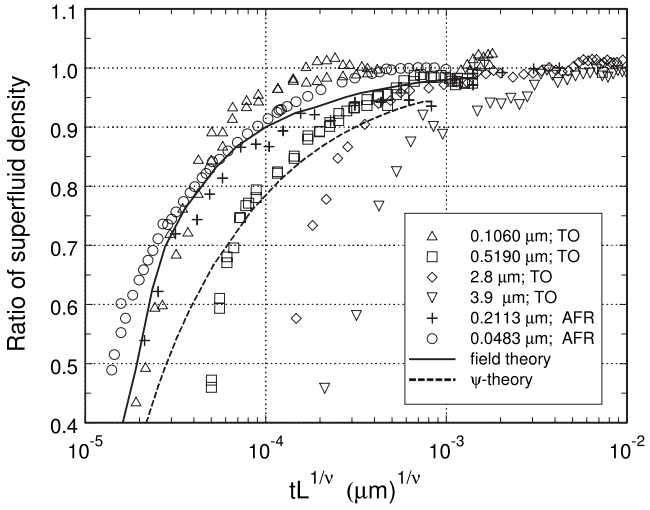

FIG. 28. The ratio of the superfluid density of ^{4}He confined to a planar geometry to the bulk superfluid density. Data over a range of sizes that span more than 80 show a distinct lack of scaling. The data are measured using either a torsional oscillator (TO) or adiabatic fountain resonance (AFR). The solid line is the field theory calculation of the scaling locus from Schmolke *et al.* (1990) and the dashed line is the ψ-theory calculation of Mooney and Gasparini (2002).

to the unbinding of vortex pairs. On the other hand, data using a torsional oscillator can be taken beyond this point. The added dissipation due to free vorticies, which can be measured, represents a relatively small effect to the overall quality factor of the oscillator. There is no sudden jump in ρ_s/ρ using this technique because of the finite-frequency rounding of the transition. This is seen most dramatically in thin films (Bishop and Reppy, 1978). A more detailed look at the region near the Kosterlitz-Thouless jump can be seen for the 0.519 μm data in Rhee *et al.* (1989). It is clear from the data that ρ_s/ρ drops more rapidly in this region, as can also be seen for the 0.519 μm data in Fig. 27 near $t \simeq 10^{-4}$. This more rapid variation is accompanied by an excess dissipation which can be attributed to the unbinding of vortex pairs (Rhee *et al.*, 1989).

The simplest scaling test of the above data is to plot ρ_s/ρ_{sb} as a function of $tL^{1/\nu}$; see Eq. (19). This is shown in Fig. 28. Far from showing a collapse on a universal locus, these data separate systematically, with the smaller confinements tending to smaller values of the scaling variable. The AFR data seem to have a slightly different dependence from the TO data; however, they show the same trend with size. The solid curve on this plot is the field-theory result from Schmolke *et al.* (1990), and the dashed line is a calculation of the scaling locus for a planar geometry from ψ theory by Mooney and Gasparini (2002). There are also results for the scaling function from numerical simulations of the 2D XY model (Schultka and Manousakis, 1997). Interestingly, these numerical simulations do not yield a collapse of the calculated data unless one adds a constant length scale to each L for which the simulation is done. We note, in contrast to this, that for a 3D XY system in a cube geometry with *periodic* boundary conditions, one obtains a good collapse of Monte Carlo data for the order-parameter distribution. This has been calculated for variation of a factor of 4 in the small dimension (Chen *et al.*, 1996).

One can calculate, in the case of ρ_s, effects of the van der Waals potential on the confining wall, which effectively will break scaling. This was done by Wang *et al.* (1990) and Mooney and Gasparini (2002) using ψ theory. The conclusion from this work was that, if one were to "correct" for the effect of the van der Waals potential according to the results from this calculation, the correction would make the disagreement with scaling even worse. This can be understood from Fig. 28. The experimental data already have the effect of the van der Waals field, thus a correction to take this into account would tend to increase $\rho_s(t,L)$. This correction would be largest for the smallest L, thus separating the data for various L's even further. Indeed, one can generalize this conclusion to any method of calculating a correction due to van der Waals effects. We note that an analysis of the TO data reported by Rhee *et al.* (1989; see their Fig. 4), shows that these data can be collapsed with an effective exponent of 1.14 as opposed to ν=0.671.

The combination of heat-capacity and superfluid density data for planar confinement indicates that on the superfluid side of the confined film and for the heat capacity in the region immediately above it the data do not scale. The reasons for this are not clear, but are not likely to be ascribed to experimental difficulties, given the different experiments involved and the different techniques used. It is not possible to resolve this result unless one considers mechanisms which differently affect the superfluid side and the region immediately above it. By contrast, the data for the normal side not

TABLE II. Various quantities for planar films. The last three columns have units of J mol^{-1} K^{-1}.

Film thickness L (μm)	Shift of C_{max} from T_λ (K)	C_{max}	$C(0,L)$	$C(t_0,\infty)$
0.0483[a]	$(2.05\pm0.13)\times10^{-3}$	44.9±0.4	31.1±0.3	38.98±0.3
0.1074[a]	$(6.22\pm0.26)\times10^{-4}$	52.6±0.6	37.2±0.4	45.40±0.4
0.2113[a]	$(2.70\pm0.15)\times10^{-4}$	59.1±0.6	42.6±0.4	50.78±0.4
0.3189[b]	$(1.2\pm0.05)\times10^{-4}$	62.0±0.2	45.6±0.4	54.03±0.4
0.5039[a]	$(6.5\pm0.5)\times10^{-5}$	67.1±0.7	50.5±0.5	57.61±0.5
0.6918[a]	$(3.9\pm0.3)\times10^{-5}$	69.7±0.7	53.6±0.5	60.06±0.5
0.9869[c]	$(2.5\pm0.2)\times10^{-5}$	71.3±0.8	55.5±0.5	62.82±0.5
57[d]	$(6.2\pm0.5)\times10^{-8}$	100.0±0.7	85.5±0.5	92.82±0.5

[a]Mehta *et al.* (1999).
[b]Diaz-Avila *et al.* (2004).
[c]Kimball *et al.* (2000).
[d]Lipa *et al.* (2000).

only scale well, but agree to a great extent with explicit theoretical predictions, and match well with the infinite limit in the sense that one obtains the correct bulk properties such as the maximum value for the bulk specific heat as $L\to\infty$ (see Table III). In addition, the specific-heat data for $T>T_\lambda$ yield the correct correlation-length exponent when the exponent is allowed to vary to achieve optimum data collapse; see Fig. 16 and Table I.

C. Thermal conductivity

The thermal conductivity for a planar geometry when heat is conducted across the planar interface is difficult to obtain for confinements comparable to those used for the specific heat and superfluid density. With such small values of L one would need large heat fluxes to measure a significant temperature difference. However, with a planar geometry and relatively large L, it is possible to measure surface effects whereby the surface thermal resistance is in series with the resistance of the remaining helium. Such measurements were carried out by Tam and Ahlers (1985), Lipa and Chui (1987), and Ahlers and Duncan (1988). These data are shown in Fig. 29 from Ahlers and Duncan (1988). What is plotted in this figure is $\hat{R}_\lambda$ defined in Eq. (46). For these experiments one has $\kappa=\kappa^\perp$ since the heat current is perpendicular to the surface. Three sets of data on this plot are at saturated vapor pressure, and the lowest set is at 22.3 bars. The solid lines show the behavior of the bulk $\hat{R}_\lambda$ (Dohm and Folk, 1981; Tam and Ahlers, 1985), while the dashed lines are the result of a fit of the data to a phenomenological model proposed by Ahlers and Duncan (1988). This model captures the initial deviations from bulk behavior but fails for smaller values of t. More importantly, this model is not in scaling form, since it predicts that $\kappa^\perp/\kappa_\infty$ is not a function of L/ξ. This was pointed out by Frank and Dohm (1989) who suggested, on the basis of renormalization-group arguments, that the surface thermal resistance should behave as

$$R_s = A_s\frac{\xi}{\kappa_\infty^\perp}\sim t^{\mu-\nu}, \tag{52}$$

where A_s is the amplitude. This behavior, as can be seen from Eq. (36) where $r_s^\perp\sim t^{\mu-\nu}$, is the same for the ther-

TABLE III. Values for the bulk specific heat at T_λ $C(0,\infty)$ determined from bulk and confined helium measurements. All values have units of J mol^{-1} K^{-1}.

Bulk data (Lipa *et al.*, 2003)	460.2±7.3
$C(0,L)$ (1D, this work, data from Fig. 34)	489±39
$C_{max}(t_m,L)$ (1D, this work, data from Fig. 34)	467±14
$C(0,L)$ (2D, this work, data from Table II)	453.8±4.3

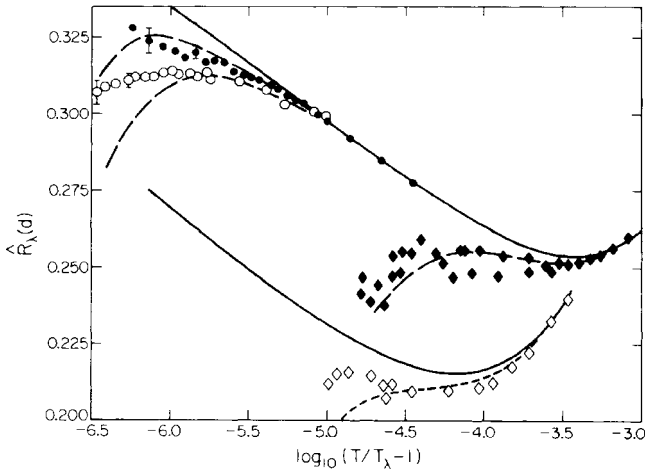

FIG. 29. The amplitude $\hat{R}_\lambda$ of the thermal conductivity above T_λ. The open and solid diamonds are the data of Tam and Ahlers (1985) with $L=0.0025$ cm for 22.3 bars and saturated vapor pressure (SVP), respectively. The open circles are the data of Lipa and Chui (1987) at SVP for $L=0.22$ cm and the solid circles are the data at SVP for $L=0.57$ cm from Ahlers and Duncan (1988). The dashed lines are from Eq. (3) of Ahlers and Duncan (1988). The solid lines are the behavior of the bulk $\hat{R}_\lambda$ based upon fits to the theory of Dohm and Folk (1981). From Ahlers and Duncan, 1988.

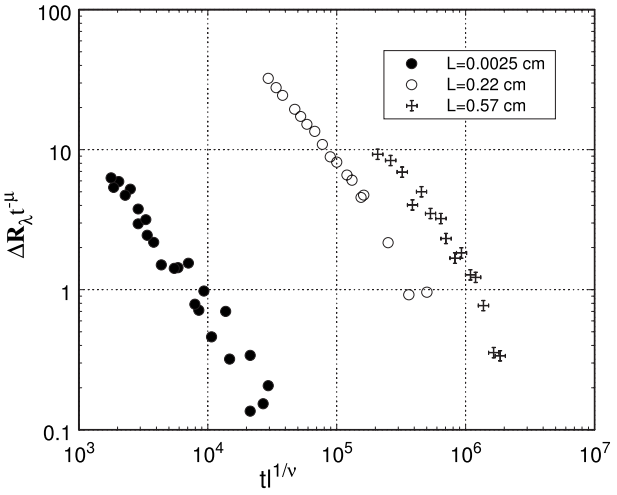

FIG. 30. Scaling of the thermal resistance of ^{4}He confined to a planar geometry above T_λ in the region where a bulk-plus-surface description applies. Data are taken from Fig. 29. These data do not collapse onto a single locus as expected. In addition, none of the data fall onto a line of slope $\nu=0.671$ as predicted by Eq. (38), but instead determine slopes greater than 1.

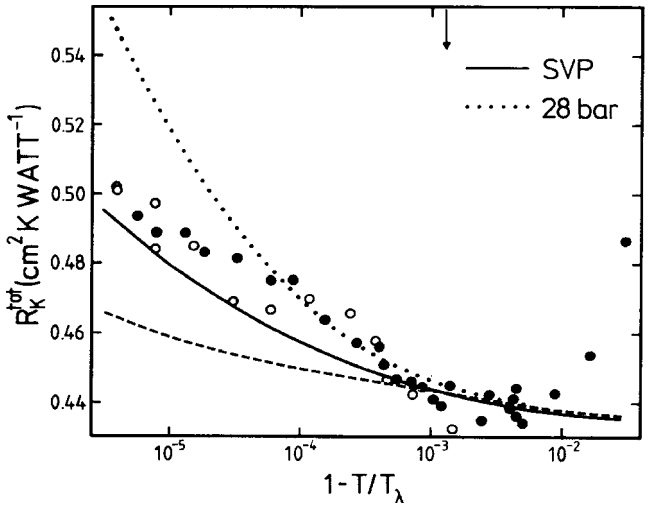

FIG. 31. The thermal boundary resistance $R_K^{\rm tot}$ between ^{4}He and a solid surface for $T<T_\lambda$. The data, open and closed circles, are from Duncan *et al.* (1987). The solid line is the renormalization-group result of Frank and Dohm (1989) and the dashed line is a hydrodynamic result based upon a theory by Landau (1941). The dotted line is the Frank and Dohm renormalization group result for 28 bars. From Frank and Dohm, 1989.

mal resistivity, as expected on the basis of the bulk-plus-surface analysis. Using the above equation, Frank and Dohm (1990) attempted to scale the data in Fig. 29 by plotting them in such a way that they should yield the constant A_s. This did not work because the data did not collapse onto a constant value but rather defined their own loci and, in addition, varied with t (see Fig. 3 in Frank and Dohm, 1990). Another way of analyzing these data is to note that the scaling of $\kappa^\perp$ in the surface region, and with confinements as large as those in Fig. 29, is the same as scaling $\hat{R}_\lambda$, since ξ and C_p in Eq. (46) will effectively have their bulk values. This can be done using Eq. (38) and recasting it in the following form:

$$[\hat{R}_\lambda(t,l)-\hat{R}_\lambda(t,\infty)]t^{-\mu}\equiv\Delta\hat{R}_\lambda t^{-\mu}\sim(tl^{1/\nu})^{-\nu}. \quad (53)$$

This is shown in Fig. 30 for the data at saturated vapor pressure of Fig. 29. For this plot we used $l=L/\xi_0^+=L/1.43\times10^{-8}$ cm, the same as for the specific heat, and $\mu=0.44$ (Tam and Ahlers, 1985). One can see from this plot that, first, the data do not collapse on a single locus, and second, they do not have the correct power-law dependence. One expects that these data would determine a line of slope $\nu=0.671$; instead, one finds that it is a value greater than 1. It is not clear what the reason is for this lack of surface scaling, but it is reminiscent of the surface superfluid density which also yields exponents greater than 1. Note also that this result for the thermal conductivity for $T>T_\lambda$ stands in contrast to the successful scaling of the specific heat for $T>T_\lambda$.

There should also be a surface contribution to the thermal resistivity below T_λ. This is expected to have a noncritical background contribution plus a critical term, which would be temperature dependent near T_λ. This is expected to behave as $t^{\mu_s^\perp}=t^{\mu-\nu}$ which is the same dependence as above T_λ. Data for this resistance can be obtained directly below T_λ because of the effectively zero thermal resistance of the superfluid at distances of several correlation lengths away from the surface. Duncan *et al.* (1987) reported such measurements for two different experimental cells at two different separations. These data do indeed show a singular dependence on the surface resistivity. Duncan *et al.* (1987) were also able to describe this behavior using a "hydrodynamic" theory proposed by Landau (1941). The data are fitted well when the amplitude of the thermal resistance is adjusted. They remark, at the same time, that there are unresolved issues principally because this theory treats the helium at the surface as having bulk properties. Frank and Dohm (1989) have calculated the prefactor A_s^- [see Eq. (52)] both within the hydrodynamic theory and using a renormalization-group approach. Their results are shown in Fig. 31. The data on this plot are from Duncan *et al.* (1987); the open circles refer to a cell where the helium is confined at $L=0.0975$ cm and the filled circles are for a cell with $L=0.2878$ cm. The dashed line represents the hydrodynamic theory while the solid line is the renormalization-group result. There are no adjustable parameters in this calculation except for the background resistance which is fixed at a temperature indicated by the arrow. The temperature dependence is given by the exponent $\mu-\nu\simeq-0.23$. It is clear that the new theoretical results do a better job but still fall below the data for small t. The calculation was also extended to higher pressures as indicated by the dotted line. Note that in Fig. 31 the factor of L from the surface resistance is absorbed in $R_\kappa^{\rm tot}$.

New data for the thermal boundary resistance have been obtained recently by Lipa and Li (2007). They found that this resistance agrees well with the theory of Frank and Dohm (1989) for $T<T_\lambda$. For $T>T_\lambda$ they find that the resistance diverges more sharply than expected, with an exponent of −0.45 instead of −0.23.

D. Thinning of saturated films

A helium film near the superfluid transition is expected to have a contribution to the surface free energy that is due to critical fluctuations (Fisher and de Gennes, 1978). This contribution will lead to a force which will be manifested between the two surfaces. If the film has a free surface, this will result in a change of thickness which will depend on the sign of the force. In the case of helium near T_λ this force is attractive, resulting in a thinning of the helium film. This was first observed by Dionne and Hallock (1989), but studied systematically by Garcia and Chan (1999) and more recently by Ganshin *et al.* (2006). This effect is an analogous manifestation in a thermodynamic system of the Casimir force (Casimir, 1948), which exists because of electromagnetic fluctuations between two conducting plates. For a review of this effect in critical systems, see Krech (1994). In the case of a helium film of thickness d near T_λ, this force can be written as (Ganshin *et al.*, 2006)

$$f_C = \frac{k_B T_\lambda}{d^3}\vartheta(d/\xi) = \frac{k_B T_\lambda}{\xi_0^3 l^3}\vartheta(lt^\nu), \tag{54}$$

where $l=d/\xi_0$. In a first series of measurements to verify this effect, Garcia and Chan (1999) used a series of five parallel-plate capacitors at various heights above a bulk helium surface. Each capacitor has a different thickness film on its plates as a result of the balance between the gravitational force and the van der Waals force between helium and the copper substrate. In addition, the Casimir force induces a rapid variation in d below T_λ in the vicinity of the superfluid onset. By measuring the capacitance one is able to deduce the thickness of the helium film and extract the scaling function. It was found initially (Garcia and Chan, 1999) that all the films had a minimum thickness at the same value of the scaling variable $tl^{1/\nu}$ as expected on the basis of Eq. (54). However, in this first series of measurements, the magnitude of the thinning, or the overall thinning curve near the transition, did not collapse on a universal locus as expected. This was attributed to the relative roughness of the polished copper surfaces upon which the films were formed. In a second series of measurements (Ganshin *et al.*, 2006) polished silicon wafers were used. Data were obtained with these for three different films. These are shown in Fig. 32. Here the change of thickness is plotted as a function of $T-T_\lambda$. One can see that each film defines its own minimum on this plot with the thinnest film, as expected, shifted by the largest amount. We have plotted this shift of the maximum thinning in Fig. 21 (shown as boxes) along with the shift in the heat-capacity maximum. This shows that within the resolution of these data the maximum in heat capacity and minimum in the film thinning define the same locus, i.e., obey the same shift equation with the same prefactor. This is perhaps not surprising, and indicates that both of these features are a reflection of the point where one has a maximum in critical fluctuations. The scaling of the data from Fig. 32 are shown in Fig. 33. Here one can see that the collapse is excellent, with none of the difficulties seen in the previous measurements. There is another interesting feature in the scaling function defined by these data. Examination of the data slightly below the minimum reveals a change in slope or kink in the data. This feature, which is most visible in the inset of Fig. 32, is not as well defined as the minimum, but its location is consistent with the onset of superfluidity in the films. These points are plotted as the open boxes on the onset plot for planar films, Fig. 24. One can see that they are consistent with the other onset data. The reason for a kink at the onset is not clear.

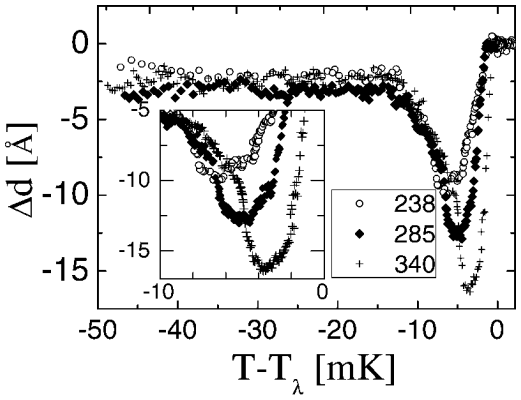

FIG. 32. Data for the critical thinning of helium films due to the thermodynamic Casimir force for three different film thicknesses. The thickness of each film is given in Å. From Ganshin *et al.*, 2006.

In the case of the heat capacity, a lack of scaling was observed near and below the specific-heat maximum (see Sec. V.A). This lack of scaling is not seen in the thinning data within the resolution of these measurements. If one were to take the variations in $f_{1\,\max}$ shown

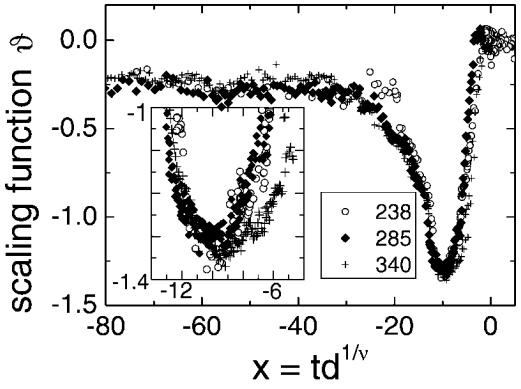

FIG. 33. The data of Fig. 32 scaled using Eq. (54). The data collapse onto a single locus using the bulk correlation-length exponent ν. From Ganshin *et al.*, 2006.

in Fig. 23 as a guide, one might expect a variation in the magnitude of the minimum of about 10% between the 238 and 340 Å data. The scatter near the minimum in Fig. 33 is about 5%, but with no systematic variations with size. It could well be that possible variations in the scaling locus are too small to be seen within the narrow range of film thickness in these data. Clearly, measurements over a wider range of film thickness, as indeed pointed out by Ganshin *et al.* (2006), would be of much interest. For Monte Carlo simulations relevant to these experiments see Hucht (2007) and Vesilyev *et al.* (2007).

VI. 3D-TO-1D CROSSOVER

In this section we discuss measurements where helium is confined in two spatial dimensions with the remaining dimension being relatively large. This is accomplished with channels or pores of length much larger than the transverse dimension, and will lead to 1D crossover. Details on how this crossover is realized will depend on the geometric cross section of the pores.

A. Specific heat

Measurements of the specific heat of helium confined to Nuclepore filters were the first to test scaling in the full critical region near T_λ (Chen and Gasparini, 1978). Data in this work were taken with four different filters ranging in pore diameter from 30 to 200 nm. In addition, in the same study, measurements were taken with films ranging in thickness from 1 to 5.3 nm formed on the surface of the 200 nm pores. In the initial analysis of these data, it was noted that both films and pores individually determined a shift of the specific-heat maximum $(T_\lambda - T_m)$ characterized by an exponent less than ν. It was then noted that all the shift data, for both pores and films, could be combined in a single plot, yielding the same exponent. This was achieved when a film of thickness L was considered equivalent to a cylinder of diameter D according to $L_{\rm eq}=0.585D$. An equivalence is expected on the basis of Eq. (9), i.e., the prefactor a is different for the two geometries, but the expected power law should be the same. This equivalence between films and pores was then carried over to the overall scaling, Eq. (5). The best collapse for the *combined* films and pores was found to take place for an exponent less than ν at a value consistent with both single-point scaling of the shift and value of the maximum; see Fig. 3 in Chen and Gasparini (1978). It is clear now that, while the single-point scaling for these data does indeed give exponents smaller than ν, combining the data for pores and films for scaling via Eq. (5) over the whole critical region is not correct. These two geometries have a different locus for the scaling functions and should not overlap simply by choosing a suitable value for $L_{\rm eq}$. Without the size "leverage" of combining thin films and larger pores, the pore data by themselves do not establish a scaling exponent via the use of the overall scaling equation [Eq. (5)] that can be claimed to be different from ν. This is especially true if the data for the 30 nm confinement are not included. The filters with the smallest pores are indeed the least homogeneous and have, in addition, the roughest surfaces, as indicated by adsorption measurements (Chen *et al.*, 1980; Gasparini and Mhlanga, 1986).

For the films formed on the Nuclepore surfaces, in comparing these original data for unsaturated films with the data for the much thicker planar films, Figs. 17, 21, and 23, one can see that these earlier data are globally consistent with the latter results. However, one can see as well from these plots that *locally* these early data by themselves do indeed have a different behavior. This is most obvious, perhaps, from the most sensitive plot of the data, Fig. 22. The increase of $f_{1\,\rm max}$ above the trend determined from the data for thick and thin films in this plot is suggestive of some film inhomogeneity for the thickest unsaturated films. It is likely that, given this trend, these thicker unsaturated films contain regions of capillary condensation within the rough surface of the pores. This would lead also to a shift exponent for the heat-capacity maximum of the films to be smaller than ν, as is indeed observed.

More recent work on the 1D crossover was done by Coleman and Lipa (1995) and Lipa *et al.* (2001) using confinement in 8-μm glass capillary arrays and 0.26-μm-diameter Anopore filters which have pores etched in an alumina matrix; and by Mooney *et al.* (2004) using patterned SiO_2 channels on a silicon wafer. These channels were capped by bonding another silicon wafer following the procedure outlined earlier. The resulting nominal dimensions of the channels are 1 μm$\times$1 μm $\times$4 mm. A measurement of the vertical height and uniformity of these channels after bonding using infrared interference is shown in Fig. 7(b). This measurement shows the vertical height to be $L\simeq 1.02\pm 0.01$ μm. This value is consistent with the thickness of the oxide growth, which was measured to be 1.016 ± 0.002 μm. All these data, for both $T>T_\lambda$ and $T<T_\lambda$, are shown on a semilogarithmic plot in Fig. 34. One can see that the behavior of these data is qualitatively similar to the planar data shown in Figs. 13 and 18. In more details, these data differ from the planar data, seen when comparisons are made. Note that the data for cylindrical pores are obtained using adiabatic calorimetry, with some contribution from bulk helium, which is subtracted from the measurement. For the 1 μm channels ac calorimetry is used with no contribution from the bulk liquid.

The overall scaling of the 1D data for $T>T_\lambda$ is plotted according to Eq. (5) in Fig. 35. For this plot specific-heat data at 0.26 and 8 μm are taken from Fig. 5 in Lipa *et al.* (2001) and then scaled using the bulk description given in that paper. There is a reasonable collapse of these data; however, the Nuclepore data tend to fall below the trend of the more recent 1D data, especially for smaller values of the scaling variable. This trend points to a greater overall value of the specific heat for helium confined in Nuclepore in a region close to T_λ, where the correlation length is largest. This will be discussed fur-

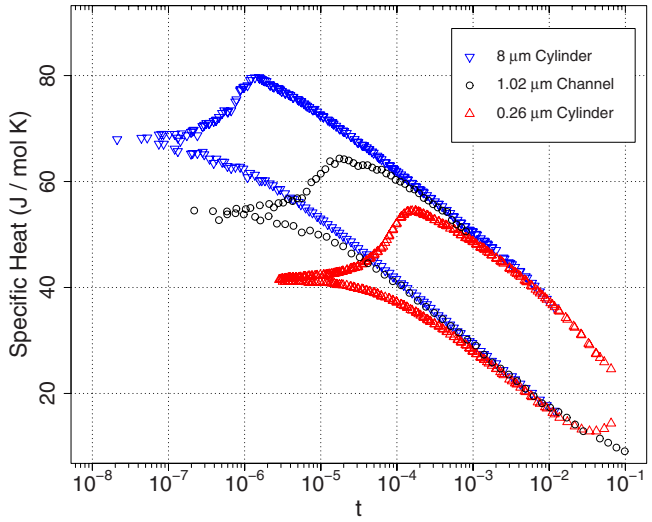

FIG. 34. (Color online) Specific heat of helium confined to uniform, one-dimensional confinements. The 8- and 0.26-μm cylinder data are from Coleman and Lipa (1995), and Lipa *et al.* (2001), respectively. The 1-μm channel data are from Mooney *et al.* (2004).

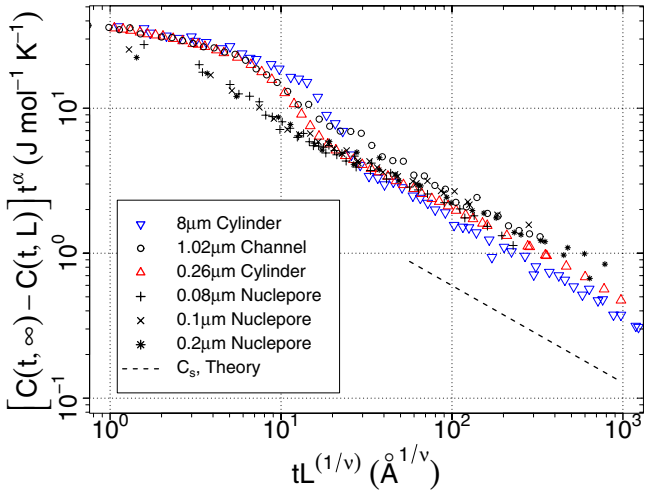

FIG. 36. (Color online) The scaling of 1D data for $T<T_\lambda$. The Nuclepore data have a different behavior than the more uniform confinements. The dashed line is the calculation of Mohr and Dohm (2000) for the surface region. This underestimates the effects of confinement below T_λ as was also seen in the planar data of Sec. V.A.

ther when single-point features are compared for 2D, 1D, and 0D crossovers, Sec. VII. Note also that on this plot the expected theoretical locus for the surface specific-heat region is shown as the dashed line (Mohr and Dohm, 2000). This region of the scaling function is governed by a power law with exponent $\alpha_s=\alpha+\nu$. The data are very close to this, as indeed are the data for the planar confinement, Fig. 16. One also notices in Fig. 35 a striking deviation of the data for the channels of square cross section for large values of the scaling variable. This deviation is evidence of an edge contribution to the confined specific heat and is governed by the exponent $\alpha_e=\alpha+2\nu$. This region will be discussed in more detail in the context of the 3D-to-0D crossover data, where the edge specific heat was first identified by Kimball *et al.* (2003; see also Kimball *et al.*, 2004). The data with pores of circular cross section do not have such a contribution from internal edges.

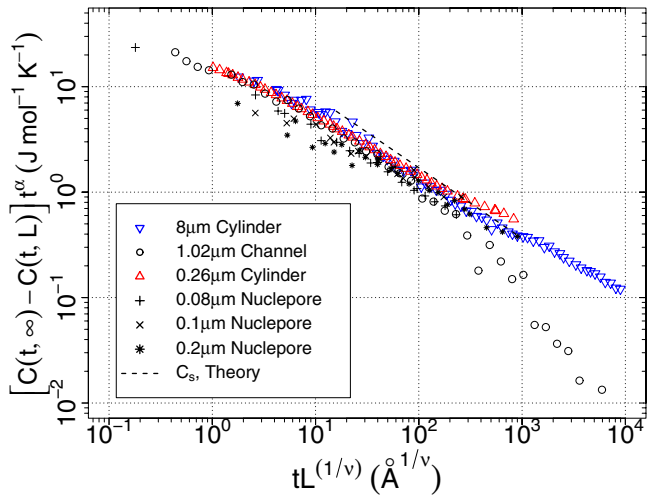

FIG. 35. (Color online) Data for 1D confinements scaled according to Eq. (5) for $T>T_\lambda$. The dashed line is the theoretical prediction for the surface region by Mohr and Dohm (2000). The 1.02-μm channel data show a unique initial deviation from bulk behavior at large values of the scaling variable due to edges in the confinement structure. The other confinements do not have such edges.

The data for $T<T_\lambda$ are shown on a scaling plot in Fig. 36. There is reasonable collapse of these data for large values of the scaling variable, but the region near the specific-heat maximum is somewhat problematic. The specific-heat maximum for 1D crossover is not as sharp as for two dimensions (see Kimball *et al.*, 2004, and also below in Sec. VII); thus the maximum appears as an inflection point rather than a minimum as it does in Fig. 20. The dashed line in this figure shows the locus of the theoretical estimate for the surface specific-heat region (Mohr and Dohm, 2000). As in the case for the planar confinement, this falls well below the data, contrary to the very good agreement for $T>T_\lambda$. This disagreement below T_λ is not unexpected since the theory is not well developed in this region and one would not expect quantitative agreement with the data. This result is still listed in Table IV, but should be understood within the limitations expressed by Mohr and Dohm (2000).

Nuclepore data fall well below the other data in the region of the maximum in Fig. 36. This is again an indication of the larger specific-heat values of these data relative to the others close to the transition. The channel data at 1 μm do not extend to large values of the scaling variable so as to reveal the edge behavior as noted for $T>T_\lambda$. This is because of an intervening resonance which becomes manifest in this experiment when the connecting channels to the filling line become superfluid. Figure 36 does not yield a clear conclusion about the collapse, or lack thereof, of the data in the region of the

TABLE IV. Values for the amplitude of surface A_s and edge A_e specific heats where available. The units for the surface and edge specific heats are J Å mol^{-1} K^{-1} and J Å^2 mol^{-1} K^{-1}, respectively.

	Surface: $T>T_\lambda$	Surface: $T<T_\lambda$	Edge: $T>T_\lambda$	Edge: $T<T_\lambda$
Planar films (expt.) (Kimball and Gasparini, 2000; Lipa *et al.*, 2000)	$A_s^+=-5.9\pm0.2$	$A_s^-=-8.6\pm0.5$	—	—
1D Channels (expt.) (Kimball *et al.*, 2004)	—	—	-370 ± 40	-1100 ± 110
Theory (Mohr and Dohm, 2000)	$A_s^+=-5.7$	$A_s^-=-2.0$	—	—

maximum. This can be seen using a scaling plot according to Eq. (8), which, setting aside the Nuclepore data, is shown in Fig. 37. One can see from this plot that near the maximum these data tend to open up. However, this behavior is not systematic with size. Thus one might conclude that the specific-heat data for 1D crossover suggest a lack of scaling in the region of the maximum, but not in the more striking and systematic way of the specific-heat data for 2D crossover. Recent data for 1.89-μm-diameter pores also support the lack of scaling seen in Fig. 37 (Aouaroun and Ahlers, 2007). However, these authors state that the lack of scaling is systematic with size near the maximum. Clearly, additional data for this geometry would be useful. See also Lipa *et al.* (2001) for comments about the region of the specific-heat maximum, and the 8 and 0.26 μm data in particular. Further discussion about the behavior of the Nuclepore data follows in the next section on the superfluid density.

B. Superfluid density

The superfluid density of helium confined in Nuclepore filters was measured by Brooks *et al.* (1979) and Schubert and Zimmermann (1981). In these measurements the Nuclepore membrane is used as a superleak separating two chambers. The walls of one of these chambers can be flexed to set up a Helmholtz resonance between the two chambers. From this, the superfluid density can be calculated (Schubert and Zimmermann, 1981). Data obtained in this way cannot approach the transition too close to the vanishing of ρ_s because of the loss of the resonance signal near T_c. Data from the above experiments have been analyzed in several ways. This is discussed in Paper I. In particular, it is shown in Paper I that a plot of these data according to Eq. (27) does not yield a collapse of the data as expected from correlation-length scaling (see Fig. 28 in Paper I). It is also shown in Paper I that one can obtain a collapse of these data with the variable tL^2. Gasparini *et al.* (1984) argued that, on the basis of the behavior of the heat capacity in Nuclepore, one might expect such scaling. However, this argument is incorrect, and is not supported by the subsequent measurements of Rhee *et al.* (1989) as discussed in Sec. III.B. These later measurements for a planar geometry, even though they do not scale with ξ, do not support a scaling with tL^2; see Fig. 20. Note that this lack of scaling for ρ_s in Nuclepore filters is a more fundamental problem than in the case of the specific heat. In the latter the data do scale among themselves, but the locus is different from that of the other 1D confinements; see Fig. 36. With ρ_s, there is no collapse of the data among themselves. This is more reminiscent of the lack of scaling for ρ_s in 2D crossover. There are no more recent measurements for 1D crossover for the superfluid density which can address the issues raised by existing data. This is clearly an area where more work needs to be done.

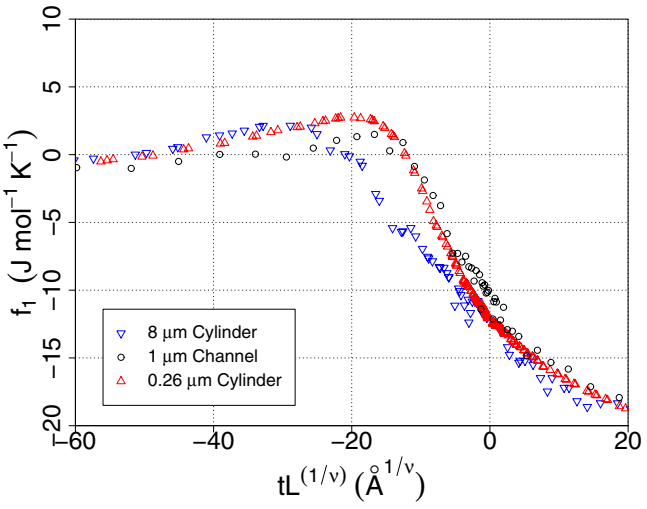

FIG. 37. (Color online) The data of Fig. 34 plotted according to the single-point scaling function f_1. While the data do not collapse near the maximum, there is no systematic opening with size as was seen in the planar data.

C. Superfluid onset

The superfluid onset T_c for helium confined in pores has been measured by numerous investigators (Notarys, 1969; Ihas and Pobell, 1974; Thomlinson *et al.*, 1975; Brooks *et al.*, 1979; Schubert and Zimmermann, 1981; Giordano, 1983). For confinement in pores, most data have been obtained with Nuclepore filters, with the exception of those of Notarys (1969), where the confinement is in pores of mica. The latter data have more of a diamond cross section than circular. The determination of the superfluid onset temperature t_c for these data is plotted in Fig. 38. Several techniques have been used to determine this: the onset of superfluid flow under a small pressure head (filled circles, Giordano, 1983; open circles, Notarys, 1969), the determination of the super-

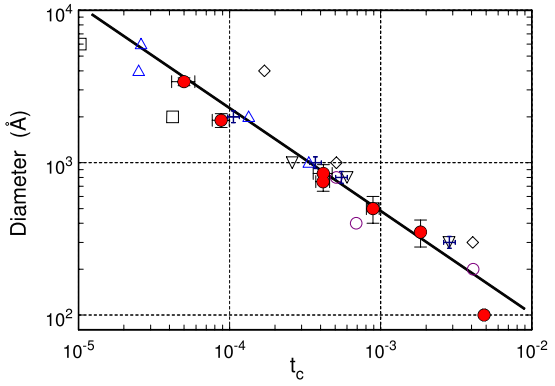

FIG. 38. (Color online) The temperature shift of superfluid onset for 1D confinements. All data except the open circles and crosses are from confinement in Nuclepore filters. The open circles are data from mica filters with pores of cross section closer to a diamond shape. The solid line is drawn with exponent ν and the data are consistent with this. The crosses are the temperature of the specific-heat maximum for confinement in Nuclepore.

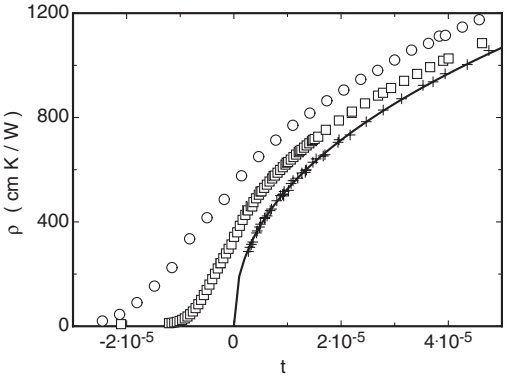

FIG. 39. The thermal resistivity of ^{4}He confined to glass cylinder arrays measured by Murphy *et al.* (2003). The circles and squares represent data from cylinders with radii of 0.5 and 1.0 μm, respectively. The plus signs are the bulk resistivity measurement of Tam and Ahlers (1985), fit to a power-law shown as the solid line. From Murphy *et al.*, 2003.

fluid fraction when the filters are the limiting flow element in a Helmholtz resonator (down triangles, Brooks *et al.*, 1979; diamonds, Schubert and Zimmermann, 1981), and the determination of the onset of second sound, where the filters are used as the driving element of a second-sound transducer (up triangles, Ihas and Pobell, 1974; squares, Thomlinson *et al.*, 1973; see Williams *et al.*, 1969, and Sherlock and Edwards, 1970, for a description of this technique). Error bars are included in Fig. 38 where available. The solid line on this plot is not a fit to these data but is drawn with exponent ν. The data are consistent with this fit. Giordano (1983), in the analysis of his own data, quoted a result of 0.65 ± 0.04. A fit of all these data is reported in Paper I with the result of 0.61 ± 0.04 (± 0.02). The uncertainty in the exponent depends on whether all the data are used or an analysis is performed in which six of the outlying data points are eliminated. These results are low relative to 0.671, but likely within the possible systematic errors.

By comparing the superfluid onset data for films, Fig. 24, with the results for filled pores, Fig. 38, one notes that there is little difference between T_c in films and in Nuclepore filters. If anything, it would appear that T_c in Nuclepore takes place somewhat *closer* to T_λ than in films. This would be unusual if the confinement truly represented 1D crossover. Further, by comparing the temperature of the specific-heat maximum T_m for Nuclepore filters with T_c, one finds that these two features are coincident within the resolution of these data; see crosses in Fig. 38 (see also Paper I, Fig. 39). This coincidence is in contrast to the behavior of films where the onset is always at a lower temperature than T_m. Thus the behavior of these single-point features for Nuclepore, when compared with films, is anomalous in several respects and contrary to what one might expect on the basis of dimensionality crossover or the relative positions of T_c and T_m.

If one compares the more limited data available from recent 1D measurements (Coleman and Lipa, 1995; Lipa *et al.*, 2001; Mooney *et al.*, 2004), one finds that indeed T_m is closer to T_λ than T_c (as judged by two thermal resistivity measurements of Murphy *et al.*, 2003; see Fig. 39). This agrees with the observation from the 2D data on the relative values of these two temperatures. Thus, ironically, it is not that the exponent for the shift in T_c is somewhat lower than expected that is problematic with the Nuclepore data, but rather that its locus does not distinguish T_c from T_m and also that it is in the wrong position, i.e., closer to T_λ, relative to the 2D data.

In summary, it would appear that confinement in Nuclepore does not represent the ideal confinement for 1D crossover. It seems that this medium, which appeared to have been an early standard for helium confinement, produces features that do not agree with more recent data for more homogeneous channels. These features also do not agree with trends that more recent data have established for 2D vs 1D crossover. The reason for this different behavior is not clear. The specific heat data, with their greater than expected values near the maximum, suggest contributions from larger characteristic confinement than the nominal pore sizes. The shift in T_c also suggests a larger size than nominal. However, in the overall scaling of the Nuclepore data compared to the more recent 1D data, one cannot make these data overlap over the full range of $tL^{1/\nu}$ with an increase in L. It seems likely that there are several factors at play with these data that go beyond the desired confinement for 1D crossover, or an increase of nominal confinement size. One interesting possibility is that there is a coupling effect in the pores of Nuclepore filters. This could take place either through interconnections of the pores (there is a finite probability that pores cross; see Smith *et al.*, 1987) or, for the determination of T_c, through an influence of bulk liquid in equilibrium with the liquid in the pores. In the case of the specific heat, one might have a coupling from a film on the surface of the filter in equilibrium with the filled pores. The coupling of the pores

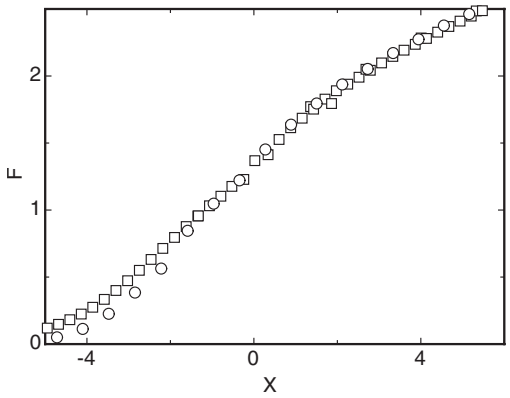

FIG. 40. The scaling of the thermal conductivity data shown in Fig. 39 using Eq. (55). The data show the expected collapse onto a single locus above T_λ but open up for temperatures below this. From Murphy *et al.*, 2003.

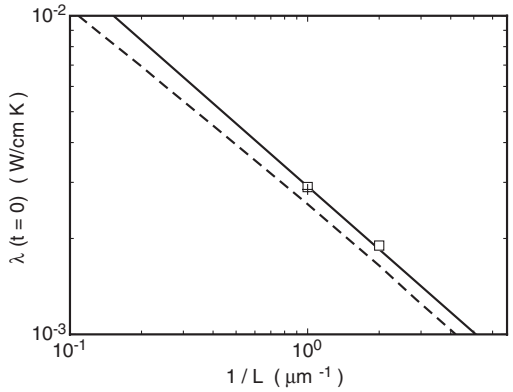

FIG. 41. The value of the thermal conductivity at T_λ from Kahn and Ahlers (1995) and Murphy *et al.* (2003) vs L^{-1} as the plus and boxes, respectively. The solid line is drawn with the expected slope of μ/ν while the dashed line is the theoretical prediction of Töpler and Dohm (2003). From Murphy *et al.*, 2003.

might well manifest itself nonuniformly as a function of temperature as the correlation length $\xi(t)$ changes. This would also generate a unique scaling locus relative to the ideal 1D crossover geometry. The effects of coupling among regions of confined helium will be discussed further in the context of 0D crossover (Sec. VII).

One could make comparisons of shift temperatures, either T_c or T_m, as functions of "size" in the case of more complex confinement geometries such as porous glasses (see, for instance, Fig. 7 in Brooks *et al.*, 1979). Such plots are more instructive in identifying differences among various confinements than for extracting shift exponents. Clearly the overall geometry and connectivity of confinement is a strong determinant of the thermodynamic response which goes beyond an average or characteristic size. Last, we note that the shift in C_m has been calculated by Chalyy (2004), where a comparison with existing data is also made and very good agreement is found. However, this calculation involves a correlation length that is not in scaling form, hence the significance of this agreement is not clear.

D. Thermal conductivity

Measurements of thermal conductivity have been performed for helium confined in cylindrical channels of glass capillary arrays with radii of 1.0 μm by Kahn and Ahlers (1995) and both 0.5 and 1.0 μm by Murphy *et al.* (2003). Data for the resistivity (ρ in this plot) from Murphy *et al.* are shown as open circles and squares, respectively, in Fig. 39. Here also plotted are data for bulk helium as well as a power-law fit to these data shown by the solid line. It is clear, as expected, that confinement increases the thermal resistance. These data can be scaled with size, and this is shown in Fig. 40. The function F plotted here can be related to the scaling function R used in the Introduction as follows:

$$F(x) = [1 + R(x)]x^{\mu}, \tag{55}$$

with $x \equiv t(L/\xi_0)^{1/\nu}$. One can see from this figure that these data, for two different confinements, scale well above T_λ ($x>0$). However, below it ($x<0$) these data do not collapse. Murphy *et al.* (2003) concluded that there is a breakdown of scaling below T_λ. Data for the earlier 1.0 μm capillary array were also analyzed by Ahlers (1999) by plotting the difference between the resistivity of the confined and bulk helium according to the scaling form $(r_\infty - r)l^{\mu/\nu}$. This should yield the scaling function $G(tl^{1/\nu})$. The data are not scaled with size, but define a region of temperature dependence where a power law with exponent of ν is obtained. If these data were in the region where a surface-plus-bulk analysis is appropriate one should obtain, for fixed l, a power law given by [see Eq. (43)]

$$(r_\infty - r)l^{\mu/\nu} \sim -t^{-(\nu-\mu)} \sim -t^{-0.23}, \tag{56}$$

at least in the region where the scaling function R is small, which is the case for the surface region. Thus an exponent of $\nu=0.671$ as obtained by Ahlers (1999) is a surprising result. Note that a plot of the data according to the alternative scaling form $(r_\infty - r)t^{-\mu}$ would produce, for small values of R, a surface region with dependence $x^{-\nu}$ [see Eq. (42)].

The data for the two cylindrical confinements also yield a check of Eq. (34) for the value of the resistivity at $t=0$. This is shown in Fig. 41 for $\lambda(0,l)=1/r(0,l)$. One finds that these values are consistent with the exponent μ/ν indicated by the solid line through the data in Fig. 41. However, the magnitude of the thermal conductivity at $t=0$ from theoretical predictions (Töpler and Dohm, 2003) is found to be smaller than that measured experimentally. This is opposite to the result found in the comparison of the specific heat $C(0,l)$. There the data have the correct scaling dependence on $l^{\alpha/\nu}$, and the theoretical results predict a larger value of $C(0,l)$ (see Fig. 17). However, it is likely that in both cases these disagreements are well within the precision of the theory. Indeed, Murphy *et al.* (2003) refer to Fig. 41 as indicating excellent agreement with the renormalization-group calculation.

Recently, data have been reported by Jerebets *et al.* (2007) for the thermal resistance of helium confined in capillary arrays with rectangular cross section, $H \times W = 1 \times 10\ \mu m^2$, and 1 mm long. This type of confinement, in the limit that the width W goes to infinity, would represent confinement in a planar geometry. What is found for these data is that the resistivity matches well the values measured for a cylindrical confinement in pores of radius 1 μm. In comparing pore confinement with planar confinement, for large values of the scaling variable (where one expects the system to be in the surface region), it is the ratio of the surface to the volume that determines the magnitude of the thermodynamic response. This is the same for both planar confinement and cylindrical confinement if the radius of the pore and the height H for the film are used as the small scaling dimension. This was discussed by Kimball *et al.* (2004) in comparing specific heats for confinement in these two geometries; see Fig. 5 in Kimball *et al.* (2004). For the experiment of Jerebets *et al.* (2007) the surface-to-volume ratio in their geometry is $2(1+H/W)/H$. This differs by 10% from that of a pore of radius H. Thus in the surface region one would expect these data to be smaller by about 10% than those for cylindrical confinement (the surface term decreases the overall conductance). Closer to the transition, one would expect these data to cross over to 1D behavior in a way somewhat different from that in a cylindrical pore. This would be reflective of the different pore cross sections. Thus the overall agreement between these data and those of cylindrical confinement is surprising. It is also observed for these data that the value of the conductivity at $t=0$ matches closely with that of cylindrical confinement (Jerebets *et al.*, 2007).

Theoretical results for the thermal conductivity from Monte Carlo simulations of the 3D XY model have been reported by Zhang *et al.* (2006). These authors simulate an $L \times L \times H$ system. To represent planar confinement L is maintained as $\geq 5H$, and, in addition, periodic boundary conditions are maintained in the $L \times L$ directions to simulate $L \sim \infty$. In the small dimension H, open-boundary conditions are maintained. Zhang *et al.* find different scaling functions for pore and planar geometry. However, as is also pointed out by Jerebets *et al.* (2007), the planar geometry scaling function can be matched to the data of Jerebets *et al.* (2007) with two adjustable parameters which do not change the shape of the scaling function. Thus for these measurements of thermal conductivity one has the experimental observation that a pore of radius H and an $H \times 10H$ channel produce data which overlap, and hence would be described by the same scaling function. Yet the Monte Carlo simulations find different scaling functions for pores and films. These observations suggest that one needs an even larger aspect ratio in W/H to represent planar confinement. The area of finite-size scaling whereby one explores the lower-dimensional crossover from laterally bounded planar films, $H \times W \times \infty$, to unbounded planar films, $H \times \infty \times \infty$, has not been studied experimentally in any great detail. Results for the superfluid density (Diaz-Avila *et al.*, 2004) of thin films with $h=9$ nm, and with varying W up to aspect ratios greater than 1000, show that the effect of finite lateral confinement can be measured even at such large aspect ratios. It is not clear, however, how these results can be extrapolated to thicker films such as those measured for the thermal conductivity.

VII. 3D-TO-0D CROSSOVER

The realization of 0D crossover requires that helium be confined in all directions. This was achieved first by Kimball *et al.* (2003; see also Kimball *et al.*, 2004). For these measurements a cell was prepared from a silicon wafer with a 1-μm-thick oxide. This was patterned into pillboxes of 1 μm diameter. An array of $\sim 10^9$ such boxes was tiled on the wafer at a center-to-center separation of 2 μm. A similar array of 2 μm boxes at 4 μm separation was subsequently used by Mooney *et al.* (2006; see also Mooney, 2006) to obtain data for a second confinement and test scaling for 0D crossover. A scanning electron microscope (SEM) image of these boxes is shown in Fig. 42. To fill the boxes a second silicon wafer was patterned with an array of channels either 1 or 2 μm wide for each respective cell. When these two wafers are bonded the resulting arrangement is one of boxes connected by channels (width $\times$ length $\times$ height) of 1 μm $\times \sim 1$ μm $\times$ 19 nm and 2 μm $\times \sim 2$ μm $\times$ 10 nm. Thus the height of the connecting channels is 19 nm for the 1 μm boxes or 10 nm for the 2 μm boxes. The length of the channels linking the boxes is not known exactly because the channels are not in registry with the boxes. Thus the shortest distance between boxes could vary between 1 and $\sqrt{2}$ times the edge-to-edge distance of the boxes. An SEM image of the 2-μm-wide channels is also shown in Fig. 42. The intent of the above design is to realize a collection of isolated boxes by having the connecting channels small enough so that the helium in them remains normal in the region where the boxes undergo their transition. In addition, one wants to have a minimum amount of helium in the channels so that the contribution to the heat capacity is negligible (finite-size effects will also suppress the specific heat of the helium in the shallow connecting channels).

With the measurements of the heat capacity of helium confined in $(1\ \mu m)^3$ boxes, data are now available to compare 2D, 1D, and 0D crossover for the same nominal smallest confinement. The actual heights of the film, the channels, and the boxes are 0.9869, 1.02, and 1.08 μm, respectively. The specific-heat data for these cases are shown in Fig. 43 on a linear scale; see also Kimball *et al.* (2004). One can see from this figure that, not unexpectedly, the crossover dimensionality has a strong influence on the magnitude and shape of the heat capacity near the maximum. All data fall below the bulk locus, the solid lines, and the maximum is shifted to successively lower temperatures as one would expect. The

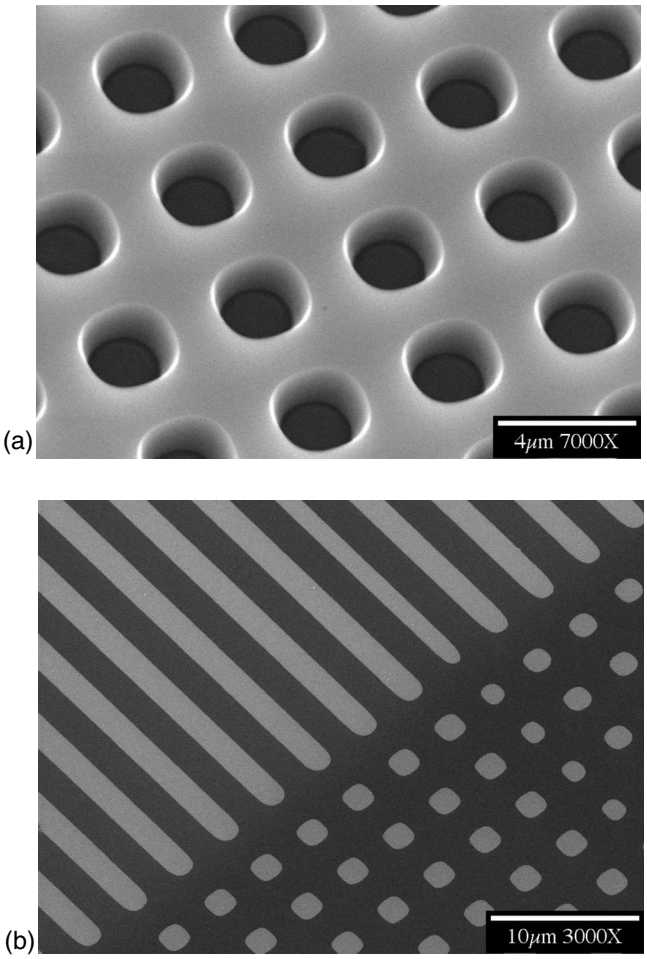

FIG. 42. Scanning electron microscope images of the structures used to confine helium to 0D (Mooney *et al.*, 2006). (a) The 2-μm^3 boxes made in SiO_2. (b) The fill channels (darker regions) that span the majority of the cell and whose cross section is 10 nm$\times$1 μm. The square oxide regions seen in (b) allow helium to flow from the cell fill hole to the channels.

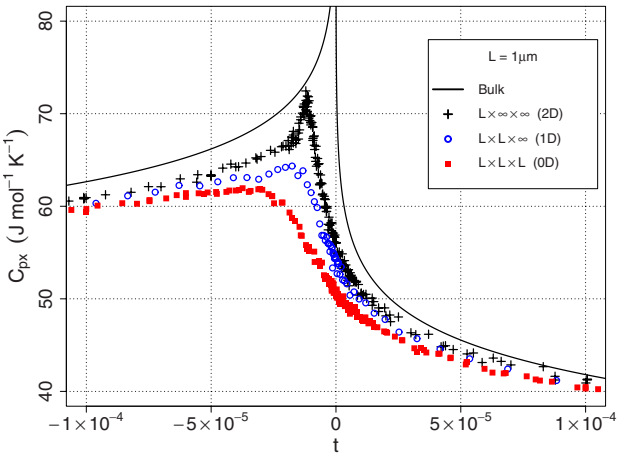

FIG. 43. (Color online) Comparison of the crossover from three dimensions to two, one, and zero dimensions where the smallest spatial length in each confinement is 1 μm. The data show the expected behavior: As more spatial dimensions are made finite, the greater the heat capacity is suppressed and the specific-heat maximum shifts to colder temperatures.

2D data are noticeably sharper than the rest indicating, perhaps, the special case of two dimensions as the lower critical dimension for helium. The scaling loci of these data according to Eq. (5) are shown in Fig. 44 for $T > T_\lambda$ (Kimball *et al.*, 2004). One can see that these data do indeed define different loci for the different crossover dimensions. There are two regions identified by straight lines on this scaling plot: one of slope $-\nu$, and the other of slope -2ν. The former, as has been seen already, is indicative of the surface specific-heat region, while the latter is indicative of the edge contribution to the specific heat. Values for the amplitudes of these specific heats are given in Table IV. From these scaling plots one can see that the deviation from bulk behavior is dictated in these data first by the presence of edges, then by surfaces. Eventually, for smaller values of $tL^{1/\nu}$, this distinction, which goes back to the consequences of Eq. (1), cannot be made, and the full scaling function takes over. Note that the 2D data have a well-developed region of surface contribution, but for one and zero dimensions there is a smooth transition from the edge to the full scaling function.

The scaling loci for $T < T_\lambda$ are shown in Fig. 45. The striking feature of this plot, as indeed one might have inferred from Fig. 43, is the region of the maximum. Here, in this difference plot, the sharpness of the maximum translates itself into a minimum for two dimensions and inflection points for one and zero dimensions. The region of surface and edge contributions can be obtained for the 0D data from the indicated slopes. The 1D data, as pointed out earlier, could not be continued into the edge region for $T < T_\lambda$ because of the onset of a superfluid resonance. A comparison of these data with

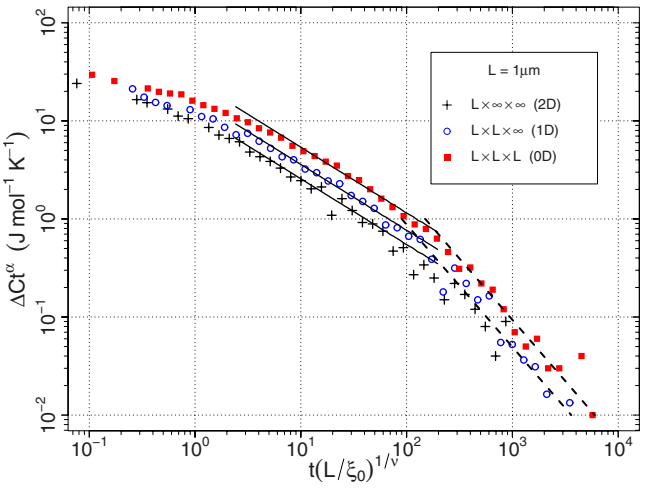

FIG. 44. (Color online) The data above T_λ in Fig. 43 cast in scaling form according to Eq. (5). The solid lines are the expected slope and magnitude of the scaling locus in the surface region for all three lower dimensionality crossovers. The dashed lines are drawn with the edge specific-heat exponent and then have their magnitude adjusted to match the 1D and 0D data.

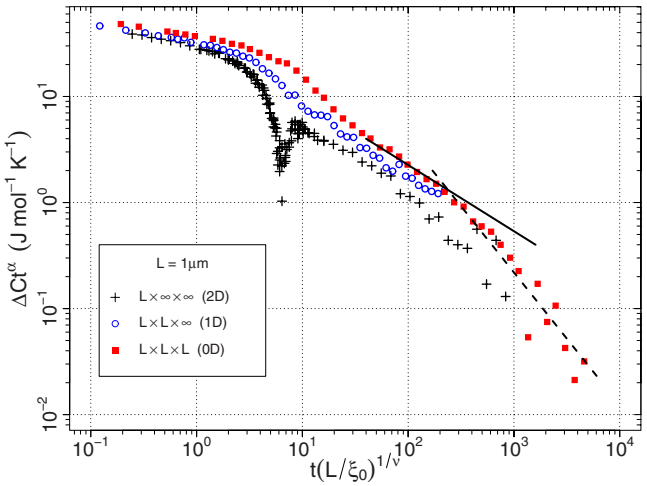

FIG. 45. (Color online) The equivalent plot to Fig. 44 for $T < T_\lambda$. The solid and dashed lines are drawn on the 0D data with slopes appropriate for the surface and edge specific-heat regions.

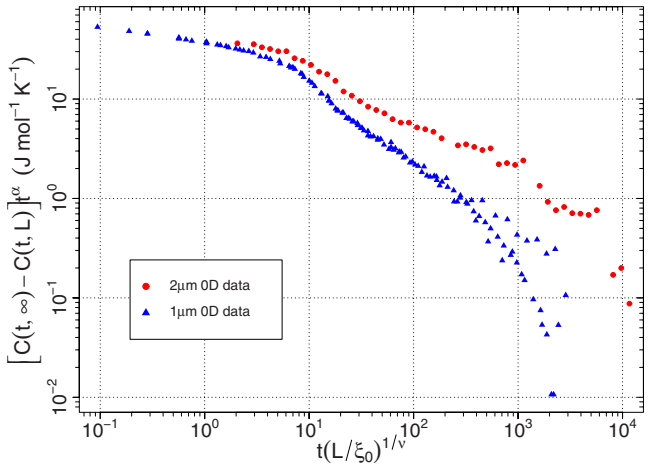

FIG. 47. (Color online) Scaling plot of the 0D data below T_λ according to Eq. (5). The lack of scaling is not surprising since the specific-heat data overlap and show little change as function of confinement size.

Monte Carlo calculations (Schultka and Manousakis, 1998) for 1D crossover has been shown by Kimball *et al.* (2004). One finds that there is good agreement except in the region near the maximum where the calculation underestimates the effects of confinement.

The heat-capacity data for the 1 and 2 μm boxes are shown in Fig. 46 on a log-linear plot (Kimball *et al.*, 2003; Mooney, 2006; Mooney *et al.*, 2006). The solid lines on this plot represent the bulk behavior. There are some features of the data which are consistent with the two different confinement dimensions: the maximum of the two data sets show the correct relative positions and magnitudes, with the 2 μm being somewhat larger in magnitude, and having a maximum closer to T_λ. However, as one moves to larger values of t, one can see that

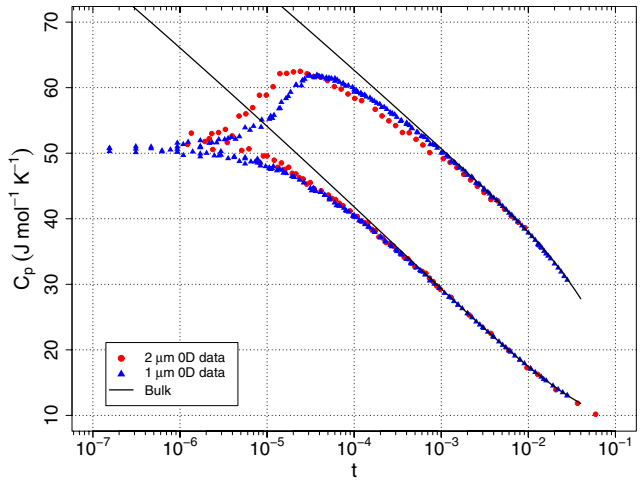

FIG. 46. (Color online) ^{4}He confined to arrays of $(1\ \mu m)^3$ and $(2\ \mu m)^3$ boxes. The shift of the maximum in the specific heat from T_λ is qualitatively as one expects; the smaller confinement has a larger shift. However, the overall magnitude of the data does not behave as expected since the two sets show little change as function of confinement.

above T_λ there is a region where both the 1 and 2 μm data are coincident while still at a value which is below the bulk. This implies that on a scaling plot, with the variable $tl^{1/\nu}$, these data will not collapse. Below T_λ, one finds that the data cross, which is again an indication that they will not collapse on a scaling plot. These data for $T < T_\lambda$ are shown in a scaling plot in Fig. 47. As expected, there is no collapse of these data. The same is found for the data at $T > T_\lambda$, and with the same trend: the data for the *smaller* boxes lie *below* those of the larger boxes. It can be seen from Fig. 16 that there are often systematic differences between data at various confinements for the same crossover dimension. However, none of the data for the other dimensionality crossover have the same systematic differences across the full range of the critical region from $T > T_\lambda$ to $T < T_\lambda$. Given this, one would assume that the lack of collapse of the two sets of 0D data stems from some physical reason. In order to understand this, one can look at the trends established for the heat capacity for the various dimensionality crossovers. The shift of the heat-capacity maximum as a function of confinement size is shown in Fig. 48. There seems to be nothing anomalous in any of these data. Each set is consistent with an exponent of ν—as indeed obtained for the full set of the planar data (see Fig. 21)—and the shift of the maximum is progressively larger for the same L as one lowers the crossover dimension. Interestingly, this shift increases by a factor of 2 for each lowering of the dimensionality. We are not aware of any theoretical prediction relevant to this observation. A similar plot to that for the shift can be made for the magnitude of the heat-capacity maximum. This is shown in Fig. 49. The variation in $C_{\max}$ with L is expected to be given by Eq. (12), $C_{\max} \sim L^{\alpha/\nu}$. The solid lines in Fig. 49 are fits to this power law. As has been discussed, the values of the specific-heat maximum for the 2D data do not yield the correct value of $C(0,\infty)$. Indeed, one can see in Fig. 49, more clearly than in

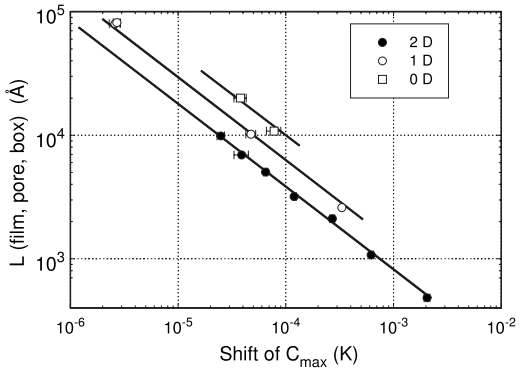

FIG. 48. Shift in the temperature of the specific-heat maximum as function of L for three crossover dimensions. The data for a given dimensionality crossover fall on lines with the expected slope of $-\nu$.

Fig. 23, the systematic deviations of the planar data from the fit to $L^{\alpha/\nu}$. For the more limited 1D data (the open circles) the value obtained for $C(0,\infty)$ is 467 ± 14 J mol^{-1} K^{-1} which is in good agreement with the determination from bulk measurement of 460.2 ± 7.3 J mol^{-1} K^{-1} (Lipa *et al.*, 2003); see Table III. However, for the present discussion, one only needs to note that the planar and cylindrical data fall on reasonably consistent trends as a function of L. In contrast, it would seem that either of the two data points for 0D crossover is incorrect in the value of $C_{\max}$. Note that there is no more than 1% uncertainty in the value of L, and less than 1% uncertainty in the magnitude.

To interpret the above results one needs to reconsider the assumption that these are measurements of a collection of *isolated* boxes. From simultaneous measurements of the superfluid density with these cells, one knows that the helium in the connecting channels becomes superfluid at $t\simeq10^{-2}$, well below the scaling region of the heat capacity shown in Fig. 47. Nevertheless, one notes that the $(2\ \mu\text{m})^3$ boxes are connected via channels which are twice as long and half as high as in the case of the $(1\ \mu\text{m})^3$ boxes. On the basis of this, one might conclude

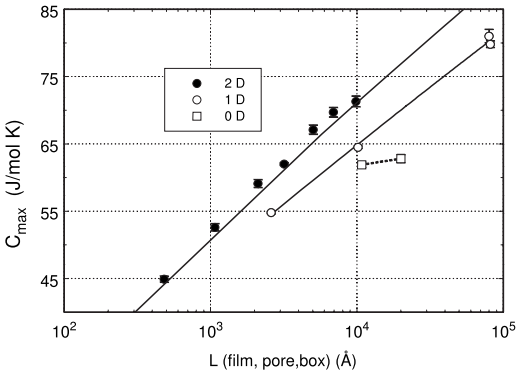

FIG. 49. The magnitude of $C_{\max}$ vs L for three crossover dimensions. Fits of the 2D and 1D data to the power law $L^{\alpha/\nu}$ are shown as solid lines though those data (the 2D fit is from the wider range of data seen in Fig. 23). The 0D data are clearly inconsistent with this.

that, if there is coupling between the boxes leading to a collective effect, then it is more likely to occur for the $(1\ \mu\text{m})^3$ data than for the $(2\ \mu\text{m})^3$ data. This would explain a relatively larger value of $C_{\max}$ for these data, and the position of these data in the scaling plot, Fig. 47, relative to the $(2\ \mu\text{m})^3$ data. If this is indeed the case, then one would expect that, as the specific heat is enhanced by a coupling via the normal channels, the superfluid density of the helium in the channels, which starts near $t\simeq10^{-2}$, be enhanced by the presence of the already superfluid boxes. We see below that there is indeed evidence of this from a series of measurements which involve determining the role of the channel width in the onset of superfluidity of a film.

The above observation on the possible coupling of superfluid boxes is somewhat outside the topic of correlation-length scaling and leads to the possibility of interesting studies of weakly coupled superfluids analogous to arrays of Josephson junctions for superconductors. In distinction to a superconductor, one would presume that in the case of a superfluid one would have a more significant role played by fluctuations near the transition. Last, we point out that, if the data for the $(1\ \mu\text{m})^3$ boxes are indeed enhanced relative to the limit of fully isolated boxes, then the true locus for these data in Fig. 43 would be even lower than indicated. The position of the maximum, however, as discussed above, is not likely to change. We note that properties of helium confined in porous media should also display these coupling phenomena. This should take place between regions where the confinement is large through regions where it is small. Given this, it should be clear that the thermodynamic responses should be unique for each porous confinement.

A Monte Carlo calculation of the specific heat of helium in a cubic geometry has been performed by Nho and Manousakis (2003). This calculation is compared to the $(1\ \mu\text{m})^3$ experimental data in scaling form and shows excellent agreement, especially considering that there are no adjustable parameters in the calculation. This stands in direct contrast to the above arguments regarding an enhanced specific heat due to coupling of individual boxes of helium. One might now conclude that it is the $(2\ \mu\text{m})^3$ data that have a problem and the above arguments regarding coupling are incorrect. However, when a similar Monte Carlo calculation is applied to a film geometry, it underestimates the effects of confinement. If this underestimation is also true for 0D confinement, one can conclude that the measured $(1\ \mu\text{m})^3$ specific heat is too large and the above arguments regarding an enhancement due to coupling hold. New experiments are needed to clarify this issue.

VIII. 2D-TO-1D CROSSOVER

A helium film of thickness L may be considered as having dimensions $L\times S\times W$ with $S,W\gg L$. Films where L is of the order of a few atomic layers and where S,W are of the order of centimeters have been studied

near their superfluid transition as examples of the Berezinskii-Kosterlitz-Thouless (BKT) transition (Berezinskii, 1971; Kosterlitz and Thouless, 1972, 1973; see also Minnhagen, 1987). Measurements of the areal superfluid density (Kagiwada *et al.*, 1969; Bishop and Reppy, 1978, 1980; Kotsubo and Williams, 1984; Agnolet *et al.*, 1989) and thermal conductance (Agnolet *et al.*, 1981; Maps and Hallock, 1981; Hess and Muirhead, 1982; Joseph and Gasparini, 1982; Finotello and Gasparini, 1985; Yu *et al.*, 1989) revealed many features of this transition which are in agreement with theoretical predictions, such as the jump in the superfluid fraction at T_c, Eq. (22), and the divergence of the convective conductance. The latter, in particular, reflects the exponential divergence of the 2D correlation length on the high-temperature side (Ambegaokar *et al.*, 1980),

$$\xi_{2D} = \xi_{2D}^0 \exp\left(\frac{2\pi}{b(1 - T/T_c)^{1/2}}\right). \tag{57}$$

This divergence is determined by two parameters which depend on the film thickness: ξ_{2D}^0 and b. The latter is not expected to be universal and may vary from substrate to substrate. The critical temperature T_c is also a function of the thickness L. For thicker films T_c is expected to obey the shift equation, Eq. (21). Data for T_c as a function of L for thinner films are plotted in Fig. 10. For thicker films, on the order of a fraction of a micrometer, the crossover from three to two dimensions masks the strictly 2D behavior until a narrow temperature region close to T_c. See, for instance, Fig. 2 of Gasparini *et al.* (1984) and also Rhee *et al.* (1989), where dissipation due to vortex pair unbinding becomes manifest in the region $t \sim 10^{-5}$–10^{-4}. This dissipation is much more striking for thin films, as can be seen from Bishop and Reppy (1978, 1980) and Agnolet *et al.* (1989). These thin films should be considered strictly 2D since the 3D correlation length plays effectively no role. For the thicker films, as one approaches T_c, the growth of the 3D correlation length is responsible for the 2D crossover until a region is reached, close to T_c, where the relevant physics is governed by the 2D correlation length.

One may consider now finite-size effects in two dimensions for a film of thickness L and some characteristic small width W, i.e., dimensions $S \times W$. For a channel one might have the length $S \simeq \infty$. In an analogous way to the 3D case one can define a shifted critical temperature—relative to $T_c(L, S \simeq \infty, W \simeq \infty)$—as the point at which $\xi_{2D} \simeq W$. Using this argument then yields the 2D shift equation (see, for instance, Barber, 1983)

$$\frac{T_c(L, \infty, \infty) - T_c(L, W, \infty)}{T_c(L, \infty, \infty)} \equiv \delta t_c(L, W) \propto \left(\frac{1}{\ln(W/\xi_{2D}^0)}\right)^2. \tag{58}$$

This is a much weaker dependence on the small dimension W than the analogous dependence of T_c on L, which is a power law; see Eq. (9). This logarithmic dependence has not been verified experimentally. In fact, it has been suggested that this prediction is incorrect because of the lateral boundary of the film where single vortices can be bound. It is predicted that the shift equation for a channel should be (Sobnack and Kusmartsev, 2001, 2002)

$$\delta t_c(L, W) = \left(\frac{2\xi_{2D}^0}{W}\right)^{1/2}. \tag{59}$$

The exponent of 1/2 in this equation depends on the geometry of the film. A film in the shape of a disk, for instance, in which $W = S$ (representing 2D to 0D crossover) would have an exponent of $(\sqrt{13} - 1)/2$ (Sobnack and Kusmartsev, 2001). Clearly, this prediction is quite different from Eq. (58), and differs markedly from the shift equation resulting from 3D crossover to lower dimensions, in which case for two, one, and zero dimensions one has a different prefactor, but the power-law shift is always governed by the 3D correlation-length exponent ν. A test of Eq. (59) was done with the data for the onset of superconductivity of aluminum films in the shape of disks of various diameters (as referenced by Sobnack and Kusmartsev, 2002). Good agreement with the prediction of Sobnack and Kusmartsev (2002) was found. For helium, the lateral confinement of a film presents an experimental challenge because of the fact that helium wets almost all surfaces. The first indication that Eq. (59) might be appropriate for helium was in the experiment of Kimball *et al.* (2003). A subsequent study by Diaz-Avila *et al.* (2004) was designed to test Eq. (59) more carefully. In this experiment a film of fixed height $L = 10$ nm was constrained in a channel of width W which is varied in the range 3–19 μm. The length of the channels was fixed at 0.2 cm. These channels are formed lithographically on a silicon wafer on which a 10 nm oxide has been grown. An example of a channel with $W = 19$ μm is shown in Fig. 50(b). This was obtained with an atomic force microscope (AFM) and represents a section of a 0.2-cm-long channel. To complete the channel structure a second silicon wafer is directly bonded to the wafer containing the shallow channels. This second wafer is prepared with a 0.319 μm oxide which is patterned in two regions separated by a solid SiO_2 ring. The two open regions have a series of small oxide posts in a similar way as described in Sec. V.A for studying of the heat capacity of 2D films. When the two wafers are bonded, the overall structure is one of two reservoirs of helium films at a thickness of 0.319 μm linked by 72 radial channels of 10 nm height across the 0.2-cm-wide oxide ring. The overall structure of the bonded wafers is visible in the infrared image of Fig. 50. The outer bright ring in this figure is the bonded SiO_2 that seals the cell. The channels of interest span the inner ring. One can detect faint spots in the reservoir regions which are the bonded SiO_2 posts. The fuzzy light bands are interference fringes from the outside top and bottom of the polished wafers. These are not indicative of inhomogeneity in the internal spacing of the wafers, but a measure of the variation in the total wafers' thicknesses. Two fringes represent a variation in thickness of 1 μm.

Adiabatic fountain resonance is used to determine the

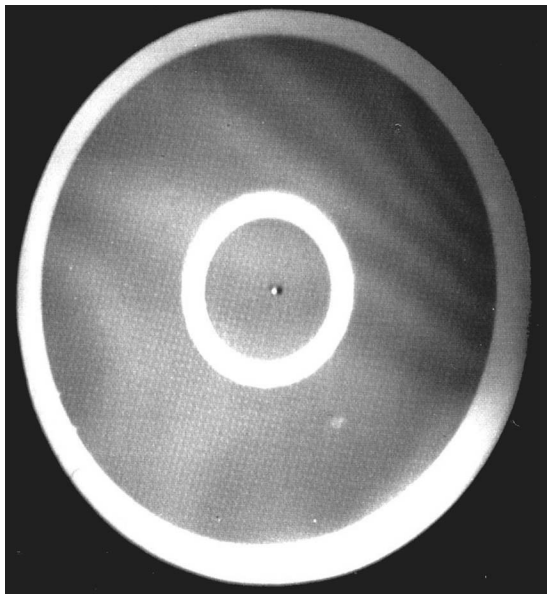

(a)

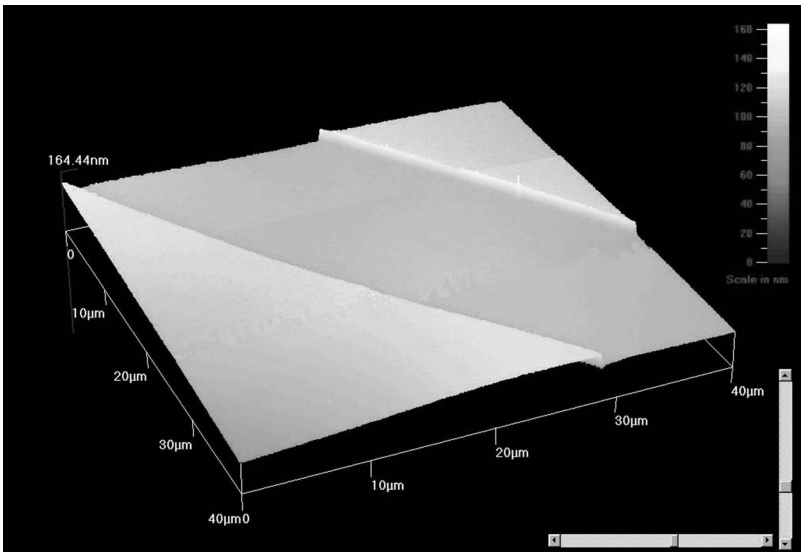

(b)

FIG. 50. The cell design used to study 2D to 1D crossover by Diaz-Avila *et al.* (2004). Shallow channels of fixed width radially span the inner oxide ring that separates the two 0.3189-μm planar regions seen in (a). One can relate the resonant frequency of helium oscillated between the two planar regions to the superfluid fraction of the helium within the channels. An AFM image of a channel section is seen in (b). Multiple cells were built where the channel height was the same but the width was varied.

superfluid fraction of helium confined in the channels. The helium is driven at resonance from one reservoir to the other, and into the filling line through the wafer hole—the bright center dot in Fig. 50(a). From the resonant frequency, or the phase shift between the heat input and thermometer response, one can determine the superfluid fraction. Further details of how this type of measurement is performed, and how ρ_s/ρ is obtained, can be found in Gasparini and Mehta (1998) and Gasparini *et al.* (2001). Note that the helium in the two 0.319 μm reservoirs is already superfluid in the region where the channels are still normal. The superfluid fraction for helium in 8- and 19-μm-wide channels is shown in Fig. 51 as a function of $t=1-T/T_\lambda$ (Diaz-Avila *et al.*, 2004). The dashed line in this plot is the locus of the bulk superfluid fraction. One finds from these data that ρ_s/ρ vanishes at a lower temperature than a film of 10 nm that is not confined laterally. The vanishing of ρ_s for a film where $W\sim\infty$ is given by the temperature at which the + symbol is located on this plot. The magnitude of

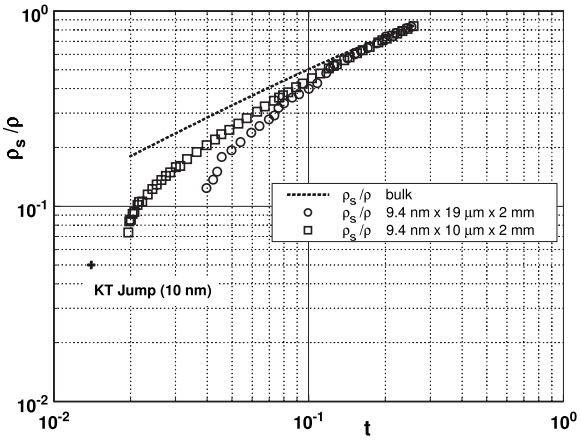

FIG. 51. Superfluid density for helium confined to channels of two different widths, 19 and 10 μm, measured by Diaz-Avila *et al.* (2004). The height and length of both channels are 10 and 2 mm, respectively. This geometry represents a dimensionality crossover from two dimensions to one dimension.

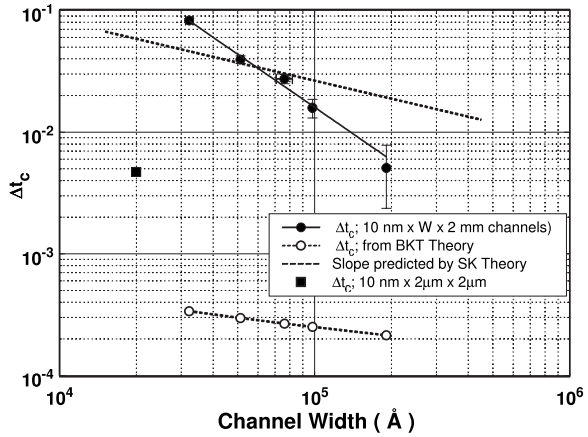

FIG. 52. The shift in the superfluid transition temperature of helium confined in finite-width channels (filled circles) relative to a channel of infinite width. Here the height and length of the channels are 10 nm and 2 mm. Also shown (open circles) is the expected temperature shift based upon the 2D shift equation of the BKT theory [Eq. (58)] and the power-law shift of Sobnack-Kusmartsev [Eq. (59)], upper dashed line. The filled box is the measured shift of the superfluid transition temperature for filling channels used to fill 0D boxes with helium.

ρ_s/ρ at the vanishing point is larger than the expected KT jump, Eq. (22); however, this can only be inferred precisely to the extent that the data can be normalized to the bulk value at the lowest temperatures. Several other channels of width as low as 3 μm were studied by Diaz-Avila (2006). However, for the narrower channels, the detailed behavior of ρ_s/ρ was not obtained as reliably because of the larger dissipation associated with the flow in these channels. The shift in T_c as a function of W for these data is plotted as filled circles in Fig. 52. The expected shift on the basis of the logarithmic dependence, Eq. (58), is also calculated using the data from Finotello *et al.* (1990) for the parameters ξ^0_{2D} and b, and shown as open circles in Fig. 52. Clearly the measured shift is much larger than that predicted from Eq. (58). This aspect is consistent with the prediction of Sobnack and Kusmartsev (2002). However, the exponent obtained from the solid line in Fig. 52 is 1.446 ± 0.089, not $1/2$ as expected from Eq. (59). This is indicated by the top dashed line on this plot. There are several sources of errors in determining the locus of δt_c: the locus of $T_c(L,\infty,\infty)$, determining the thicknesses of the nominal 10 nm oxide (this is done with ellipsometry of the oxide and AFM on the open channels), and the width of the channels as measured with AFM. These errors are indicated with error bars in Fig. 52. Even within these errors it seems clear that these data do not support an exponent of $1/2$.

Williams (2006) calculated the superfluid function for helium films confined in finite-width channels. He found that the superfluid fraction is anisotropic for directions parallel and perpendicular to the lateral walls. For the parallel component, which presumably corresponds to what is measured experimentally, he found a 15% decrease in T_c which is independent of W, and a broadening of the transition which varies as $\sim(\ln W)^{-2}$. The measured shifts shown in Fig. 52 do not support a constant decrease in T_c.

Also shown in Fig. 52, as the full box, is the data point associated with the onset of superfluidity in channels used in the 3D to 0D heat-capacity measurement discussed in Sec. VII. The dimensions of these channels, $L\times S\times W$, are $10\ \text{nm}\times\sim 2\ \mu\text{m}\times 2\ \mu\text{m}$. One can see from the location of Δt_c for these channels that the onset of superfluidity is much closer to T_λ than the closed circles, which represent channels 2000 μm long. If one argues that having the length comparable to the width makes the connecting channels fully finite, then they will represent 2D to 0D crossover with an expected Δt_c *larger* than the filled circles. The opposite is true. Hence one would have to conclude that these short channels, connecting the already superfluid boxes, have their T_c *enhanced* by this contact. This proximity effect is the other side of the coin in the connected-box measurements: we have seen that the specific heat is enhanced via the coupling through the normal channels, and now see that the onset of superfluidity in the channels themselves is enhanced by the presence of the superfluid boxes. These are both interesting effects that need to be pursued more systematically in future experiments.

IX. FINITE-SIZE SCALING AND UNIVERSALITY

A. Specific heat

The superfluid transition in helium varies as a function of pressure P and ^{3}He concentration x, thus defining a surface as a function of these variables $T_\lambda(P,x)$. This surface ends at higher pressures at the solid-liquid boundary, and, at higher concentrations, at the tricritical point where it meets the surfaces of phase separation (Graf *et al.*, 1967). The superfluid transition along the two λ lines, $T_\lambda(P,x=0)$ and $T_\lambda(P_{\text{sat}},x)$, where P_{sat} is the saturated vapor pressure, has been studied in a number of experiments as a test of the expected universal behavior of critical exponents and amplitude ratios. In the case of the heat capacity, the exponent α, and the ratio of the specific-heat amplitudes above and below the transition, are shown in Fig. 53. These results are plotted as a function of $T_\lambda(P_{\text{sat}},x=0)-T_\lambda(P,x)$. This way, results as a function of pressure at $x=0$ and as a function of x at P_{sat} can be plotted together. The exponents and amplitude ratios are from the specific-heat data of bulk helium mixtures from Gasparini and Moldover (1975) and Takada and Watanabe (1980) (solid and open circles, respectively), the measurement of the thermal-expansion coefficient as a function of pressure by Mueller *et al.* (1975) (solid up triangles), and the mixture data of Lipa and Chui (1984) as analyzed by Kimball (open up triangle, this work). Data at saturated vapor pressure and zero concentration are from the specific-heat measurements of Ahlers (1971) (open square), Gasparini and Moldover (1975) (solid circles), and an analysis of Mehta *et al.* (1999) (star) which combines the above two sets of

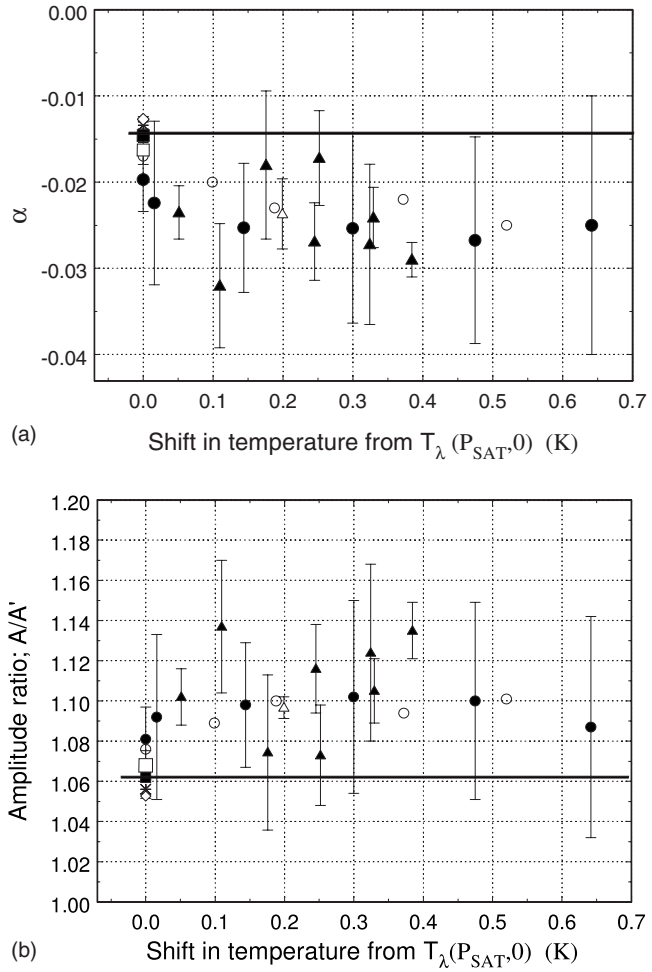

FIG. 53. The measured specific-heat critical exponent α (a) and the ratio of the specific-heat amplitudes above and below the superfluid transition A/A' (b) vs $T_\lambda(P_{\rm sat}, x=0)-T_\lambda(P,x)$. The symbols are defined in the opening paragraph of Sec. IX.A. The solid line is the theoretical result of Campostrini *et al.* (2001).

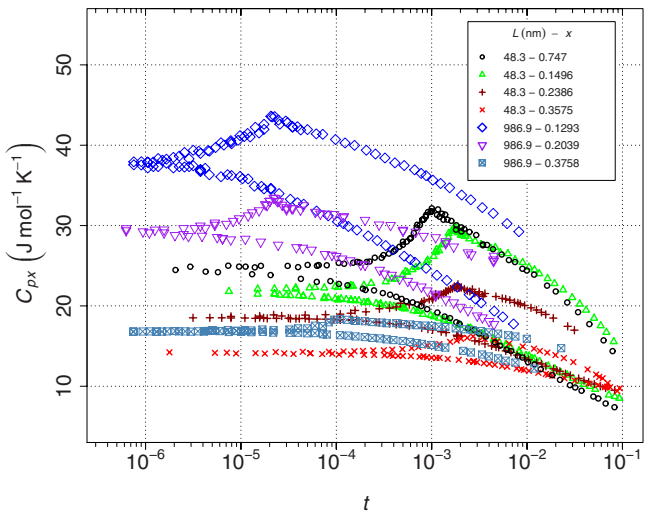

FIG. 54. (Color online) Data for the specific heat measured at constant pressure and concentration with two planar confinements that differ by a factor of 20 in height. From Kimball and Gasparini, 2005.

data plus measurements of Chen and Gasparini (1978) and Lipa and Chui (1983) to give an overall exponent and amplitude ratio. The specific-heat measurement of helium in microgravity by Lipa *et al.* (2003) is given by the open diamonds, and the theoretical values by Campostrini *et al.* (2001) as the filled squares. At $(P_{\rm sat},x=0)$ the exponents cluster around $\alpha\simeq-0.015$ with the most recent and precise value (Lipa *et al.*, 2003) at $\alpha=-0.0127\pm0.0003$. The solid line is drawn at the expected theoretical value (Campostrini *et al.*, 2001). Away from $(P_{\rm sat},x=0)$, one can see that a more negative value closer to $\alpha\simeq-0.025$ is preferred by all these data. The reason for this lack of universality in α is not clear, but it has repercussions in the finite-size scaling analysis. The leading amplitude ratio for the specific heat A/A' shows that there is a similar evolution from a value $A/A'\simeq1.05$ at $(P_{\rm sat},x=0)$ to a value close to 1.10 as one moves away from $(P_{\rm sat},x=0)$. For the superfluid fraction and the exponent ν, one would expect, using the hyperscaling relation, that ν would vary between 0.671 and 0.675 to reflect the variation in α shown in Fig. 53. There are at present no bulk data which are precise enough to test this relatively small variation in ν along the λ lines.

The universality of finite-size scaling for the specific heat was tested in a series of experiments for 2D crossover by Kimball and Gasparini (2002, 2005, 2006), and for 1D crossover by Mooney (2006). These measurements were done in experimental cells described in Secs. V and VI using a series of ^{3}He concentrations up to $x\sim0.4$. Data for $C_{px}(t,L)$ and planar confinement are shown in Fig. 54. These data are obtained with two different confinements, $L=48.3$ nm and 986.9 nm. To analyze these data for universality it is necessary to convert the measured data taken at constant concentration to the corresponding heat capacity $C_{p\phi}(\theta,L)$ where $\phi\equiv\mu_3-\mu_4$, the difference in the chemical potentials of ^{3}He and ^{4}He. One must also introduce a new reduced temperature $\theta\equiv|1-T/T_\lambda(\phi)|$, which measures the distance to the bulk transition along a path of $\phi=$const. The need for this conversion to a particular thermodynamic path is motivated by Kimball and Gasparini (2005). The thermodynamics of the conversion has been discussed by Gasparini and Moldover (1975).

The finite-size scaling function has to reflect for the mixtures the nonuniversal specific-heat amplitude $A_\phi(x)$. Thus Eq. (5) has to be modified to (Kimball and Gasparini, 2002, 2005)

$$\Delta C_{p\phi}\theta^{\alpha_\phi}\left|\frac{\alpha_\phi}{A_\phi(x)}\right|=g_2\left[\left(\frac{L}{\xi(x,t)}\right)^{1/\nu}\right], \tag{60}$$

where $\Delta C_{p\phi}\equiv C_{p\phi}(\theta,\infty)-C_{p\phi}(\theta,L)$. Note that for $x=0$ there was no need to retain the ratio of α/A on the left-hand side of Eq. (60) because these quantities were constant and could be absorbed in g_2. For the mixtures, one needs the factor $1/A_\phi$ because this is not universal, and the factor of α_ϕ is retained in view of the discussion

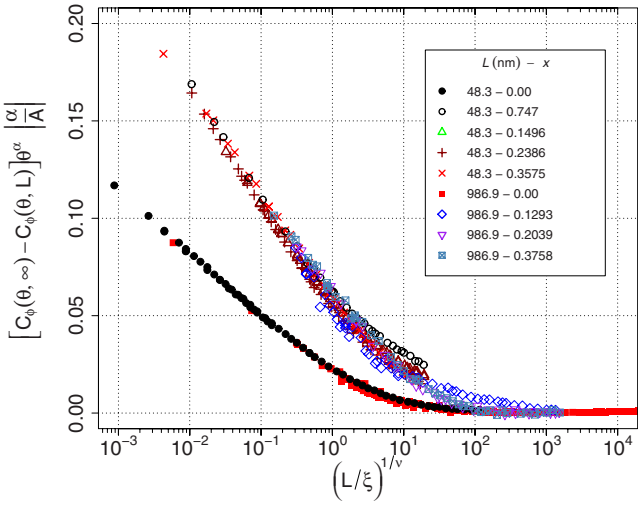

FIG. 55. (Color online) The specific-heat data shown in Fig. 54 above T_λ cast in scaling form according to Eq. (60). The mixtures with $x>0$ show good collapse amongst themselves but define a locus that is dramatically different from that defined by the $x=0$ data. The values of α and A in the scaling function come from fitting bulk data at each concentration. From Kimball and Gasparini, 2005.

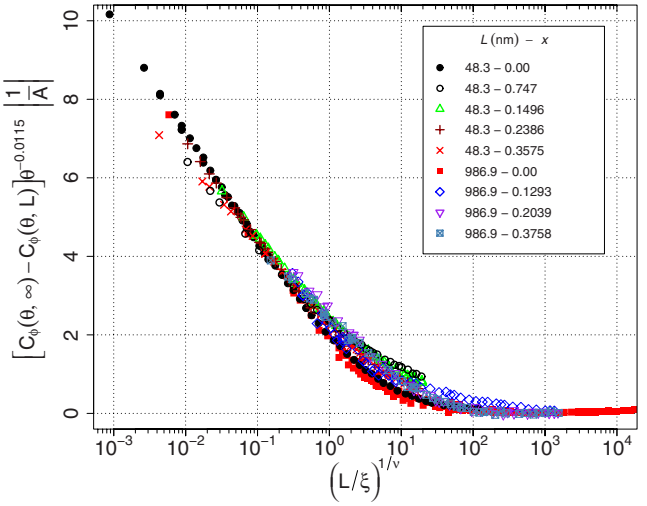

FIG. 56. (Color online) The same data as Fig. 55 except the value of α used in the scaling function is taken to be that from the $x=0$ data. This produces a reasonable collapse of all the data but is a less consistent analysis. From Kimball and Gasparini, 2005.

above and the results of Fig. 53. It is interesting to note that Eq. (60) is more sensitive to possible variations in α_ϕ than the bulk specific heat itself because α_ϕ appears not only in the term θ^{α_ϕ}—which, with α_ϕ near zero, has a weak dependence on α_ϕ—but also as a multiplicative factor.

Two ingredients are necessary to implement Eq. (60), the value of the correlation length of mixtures, and the behavior of the bulk specific heat corresponding to the mixtures listed in Fig. 54. For the former one can use the relationship between the correlation length ξ and the superfluid density ρ_s (Ferrell *et al.*, 1968; Halperin and Hohenberg, 1969). This can be cast in such a way as to relate $\xi_0(x)$ to $\xi_0(0)$,

$$\xi_0(x) = \xi_0(0)\frac{T_\lambda(x)}{T_\lambda(0)}\frac{\rho(0)}{\rho(x)}\frac{k(0)}{k(x)}, \tag{61}$$

where the transition temperature T_λ, the density ρ, and the prefactor of the superfluid fraction k are functions of concentration x. For the bulk specific heat one can interpolate existing data (Gasparini and Moldover, 1975; Takada and Watanabe, 1980) to the desired values of x (Gasparini and Moldover, 1975; Takada and Watanabe, 1980). The resulting scaling plot for all the concentrations shown in Fig. 54, and for $x=0$, for $T>T_\lambda$, is shown in Fig. 55. One can see that all the mixtures for both confinement sizes collapse on a universal locus, but this differs from the locus of the $x=0$ data. This result represents a lack of universality between $x=0$ and $x\neq 0$ for finite-size scaling, and this is a reflection of the lack of universality of α of the bulk system; Fig. 53. Note that for this plot the values of α_ϕ and A_ϕ come from fitting the bulk data at each concentration to Eq. (44) with $E=F=0$. For $x=0$ the value of $\alpha=-0.0115$ corresponding to $\nu=0.6705$ (Goldner and Ahlers, 1992) is used. Various other analyses have been discussed by Kimball and Gasparini (2005). The only analysis that seems to achieve a reasonable collapse of all the data is to fix α_ϕ to a universal exponent while at the same time retaining the values of A_ϕ which correspond to the best-fit exponent at a given x. This analysis, although not self-consistent, yields the scaling plot of Fig. 56. The collapse here is reasonable, although the data for $x=0$ still seem to have a slightly different dependence on the scaling variable. Note that, since $\xi_0(x)$ varies by a factor of about 1.9 in the range of concentrations in Fig. 53, the effective range in L which is tested by these data is a factor of about 39.

The analogous scaling plot to Fig. 55 is shown in Fig. 57 for $T<T_\lambda$. The overall picture is similar as for $T>T_\lambda$ with the mixture data separating from the locus of the $x=0$ data. However, the mixtures do not collapse as well among themselves as for $T>T_\lambda$. Note also that there is a tendency for the 48.3 nm data to be higher than the 986.9 nm data near the value of 10 in the scaling variable. This is consistent with the observation at $x=0$, seen most clearly in Fig. 20. However, the scatter in the mixture data is too large in this region to be able to make a strong statement about this. Finally, we note that an analogous analysis as for Fig. 57 can also be carried out for $T<T_\lambda$ with similar results as for $T>T_\lambda$ (see Fig. 5 in Kimball and Gasparini, 2005).

Data were also obtained for two mixtures for 1D crossover by Mooney (2006). These data were analyzed as described above and yield the scaling plots for $T>T_\lambda$ and $T<T_\lambda$ shown in Figs. 58 and 59, respectively. One can see that similar results are obtained for one as for two dimensions: the two mixtures collapse upon themselves, but on a different locus from that of $x=0$. These data were also analyzed by forcing a universal α_ϕ

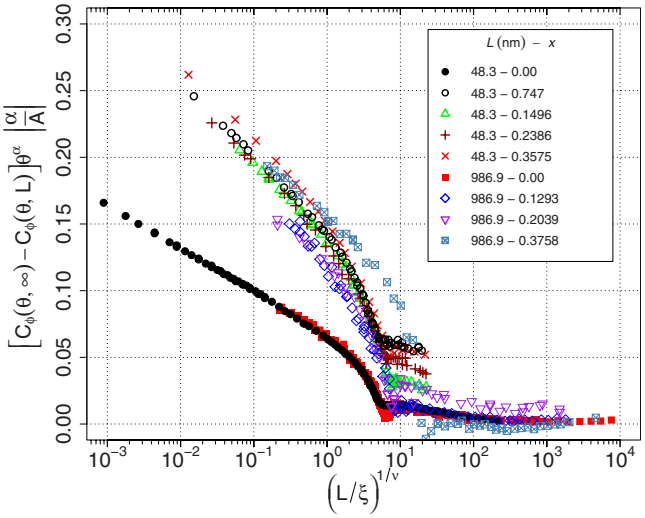

FIG. 57. (Color online) Scaling of the data from Fig. 54 below T_λ. This plot is analogous to Fig. 55. The mixture data with $x>0$ stand apart from the $x=0$ data.

and retaining A_ϕ as the best-fit amplitude as done for the 2D data. The data tend to collapse now with only small residual systematic deviations of the mixtures from the $x=0$ data.

In summary, the present specific-heat data, in a self-consistent analysis, show that for $x\neq 0$ one obtains good universal collapse for $T>T_\lambda$. This is true for both 2D and 1D crossover. This must be viewed as strong support of universality. The fact that one obtains a different scaling locus for $x=0$ is more indicative of the fact that the bulk system, as evidenced in Fig. 53, yields an exponent α_ϕ which appears not to be universal.

B. Superfluid density

The superfluid density for ^{3}He-^{4}He mixtures confined in a planar cell at $L=48.3$ nm was reported by Kimball and Gasparini (2001). These data were obtained using the same cell as used for the heat capacity; see Sec. V.A. The AFR technique was used for these measurements whereby the superfluid was driven in resonance between the cell and the filling line; see Fig. 11. Because this cell was designed for heat-capacity measurements, the center section, as shown in Fig. 12, had a series of filling channels 48.3 nm high, 3 μm wide, and 4 mm long. Thus the measured superfluid fraction is characteristic of this geometry. The data for three concentrations and for $x=0$ are shown in Fig. 60. The solid line in this figure represents the bulk superfluid fraction (Greywall and Ahlers, 1973). For the mixtures, the data are normalized to bulk values as given by Schubert and Zimmermann (1981). The + sign on this plot represents the expected jump in ρ_s/ρ at T_c for $x=0$ according to Kosterlitz-Thouless theory [see Eq. (22)]. One can see that the data end close to this value which cannot be reached because

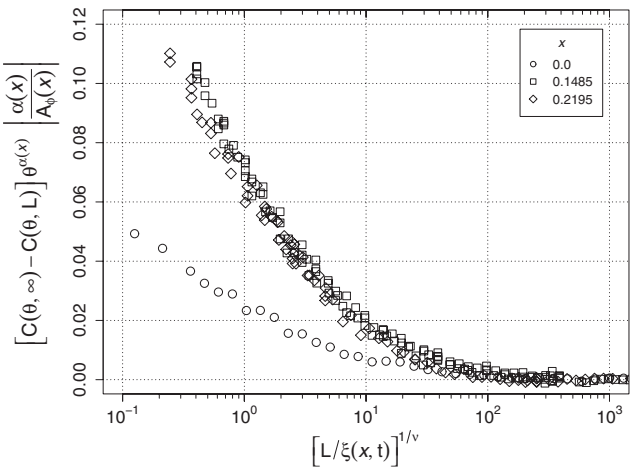

FIG. 58. Data above T_λ for mixtures confined to 1D channels scaled according to Eq. (60) (Mooney, 2006). As seen in the planar data, the mixtures with $x>0$ define a locus that differs from the one defined by the $x=0$ data.

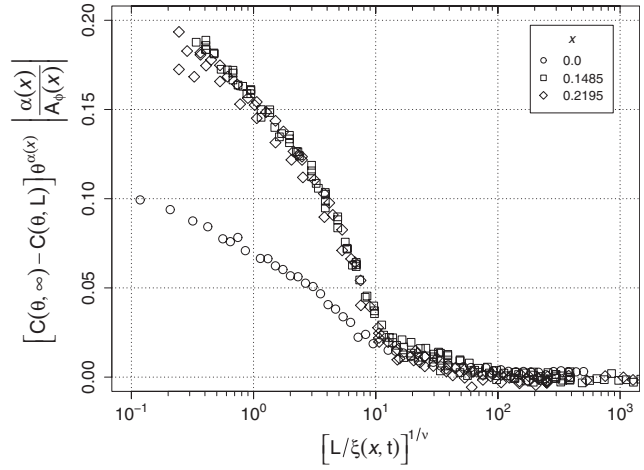

FIG. 59. The equivalent plot to Fig. 58 below T_λ. The mixtures data for $x>0$ define a separate locus from the $x=0$ data.

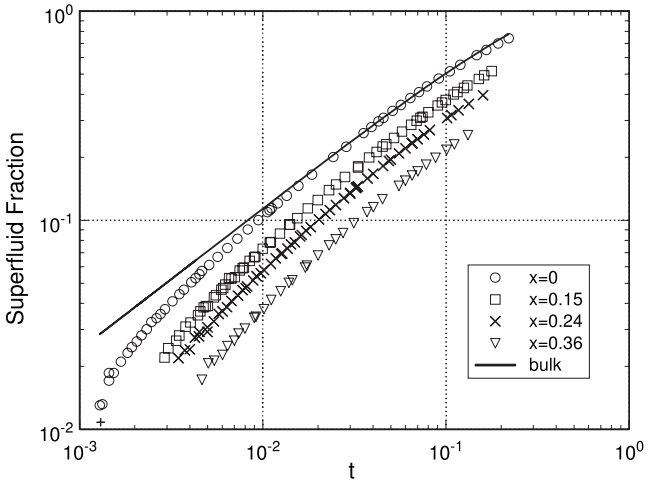

FIG. 60. The superfluid fraction of both pure ^{4}He and mixtures of ^{2}He-^{4}Heconfined to a 48.3-nm-high and 3-μm-wide channel. The solid line is the superfluid fraction for bulk pure ^{4}He. The bulk data for the $x>0$ mixtures have been omitted for clarity. From Kimball and Gasparini, 2001.

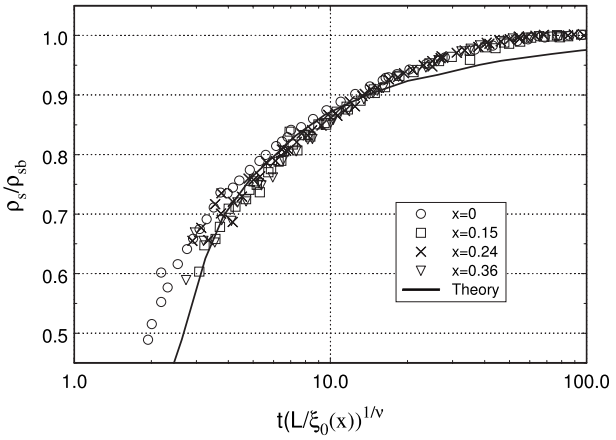

FIG. 61. The scaling of the superfluid fraction of helium mixtures confined to a 48.3-nm planar geometry according to Eq. (62). The solid line is the field-theory calculation of Schmolke *et al.* (1990). Adapted from Kimball and Gasparini, 2001.

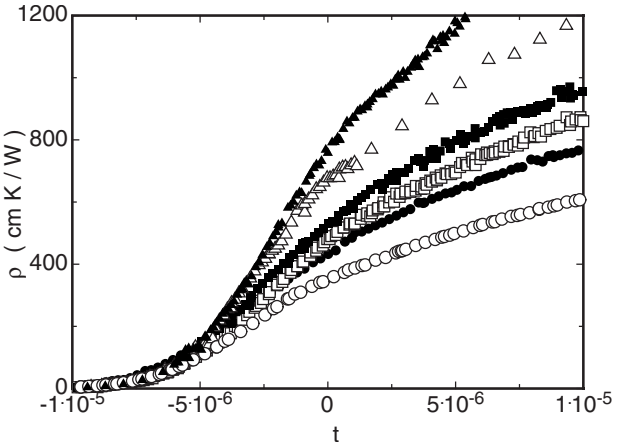

FIG. 62. The thermal resistivity near $T_\lambda(P)$ of helium confined to 1-μm-diameter glass capillaries as function of pressure. The data are as follows: open circles, SVP; solid circles, 6.95 bars; open squares, 11.25 bars; solid squares, 14.73 bars; open triangles, 22.31 bars; solid triangles, 28.00 bars. From Murphy *et al.*, 2003.

of the increased dissipation in the resonance (see Fig. 4 in Kimball and Gasparini, 2001). The shift in T_c from T_λ is as expected for a planar film which is not laterally confined; see Fig. 24. Thus it appears that for a 48-nm-thick film in a 3-μm-wide channel, the effects described for the laterally confined 10-nm films are too small to be observed. It would appear that for these effects to be manifest a thin film that represents more closely a strictly 2D geometry is necessary. It is interesting to note that the aspect ratio between the width and height of the 48 nm film was ~62 while this ratio for the 10-nm-thin films discussed in Sec. VIII was between 300 and 1900.

To scale the data in Fig. 60, one can use the following:

$$\frac{\rho_s(t,L)}{\rho} = \frac{\rho_s(t,\infty)}{\rho} G\left[t\left(\frac{L}{\xi_0(x)}\right)^{1/\nu}\right]. \tag{62}$$

This is basically the same as Eq. (19) with the function $G=1-X$, except here the amplitude of the correlation length is a function of the ^{3}He concentration. One can obtain values for $\xi_0(x)$ from Eq. (61). We note that in the analysis of the superfluid fraction there is no need for a thermodynamic path correction because, unlike the specific heat, the superfluid fraction has a unique value at any (t,x) which is not dependent on a path constraint of constant concentration or chemical potential. The scaling plot for these data is shown in Fig. 61. One can see that there is good collapse of these data, with perhaps a tendency for the mixtures to lie below the pure system for values of the scaling variable less than about 10. However, this is relatively benign when compared with the behavior of the specific heat as seen in Figs. 55 and 58. It has also been suggested that this small discrepancy might be attributed to concentration gradients near the walls (Kimball and Gasparini, 2001). The solid curve on this plot is the result of the field-theory calculation of Schmolke *et al.* (1990). The theory, which has no adjustable parameters, agrees quite well with these data, especially in the midrange of the scaling variable. Another way to look at these data is to realize that, as $\xi_0(x)$ increases with concentration, the confinement at $L=48.3$ nm appears smaller to the mixtures. One may look then at a mixture as effectively being confined in a size relative to $x=0$ given by $L_{\text{effective}}=L[\xi_0(0)/\xi_0(x)]$. At the highest concentration this is $L_{\text{effective}}=25.7$ nm (Kimball and Gasparini, 2001). Thus a range in L of a factor of ~1.9 is explored this way. A more global look at the scaling of the superfluid density at $x=0$, for a range of L of about 80, is shown in Fig. 28. There is no collapse of these data. In light of this, one might conclude that the collapse of the data in Fig. 61 is a reflection of the relatively narrow range of $L_{\text{effective}}$ probed.

C. Thermal conductivity

The thermal conductivity of confined helium has been measured by Murphy *et al.* (2003) as a function of pressure. These data were obtained for helium confined in a cylindrical geometry of glass capillary arrays. Part of this work was discussed already in Sec. VI.D in the context of scaling for 1D crossover. Here we are interested in the portion of these data which were obtained as a function of pressure and can be used to test universality. These data are shown in Fig. 62. Pressures range from saturated vapor pressure (SVP) (0.05 bar) to 28 bars. The confinement is in pores of 1-μm radius. Note that for this plot ρ is the thermal resistivity r as used in the Introduction. To test universality the following scaling function is used:

$$\frac{r(t,P,L)}{r_0(P)}\left(\frac{L}{\xi_0(P)}\right)^{1/\nu} = F\left[t\left(\frac{L}{\xi_0(P)}\right)^{1/\nu}\right]. \tag{63}$$

Comparing this to the scaling function R used in the Introduction, one has

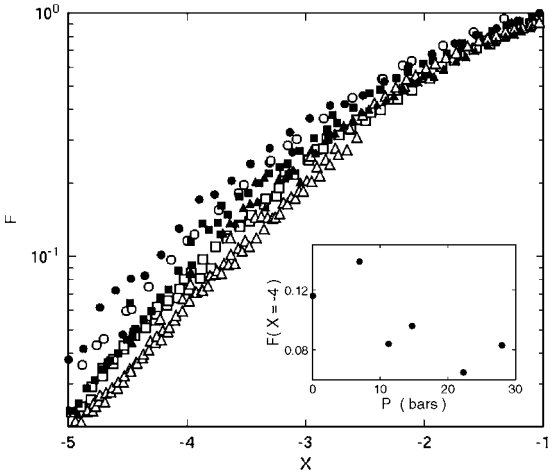

FIG. 63. The thermal resistivity data shown in Fig. 62 below T_λ scaled according to Eq. (63). For $X>-2$, the data show a collapse within their precision. Below this, they show a systematic opening with pressure. The trend with pressure is more easily seen in the inset. From Murphy *et al.* (2003).

$$R = (F)\left(\frac{L}{\xi}\right)^{-\mu/\nu} - 1. \tag{64}$$

As noted in the Introduction, scaling using the function R yields an equation analogous to that of the specific heat [see Eqs. (5) and (32)].

Using Eq. (63), Murphy *et al.* (2003) found that, to first order, there is reasonable collapse of these data on a universal locus. However, a closer look at the data below T_λ shows that some systematic differences are manifest. This is shown in Fig. 63. In this plot one has $X \equiv t[L/\xi(P)]^{1/\nu}$. The data do indeed open up for negative X, the region for $T<T_\lambda$. The inset in this figure emphasizes the trend with pressure by indicating how F varies at the fixed value $X=-4$.

In comparing these results for thermal resistivity as a function of pressure with the specific heat as a function of concentration, we note that the latter fails to collapse on the locus defined by the $x=0$ data, while it collapses on its own locus for all concentrations. For the resistivity, the data at various pressures (analogous to various concentrations) open up systematically as a function of pressure. In the case of the specific heat it seems clear that its behavior, to first order, is due to the fact that the exponent α_ϕ [see Eq. (60)] changes by a factor ~ 2 in going from $x=0$ to $x\neq 0$. This affects both sides of the transition, $T>T_\lambda$ and $T<T_\lambda$. In the case of the resistivity, the analogous exponent μ changes by only $\sim 6\%$ over the range of the data. Thus it would not seem that this would be principally responsible for the behavior seen in Fig. 63. Indeed, if it were simply the variations in this exponent which causes lack of universality, it should be seen on both sides of T_λ, as is observed for the specific heat. We note that over the range of the pressure data $\xi_0(P)$ and $r_0(P)$ change by 8.2% and 81%, respectively, between SVP and 28 bars. For the mixture data, the analogous quantities $\xi_0(x)$ and $A_\phi(x)$ change by 90% and 60% from $x=0$ to the highest concentrations measured.

X. SUMMARY

The experimental results reviewed in this paper allow us to make some general conclusions about correlation-length scaling; however, at the same time, they leave a number of questions unanswered. Irrespective of this, the amount of data available for the superfluid transition of confined helium represents the most comprehensive experimental work that probes correlation-length scaling and universality in a critical system.

The most coherent results are obtained from studies of helium in a planar confinement for 2D crossover. Here, the picture that emerges is fairly clear: in the region where the helium remains normal there is excellent scaling over a wide range of confinements. The scaling yields the correct critical exponent ν and, independent from the bulk specific heat, produces a value of $C(0,\infty)$ which agrees with the analysis of most recent bulk data. These data also yield a value for the surface specific heat which is in agreement with theory. These results must be viewed not only as support of correlation-length scaling when the helium is normal, but also as an indication of the internal consistency of all these data.

The region near the specific-heat maximum and for lower temperatures, where the helium becomes superfluid, is problematic. The magnitude of the specific-heat maximum does not scale properly and the superfluid fraction, obtained in independent experiments, fails to scale altogether. Overall this suggests that for 2D crossover, when fluctuations are large, scaling the confined film with the 3D correlation length fails, as indeed it fails below the superfluid onset where the order parameter is not zero. Interestingly, the *temperature* of the specific-heat maximum—as opposed to the *value* of the maximum—as well as the temperature for the onset of superfluidity, scale properly and yield, in an independent way from the overall scaling, the correct correlation-length exponent. These results emphasize the fact that single-point (or-temperature) features of the data such as the shift of $C_{\max}$ or the onset T_c might well scale, even though there might be no overall scaling of the data over a range of the scaling variable. In contrast to the specific-heat and superfluid density results, data for thinning of helium films show good overall collapse for both the normal and the superfluid sides. These data, however, span only a range of 1.3 in L as opposed to over 1000 and 80 for the specific heat and superfluid density, respectively. Thus these data might well miss trends which become visible over a wider range of confinements. Interestingly, the maximum in the thinning region agrees identically with the position of the specific-heat maximum. Further, a feature in these data suggests that the superfluid onset is also in agreement with the onset obtained from measurements of the superfluid density and thermal conductivity of films.

In the case of 1D crossover, data are not as plentiful as for 2D crossover. In particular, it appears that experi-

ments with Nuclepore filters, which have been used to confine helium in many experiments, represent a confinement that is not strictly 1D. Specifically, there are issues with connectivity and coupling of the pores in these filters. The specific heat over a narrow range of pore sizes can be scaled, but the scaling locus differs from that of the most recent experiments for 1D crossover. These recent experiments can be scaled on both the normal and superfluid sides with some lack of collapse near the heat-capacity maximum. However, this lack of scaling near the maximum is not systematic with size, and might well represent experimental problems. Interestingly, the magnitude of the specific-heat maximum for 1D crossover yields the correct value for $C(0,\infty)$ in contrast to the 2D crossover case. Additional data for 1D crossover are needed to possibly confirm scaling and hence the possibility that 2D crossover is unique in the lack of scaling.

Also, for 1D crossover, there are data for the superfluid fraction using Nuclepore filters as well as for the onset of superflow. The latter, coming from several investigators, is consistent with a shifted onset temperature governed by the exponent ν. The former, which involves the temperature dependence of the superfluid fraction over the full critical region, does not scale properly. It is not clear at this time whether this represents difficulties with the homogeneity or the uniqueness of the confinement—as remarked in the case of the specific heat—or, as the data for 2D crossover indicate, a lack of scaling in a region where the order parameter is not zero. This would clearly be a more fundamental conclusion. There are no other data for 1D confinement that can be brought to bear on this issue. This is an area where future experiments would be most revealing.

Thermal conductivity data for 1D crossover have been obtained for confinement in glass capillary arrays for two pore sizes differing by a factor of 2. These data indicate scaling in the region above T_λ and show lack of scaling below. These data behave in an analogous way to the specific heat for 2D crossover, but not the specific heat for 1D crossover. These data also correlate in behavior with the superfluid density for 1D crossover in Nuclepore filters where there is also a lack of scaling. However, given the possible ambiguity with the Nuclepore confinement representing true 1D crossover, data over a wider range of sizes for the thermal conductivity are needed to confirm these conclusions.

Data for 0D crossover are available only for the specific heat with two characteristic sizes differing by a factor of 2. The realization of this confinement is via a collection of boxes made lithographically on an oxidized silicon wafer. These are connected with shallow channels where the helium remains normal over the full range in which data are taken. While these data for 0D crossover do reflect the expected trends with lower-dimensionality crossover established by the 2D and 1D data, they cannot be scaled with size. The evidence suggests that, even though the connecting channels remain normal, they provide a coupling among the boxes which adds an element of collective behavior to the desired behavior of isolated boxes. It is also evident from the superfluid onset in the connecting channels that this is in turn influenced by the already superfluid helium in the boxes. Thus the present data provide an interesting possibility of studying collective effects in coupled superfluids in a well-defined geometry. Experiments in which boxes are separated at much larger distances are necessary to realize truly isolated 0D superfluids. A bonus from these studies is the realization that the presence of bulk helium in equilibrium with the confined helium will affect the behavior of the confined helium in a way that cannot be corrected by a simple subtraction. Further, in the case of Nuclepore filters the uniqueness of their confinement, as far as the specific heat is concerned, might well come not only from the connectivity of the pores but also from the coupling of the pores via a film which is in equilibrium with the filled pores. The data for 0D crossover suggest that this can take place even if such a film is normal.

Data for crossover from 2D to 1D can be obtained using a geometry of a shallow and long channel that has a finite width. Such data are of interest to see if simple scaling with the 2D correlation length is appropriate, or if the lateral confinement plays a more significant role. One finds that the shift in the transition temperature in this geometry is a power law as opposed to the logarithmic behavior expected from scaling with the 2D correlation length. This power-law behavior has been predicted theoretically; however, the magnitude of the exponent does not seem to agree.

There are a number of experiments that have tested the expected universality along the lambda lines as a function of ^{3}He concentration and pressure. For the specific heat of mixtures, for both 2D and 1D crossover, one finds that the data for mixtures fall on a universal locus that differs from the locus at zero concentration. This collapse of the mixtures among themselves, but not on the pure system, reflects the variation of the exponent α as one moves away from the point at saturated vapor pressure and zero concentration. It is thus a problem in the bulk system rather than the confined system. The confined specific heat is more sensitive to variations in α than the bulk data. The thermal conductivity has also been measured as a function of pressure to check on the expected universal behavior. One finds that these data collapse on a universal locus above T_λ, but indicate lack of scaling below T_λ.

ACKNOWLEDGMENTS

We are grateful to the U.S. National Science Foundation for over 30 years of support of our research efforts. In particular, we acknowledge our current grant, Grant No. DMR-0605716. We are also grateful for the support and access to the Cornell NanoScale Science and Technology Facility who has supported our work with silicon wafers through Project No. 526-94 since 1994. We acknowledge as well the support of the Cryogenic Facility of the University at Buffalo's Instrument Facility.

REFERENCES

Adams, P. W., 1978, Ph.D. thesis (Rutgers University, New Brunswick, NJ).

Adams, P. W., and W. I. Glaberson, 1987, "Vortex dynamics in superfluid helium films," Phys. Rev. B **35**, 4633–4652.

Agnolet, G., D. F. McQueeney, and J. D. Reppy, 1989, "Kosterlitz-Thouless transition in helium films," Phys. Rev. B **39**, 8934–8958.

Agnolet, G., S. L. Teitel, and J. D. Reppy, 1981, "Thermal transport in a ^{4}He film at the Kosterlitz-Thouless transition," Phys. Rev. Lett. **47**, 1537–1540.

Ahlers, G., 1971, "Heat capacity near the superfluid transition in ^{4}He at saturated vapor pressure," Phys. Rev. A **3**, 696–716.

Ahlers, G., 1973, "Thermodynamics and experimental tests of static scaling and universality near the superfluid transition in ^{4}He under pressure," Phys. Rev. A **8**, 530–568.

Ahlers, G., 1999, "Finite-size and gravity effects on the thermal conductivity of ^{4}He near the λ line," J. Low Temp. Phys. **115**, 143–172.

Ahlers, G., and R. V. Duncan, 1988, "Finite-size effects on the thermal conductivity of ^{4}He near the superfluid transition," Phys. Rev. Lett. **61**, 846–848.

Ahlers, G., P. C. Hohenberg, and A. Kornblit, 1982, "Nonlinear renormalization-group analysis of the thermal conductivity of ^{4}He for $T<T_\lambda$," Phys. Rev. B **25**, 3136–3167.

Ambegaokar, V., B. I. Halperin, D. R. Nelson, and E. D. Siggia, 1980, "Dynamics of superfluid films," Phys. Rev. B **21**, 1806–1826.

Andronikashvili, E. L., 1946, "Direct observation of two types of motion in helium II," J. Phys. (Moscow) **10**, 201.

Aouaroun, T., and G. Ahlers, 2007, "Specific heat of ^{4}He confined in cylindrical micro-channels and near the superfluid transition," J. Low Temp. Phys. **149**, 209–221.

Baker, G. A., Jr., 1990, *Quantitative Theory of Critical Phenomena* (Academic, Boston).

Barber, M. N., 1973, "Critical phenomena in systems of finite thickness. II. Ideal Bose gas," Aust. J. Phys. **26**, 483–500.

Barber, M. N., 1977, "Helicity modulus for an ideal Bose fluid," J. Phys. A **10**, 1335–1343.

Barber, M. N., 1983, in *Phase Transitions and Critical Phenomena*, edited by C. Domb and J. Lebowitz (Academic, New York), Vol. 8, pp. 146–259.

Barber, M. N., and M. E. Fisher, 1973, "Critical phenomena in systems of finite thickness. III. Specific heat of an ideal boson film," Phys. Rev. A **8**, 1124–1135.

Barmatz, M., I. Hahn, J. Lipa, and R. Duncan, 2007, "Critical phenomena in microgravity: Past, present, and future," Rev. Mod. Phys. **79**, 1–52.

Berezinskii, V., 1971, "Destruction of long range order in one-dimensional and two-dimensional systems having a continuous symmetry group. I. Classical systems," Sov. Phys. JETP **32**, 493.

Bhattacharjee, J. K., and R. A. Ferrell, 2003, "Effect of confinement on the critical specific heat of liquid helium near the lambda point," J. Low Temp. Phys. **132**, 55–76.

Bishop, D. J., and J. D. Reppy, 1978, "Study of the superfluid transition in two-dimensional ^{4}He films," Phys. Rev. Lett. **40**, 1727–1730.

Bishop, D. J., and J. D. Reppy, 1980, "Study of the superfluid transition in two-dimensional ^{4}He films," Phys. Rev. B **22**, 5171–5185.

Blöte, H. W. J., and M. P. Nightingale, 1982, "Critical behaviour of the two-dimensional Potts model with a continuous number of states; A finite size scaling analysis," Physica A **112**, 405–465.

Bretz, M., 1973, "Heat capacity of multilayer ^{4}He on graphite," Phys. Rev. Lett. **31**, 1447–1450.

Brewer, D. F., 1970, "Some thermal, magnetic, and flow properties of adsorbed He and He3-He4 mixtures," J. Low Temp. Phys. **3**, 205–224.

Brewer, D. F., and K. Mendelssohn, 1961, "Transfer of the unsaturated helium II film," Proc. R. Soc. London, Ser. A **260**, 1–12.

Brewer, D. F., A. J. Symonds, and A. L. Thomson, 1965, "Gapless surface excitations in liquid helium," Phys. Rev. Lett. **15**, 182–184.

Brézin, E., 1982, "An investigation of finite size scaling," J. Phys. (France) **43**, 15–22.

Brooks, J. S., B. B. Sabo, P. C. Schubert, and W. Zimmermann, Jr., 1979, "Helmholtz-resonator measurements of the superfluid density of liquid ^{4}He in submicrometer-diameter channels," Phys. Rev. B **19**, 4524–4544.

BURLE Electro-Optics Inc., Sturbridge Business Park, P.O. Box 1165, Sturbridge, MA 01566.

Campostrini, M., M. Hasenbusch, A. Pelissetto, P. Rossi, and E. Vicari, 2001, "Critical behavior for the three-dimensional *XY* universality class," Phys. Rev. B **63**, 214503.

Cardy, J. L., 1988, Ed., *Finite-Size Scaling, Current Physics—Sources and Comments* No. 2 (North-Holland, Amsterdam).

Casimir, H. B. G., 1948, "On the attraction between two perfectly conducting plates," Proc. K. Ned. Akad. Wet. **51**, 793.

Chalyy, K., 2004, "Heat capacity of cylindrically confined helium: Theoretical predictions versus experimental data," Low Temp. Phys. **30**, 686–690.

Chen, T.-P., 1978, Ph.D. thesis (University at Buffalo, the State University of New York, Buffalo).

Chen, T. P., M. J. DiPirro, B. Bhattacharyya, and F. M. Gasparini, 1980, "Some properties of Nuclepore filters," Rev. Sci. Instrum. **51**, 846–848.

Chen, T.-P., and F. M. Gasparini, 1977, "Specific heat of unsaturated ^{4}He films near T_λ," Phys. Lett. **62A**, 231–233.

Chen, T.-P., and F. M. Gasparini, 1978, "Scaling of the specific heat of confined helium near T_λ," Phys. Rev. Lett. **40**, 331–333.

Chen, X. S., and V. Dohm, 1999, "Violation of finite-size scaling in three dimensions," Eur. Phys. J. B **10**, 687–703.

Chen, X. S., and V. Dohm, 2000, "Relation between bulk order-parameter correlation function and finite-size scaling," Eur. Phys. J. B **15**, 283–296.

Chen, X. S., and V. Dohm, 2004, "Nonuniversal finite-size scaling in anisotropic systems," Phys. Rev. E **70**, 056136.

Chen, X. S., V. Dohm, and N. Schultka, 1996, "Order-parameter distribution function of finite $O(n)$ symmetric systems," Phys. Rev. Lett. **77**, 3641–3644.

Cheng, E., M. W. Cole, W. F. Saam, and J. Treiner, 1991, "Helium prewetting and nonwetting on weak-binding substrates," Phys. Rev. Lett. **67**, 1007–1010.

Chester, M., and L. C. Yang, 1973, "Superfluid fraction in thin helium films," Phys. Rev. Lett. **31**, 1377–1380.

Clow, J. R., and J. D. Reppy, 1966, "Temperature dependence of the superfluid density in He II near T_λ," Phys. Rev. Lett. **16**, 887–889.

Cole, M. W., and W. F. Saam, 1974, "Excitation spectrum and thermodynamic properties of liquid films in cylindrical pores," Phys. Rev. Lett. **32**, 985–988.

Coleman, M., and J. A. Lipa, 1995, "Heat capacity of helium confined to 8-μm cylinders near the λ point," Phys. Rev. Lett. **74**, 286–289.

De Dominicis, C., and L. Peliti, 1978, "Field-theory renormalization and critical dynamics above T_c: Helium, antiferromagnets, and liquid-gas systems," Phys. Rev. B **18**, 353–376.

Diaz-Avila, M., 2006, Ph.D. thesis (University at Buffalo, the State University of New York, Buffalo).

Diaz-Avila, M., F. M. Gasparini, and M. O. Kimball, 2004, "Behavior of ^{4}He near T_λ in films of infinite and finite lateral extent," J. Low Temp. Phys. **134**, 613–618.

Dingus, M., F. Zhong, and H. Meyer, 1986, "Thermal transport properties in helium near the superfluid transition. I. ^{4}He in the normal phase," J. Low Temp. Phys. **65**, 185–212.

Dionne, R. J., and R. B. Hallock, 1989, in *Quantum Fluids and Solids—1991*, edited by G. G. Ihas and Y. Takano, AIP Conf. Proc. No. 194 (AIP, New York), pp. 199–200.

Dohm, V., 1978, "Discontinuity of the dynamic critical exponents of O(n)-symmetric systems," Z. Phys. B **31**, 327–331.

Dohm, V., 1985, "Nonuniversal critical phenomena along the lambda line of ^{4}He. II. Thermal conductivity in three dimensions," Z. Phys. B: Condens. Matter **61**, 193–204.

Dohm, V., 1991, "Renormalization-group flow equations of model F," Phys. Rev. B **44**, 2697–2712.

Dohm, V., 1993, "The superfluid transition in confined ^{4}He: Renormalization-group theory," Phys. Scr. **T49**, 46–58.

Dohm, V., 2006, "Model F in two-loop order and the thermal conductivity near the superfluid transition of ^{4}He," Phys. Rev. B **73**, 092503.

Dohm, V., 2008, e-print arXiv:0801.4096v1.

Dohm, V., and R. Folk, 1981, "Nonlinear dynamic renormalization-group analysis above and below the superfluid transition in ^{4}He," Phys. Rev. Lett. **46**, 349–352.

Domb, C., 1996, *The Critical Point* (Taylor & Francis, London).

Duncan, R. V., G. Ahlers, and V. Steinberg, 1987, "Singularity in the Kapitza resistance between gold and superfluid ^{4}He near T_λ," Phys. Rev. Lett. **58**, 377–380.

Dzyaloshinskii, I. E., E. M. Lifshitz, and L. P. Pitaevskii, 1961, "The general theory of van der Waals forces," Adv. Phys. **10**, 165–209.

Ferdinand, A. E., and M. E. Fisher, 1969, "Bounded and inhomogeneous Ising models. I. Specific-heat anomaly of a finite lattice," Phys. Rev. **185**, 832–846.

Ferrell, R. A., N. Menyhárd, H. Schmidt, F. Schwabl, and P. Szépfalusy, 1967, "Dispersion in second sound and anomalous heat conduction at the lambda point of liquid helium," Phys. Rev. Lett. **18**, 891–894.

Ferrell, R. A., N. Menyhard, H. Schmidt, F. Schwabl, and P. Szépfalusy, 1968, "Fluctuations and lambda phase transition in liquid helium," Ann. Phys. (N.Y.) **47**, 565.

Finotello, D., and F. M. Gasparini, 1985, "Universality of the Kosterlitz-Thouless transition in ^{4}He films as a function of thickness," Phys. Rev. Lett. **55**, 2156–2159.

Finotello, D., Y. Y. Yu, and F. M. Gasparini, 1990, "Universal behavior of ^{4}He films as a function of thickness near the Kosterlitz-Thouless transition," Phys. Rev. B **41**, 10994–11010.

Fisher, M., and P.-G. de Gennes, 1978, "Wall phenomena in a critical binary mixture," C. R. Acad. Sci., Ser. B **287**, 207–209.

Fisher, M. E., 1971, in *Critical Phenomenon, Proceedings of the 51st "Enrico Fermi" Summer School, Varenna, Italy*, edited by M. Green (Academic, New York), pp. 1–97.

Fisher, M. E., and M. N. Barber, 1972, "Scaling theory for finite-size effects in the critical region," Phys. Rev. Lett. **28**, 1516–1519.

Fisher, M. E., and R. J. Burford, 1967, "Theory of critical-point scattering and correlations. I. The Ising model," Phys. Rev. **156**, 583–622.

Fisher, M. E., and A. E. Ferdinand, 1967, "Interfacial, boundary, and size effects at critical points," Phys. Rev. Lett. **19**, 169–172.

Folk, R., and G. Moser, 2002, "Dynamic critical behavior near the superfluid transition in ^{3}He-^{4}He Mixtures in two loop order," Phys. Rev. Lett. **89**, 125301.

Frank, D., and V. Dohm, 1989, "Critical thermal boundary resistance of ^{4}He near T_λ," Phys. Rev. Lett. **62**, 1864–1867.

Frank, D., and V. Dohm, 1990, "Critical thermal resistance of confined 4He above T_λ," Physica B **165-166**, 543–544.

Frederikse, H. P. R., 1949, "On the specific heat of adsorbed helium," Physica (Amsterdam) **15**, 860–862.

Ganshin, A., S. Scheidemantel, R. Garcia, and M. H. W. Chan, 2006, "Critical Casimir force in ^{4}He films: Confirmation of finite-size scaling," Phys. Rev. Lett. **97**, 075301.

Garcia, R., and M. H. W. Chan, 1999, "Critical fluctuation-induced thinning of ^{4}He films near the superfluid transition," Phys. Rev. Lett. **83**, 1187–1190.

Gasparini, F. M., G. Agnolet, and J. D. Reppy, 1984, "Failure of bulk-correlation-length scaling for the superfluid density of confined ^{4}He," Phys. Rev. B **29**, 138–149.

Gasparini, F. M., T.-P. Chen, and B. Bhattacharyya, 1981, "Corrections to scaling and surface specific heat of confined helium," Phys. Rev. B **23**, 5797–5814.

Gasparini, F. M., and A. A. Gaeta, 1978, "Universality of the specific heat of ^{3}He-^{4}He mixtures at the λ transition," Phys. Rev. B **17**, 1466–1471.

Gasparini, F. M., M. O. Kimball, and S. Mehta, 2001, "Adiabatic fountain resonance for ^{4}He and ^{3}He-^{4}He mixtures," J. Low Temp. Phys. **125**, 215–238.

Gasparini, F. M., and S. Mehta, 1998, "Temperature oscillations of an adiabatic superleak," J. Low Temp. Phys. **110**, 293–296.

Gasparini, F. M., and S. Mhlanga, 1986, "Fractal surface dimensionality and finite-size scaling at the superfluid transition of confined ^{4}He," Phys. Rev. B **33**, 5066–5069.

Gasparini, F. M., and M. R. Moldover, 1969, "Specific heat of mixtures mixtures very near the λ line," Phys. Rev. Lett. **23**, 749–752.

Gasparini, F. M., and M. R. Moldover, 1975, "Specific heat of ^{4}He and ^{3}He-^{4}He mixtures at their λ transition," Phys. Rev. B **12**, 93–113.

Gasparini, F. M., and I. Rhee, 1992, in *Progress in Low Temperature Physics*, edited by D. F. Brewer (North-Holland, New York), Vol. 13, pp. 1–90.

Genio, E., D. Murphy, G. Ahlers, F. Liu, and Y. Liu, 2005, "Scaling and universality of the thermal conductivity of liquid ^{4}He near the superfluid transition and in restricted geometries," Adv. Space Res. **35**, 87–91.

Ginzburg, V. L., and L. P. Pitaevskii, 1958, "On the theory of superfluidity," Zh. Eksp. Teor. Fiz. **34**, 1240 [Sov. Phys. JETP **7**, 858 (1958)].

Ginzburg, V. L., and A. A. Sobyanin, 1976, "Superfluidity of helium II near the λ-point," Sov. Phys. Usp. **10**, 773.

Ginzburg, V. L., and A. A. Sobyanin, 1982, "On the theory of superfluidity of helium II near the λ point," J. Low Temp. Phys. **49**, 507–543.

Ginzburg, V. L., and A. A. Sobyanin, 1987, "Superfluidity of helium II near the λ—point," Jpn. J. Appl. Phys., Part 1 **26**, 1785.

Giordano, N., 1983, "Experimental study of the flow of liquid ^{4}He through very small channels: Finite-size effects near T_λ," Phys. Rev. B **27**, 5447–5459.

Goldner, L. S., and G. Ahlers, 1992, "Superfluid fraction of ^{4}He very close to T_λ," Phys. Rev. B **45**, 13129–13132.

Goldner, L. S., N. Mulders, and G. Ahlers, 1993, "Second sound very near T_λ," J. Low Temp. Phys. **93**, 125–176.

Gösele, U., and Q.-Y. Tong, 1998, "Semiconductor wafer bonding," Annu. Rev. Mater. Sci. **28**, 215–239.

Graf, E. H., D. M. Lee, and J. D. Reppy, 1967, "Phase separation and the superfluid transition in liquid ^{3}He-^{4}He Mixtures," Phys. Rev. Lett. **19**, 417–419.

Greywall, D. S., and G. Ahlers, 1972, "Second-sound velocity, scaling, and universality in He II under pressure near the superfluid transition," Phys. Rev. Lett. **28**, 1251–1254.

Greywall, D. S., and G. Ahlers, 1973, "Second-sound velocity and superfluid density in ^{4}He under pressure near T_λ," Phys. Rev. A **7**, 2145–2162.

Griffiths, R. B., 1970, "Dependence of critical indices on a parameter," Phys. Rev. Lett. **24**, 1479–1482.

Halperin, B. I., and P. C. Hohenberg, 1967, "Generalization of scaling laws to dynamical properties of a system near its critical point," Phys. Rev. Lett. **19**, 700–703.

Halperin, B. I., and P. C. Hohenberg, 1969, "Scaling laws for dynamic critical phenomena," Phys. Rev. **177**, 952–971.

Halperin, B. I., P. C. Hohenberg, and E. D. Siggia, 1974, "Renormalization-group calculations of divergent transport coefficients at critical points," Phys. Rev. Lett. **32**, 1289–1292.

Henkel, R. P., 1971, Ph.D. thesis (Cornell University, Ithaca, NY).

Henkel, R. P., E. N. Smith, and J. D. Reppy, 1969, "Temperature dependence of the superfluid healing length," Phys. Rev. Lett. **23**, 1276–1279.

Hess, G. B., and R. J. Muirhead, 1982, "Superfluidity in thin ^{4}He films: Comparison of onset on particular crystal facets and on disordered substrates," J. Low Temp. Phys. **49**, 481–506.

Hohenberg, P. C., and B. I. Halperin, 1977, "Theory of dynamic critical phenomena," Rev. Mod. Phys. **49**, 435–479.

Hucht, A., 2007, "Thermodynamic Casimir effect in ^{4}He films near T_λ: Monte Carlo results," Phys. Rev. Lett. **99**, 185301.

Huhn, W., and V. Dohm, 1988, "Possible resolution of the finite-size scaling problem in ^{4}He," Phys. Rev. Lett. **61**, 1368–1371.

Ihas, G. G., and F. Pobell, 1974, "Correlation length, finite-geometry effects, and universality in pressurized superfluid helium near T_λ," Phys. Rev. A **9**, 1278–1296.

Ikushima, A., and G. Terui, 1973, "Superfluid density near the lambda point of ^{4}He under pressure," J. Low Temp. Phys. **10**, 397–405.

Jerebets, S., Y. Liu, F. Liu, and G. Ahlers, 2007, "Finite-size effects on the thermal resistivity of ^{4}He near the superfluid transition," J. Low Temp. Phys. **146**, 471–483.

Joseph, R. A., and F. M. Gasparini, 1982, "Conductance and non-linear behavior of a ^{4}He film at the superfluid transition," Physica B & C **109-110**, 2102–2104.

Josephson, B. D., 1966, "Relation between the superfluid density and order parameter for superfluid He near T_c," Phys. Lett. **21**, 608–609.

Kadanoff, L. P., 1971, in *Critical Phenomenon Proceedings of the 51st "Enrico Fermi" Summer School, Varenna, Italy*, edited by M. Green (Academic, New York), pp. 100–151.

Kagiwada, R. S., J. C. Fraser, I. Rudnick, and D. Bergman, 1969, "Superflow in helium films: Third-sound measurements," Phys. Rev. Lett. **22**, 338–342.

Kahn, A. M., and G. Ahlers, 1995, "Thermal conductivity of ^{4}He near the superfluid transition in a restricted geometry," Phys. Rev. Lett. **74**, 944–947.

Kimball, M. O., 2005, Ph.D. thesis (University at Buffalo, the State University of New York, Buffalo).

Kimball, M. O., M. Diaz-Avila, and F. M. Gasparini, 2003, "^{4}He confined to 1 μm^3 boxes, 0D crossover, surface and edge effects," Physica B **329-333**, 286.

Kimball, M. O., and F. M. Gasparini, 2000, "Specific heat of ^{4}He confined to 9869 Å planar geometry," Physica B **284-288**, 47–48.

Kimball, M. O., and F. M. Gasparini, 2001, "Superfluid fraction of ^{3}He-^{4}He mixtures confined at 0.0483 μm between silicon wafers," Phys. Rev. Lett. **86**, 1558–1561.

Kimball, M. O., and F. M. Gasparini, 2002, "Critical behavior and scaling of confined ^{3}He-^{4}He Mixtures," J. Low Temp. Phys. **126**, 103–108.

Kimball, M. O., and F. M. Gasparini, 2005, "Universality and finite-size scaling of the specific heat of ^{3}He-^{4}He mixtures," Phys. Rev. Lett. **95**, 165701.

Kimball, M. O., and F. M. Gasparini, 2006, in *24th International Conference on Low Temperature Physics (LT24)*, edited by Y. Takano, S. P. Hershfield, S. O. Hill, P. J. Hirschfeld, and A. M. Goldman, AIP Conf. Proc. No. 850 (AIP, Melville, NY), pp. 125–126.

Kimball, M. O., S. Mehta, and F. M. Gasparini, 2000, "Specific heat near the superfluid transition of a 0.9869 μm ^{4}He film," J. Low Temp. Phys. **121**, 29–51.

Kimball, M. O., K. P. Mooney, and F. M. Gasparini, 2004, "Three-dimensional critical behavior with 2D, 1D, and 0D dimensionality crossover: Surface and edge specific heats," Phys. Rev. Lett. **92**, 115301.

Kleinert, H., 2000, "Theory and satellite experiment for critical exponent α of λ-transition in superfluid helium," Phys. Lett. A **277**, 205–211.

Kosterlitz, J. M., and D. J. Thouless, 1972, "Long range order and metastability in two dimensional solids and superfluids," J. Phys. C **5**, L124.

Kosterlitz, J. M., and D. J. Thouless, 1973, "Ordering, metastability and phase transitions in two-dimensional systems," J. Phys. C **6**, 1181–1203.

Kotsubo, V., and G. A. Williams, 1984, "Kosterlitz-Thouless superfluid transition for helium in packed powders," Phys. Rev. Lett. **53**, 691–694.

Krech, M., 1994, *The Casimir Effect in Critical Systems* (World Scientific, Singapore).

Krech, M., and S. Dietrich, 1992, "Free energy and specific heat of critical films and surfaces," Phys. Rev. A **46**, 1886–1921.

Landau, L. D., 1937, Phys. Z. Sowjetunion **11**, 545.

Landau, L. D., 1941, J. Phys. (USSR) **5**, 71.

Landau, L. D., 1965, in *Collected Papers of L. D. Landau*, edited by D. T. Haar (Pergamon, Oxford), pp. 193–216.

Landau, L. D., and E. M. Lifshitz, 1959, *Statistical Physics* (Pergamon, Oxford).

Lee, S. D., 1977, Ph.D. thesis (University at Buffalo, the State Univeristy of New York, Buffalo).

Lipa, J. A., and T. C. P. Chui, 1983, "Very high-resolution heat-

capacity measurements near the lambda point of helium," Phys. Rev. Lett. **51**, 2291–2294.
Lipa, J. A., and T. C. P. Chui, 1984, "Preliminary results from high resolution heat capacity measurements near the lambda-line of ^{2}He-^{4}He mixtures," Physica B & C **126**, 481–482.
Lipa, J. A., and T. C. P. Chui, 1987, "High-resolution thermal-conductivity measurements near the lambda point of helium," Phys. Rev. Lett. **58**, 1340–1343.
Lipa, J. A., M. Coleman, and D. A. Stricker, 2001, "Specific heat of helium confined to cylinders near the lambda point," J. Low Temp. Phys. **124**, 443–460.
Lipa, J. A., and Q. Li, 2007, "Thermal conductivity and critical boundary resistance of helium near the lambda point," J. Low Temp. Phys. **149**, 1–27.
Lipa, J. A., J. A. Nissen, D. A. Stricker, D. R. Swanson, and T. C. P. Chui, 2003, "Specific heat of liquid helium in zero gravity very near the lambda point," Phys. Rev. B **68**, 174518.
Lipa, J. A., D. R. Swanson, J. A. Nissen, Z. K. Geng, P. R. Williamson, D. A. Stricker, T. C. P. Chui, U. E. Israelsson, and M. Larson, 2000, "Specific heat of helium confined to a 57 μm planar geometry near the lambda point," Phys. Rev. Lett. **84**, 4894–4897.
Lipa, J. A., D. R. Swanson, J. A. Nissen, P. R. Swanson, J. A. Nissen, P. R. Williamson, Z. K. Geng, D. A. Stricker, T. C. P. Chui, U. E. Israelsson, and M. Larson, 1998, "Preliminary results from a shuttle mission to measure the heat capacity of confined helium near the lambda point," J. Low Temp. Phys. **113**, 849–860.
Long, E., and L. Meyer, 1955, "Superfluidity and heat transport in the unsaturated helium-II film," Phys. Rev. **98**, 1616–1622.
Lutz, H., P. Scoboria, J. E. Crow, and T. Mihalisin, 1978, "Effects of finite size on critical phenomena: The resistivity anomaly in Ni films," Phys. Rev. B **18**, 3600–3611.
Magnum, B. W., and G. T. Furukawa, 1990, "Guidelines for realizing the international temperature scale of 1990 (ITS-90)," NIST Technical Note 1265.
Mamaladze, Y. G., 1967, "Parameters of phenomenological superfluidity theory and the λ-point shift," Sov. Phys. JETP **25**, 479–484.
Maps, J., and R. B. Hallock, 1981, "Onset of superfluid flow in ^{4}He films adsorbed on mylar," Phys. Rev. Lett. **47**, 1533–1536.
Mastrangelo, S. V. R., and J. G. Aston, 1951, "Thermodynamic data and some notes on the nature of adsorbed helium," J. Chem. Phys. **19**, 1370–1375.
Maynard, J. D., and M. H. W. Chan, 1982, "Third sound on HOPG surface," Physica B & C **109-110**, 2090–2092.
McQueeney, D. F., 1988, Ph.D. thesis (Cornell University, Ithaca NY).
Mehta, S., 1998, Ph.D. thesis (University at Buffalo, the State University of New York, Buffalo).
Mehta, S., and F. M. Gasparini, 1997, "Specific heat and scaling of ^{4}He confined in a planar geometry," Phys. Rev. Lett. **78**, 2596–2599.
Mehta, S., and F. M. Gasparini, 1998, "High resolution calorimetry on μ mole samples of ^{4}He near T_λ," J. Low Temp. Phys. **110**, 287–292.
Mehta, S., M. O. Kimball, and F. M. Gasparini, 1998, "^{4}He confined in 0.0483 μm planar geometry, specific heat and scaling near T_λ," J. Low Temp. Phys. **113**, 435.
Mehta, S., M. O. Kimball, and F. M. Gasparini, 1999, "Superfluid transition of ^{4}He for two-dimensional crossover, heat capacity, and finite-size scaling," J. Low Temp. Phys. **114**, 467–521.
Minnhagen, P., 1987, "The two-dimensional Coulomb gas, vortex unbinding, and superfluid-superconducting films," Rev. Mod. Phys. **59**, 1001–1066.
Mohr, U., and V. Dohm, 2000, "Surface specific heat of confined ^{4}He above and below T," Physica B **284**, 43–44.
Mooney, K. P., 2006, Ph.D. thesis, (University at Buffalo, the State University of New York, Buffalo).
Mooney, K. P., and F. M. Gasparini, 2002, "van der Waals effects at the superfluid transition of confined ^{4}He," J. Low Temp. Phys. **126**, 247–253.
Mooney, K. P., M. O. Kimball, and F. M. Gasparini, 2004, "Specific heat of ^{4}He confined in channels of 1 m square cross-section," J. Low Temp. Phys. **134**, 607–612.
Mooney, K. P., M. O. Kimball, and F. M. Gasparini, 2006, "Specific heat of helium in 2 μm^3 boxes, coupled or uncoupled?," *24th International Conference on Low Temperature Physics (LT24)*, edited by Y. Takano, S. P. Hershfield, S. O. Hill, P. J. Hirschfeld, and A. M. Goldman, AIP Conf. Proc. No. 850 (AIP, Melville, NY), pp. 129–130.
Mueller, K. H., F. Pobell, and G. Ahlers, 1975, "Thermal-expansion coefficient and universality near the superfluid transition of ^{4}He under pressure," Phys. Rev. Lett. **34**, 513–516.
Murphy, D., E. Genio, G. Ahlers, and F. L. Y. Liu, 2003, "Finite-size scaling and universality of the thermal resistivity of liquid ^{4}He near T_λ," Phys. Rev. Lett. **90**, 025301.
Nacher, P. J., and J. Dupont-Roc, 1991, "Experimental evidence for nonwetting with superfluid helium," Phys. Rev. Lett. **67**, 2966–2969.
Nelson, D. R., and J. M. Kosterlitz, 1977, "Universal jump in the superfluid density of two-dimensional superfluids," Phys. Rev. Lett. **39**, 1201–1205.
Nho, K., and E. Manousakis, 2003, "Heat-capacity scaling function for confined superfluids," Phys. Rev. B **68**, 174503.
Nightingale, M. P., 1976, "Scaling theory and finite systems," Physica A **83**, 561–572.
Nissen, J. A., D. R. Swanson, Z. K. Geng, K. Kim, P. Day, and J. A. Lipa, 2000, "Superfluid density as a function of temperature and pressure near the lambda line," Physica B **284-288**, 51–52.
Notarys, H. A., 1969, "Pressure-driven superfluid helium flow," Phys. Rev. Lett. **22**, 1240–1242.
Okaji, M., and T. Watanabe, 1978, "Heat capacity near the lambda point in ^{4}He under pressure. Experimental test of scaling laws and universality," J. Low Temp. Phys. **32**, 555–569.
Onsager, L., 1944, "Crystal statistics. I. A two-dimensional model with an order-disorder transition," Phys. Rev. **65**, 117–149.
Privman, V., 1990, "Finite-size scaling theory," in *Finite Size Scaling and Numerical Simulations of Statistical Systems*, edited by V. Privman (World Scientific, Singapore), pp. 1–98.
Privman, V., and M. E. Fisher, 1984, "Universal critical amplitudes in finite-size scaling," Phys. Rev. B **30**, 322–327.
Privman, V., P. C. Hohenberg, and A. Aharony, 1991, in *Phase Transitions and Critical Phenomena*, edited by C. Domb and J. L. Lebowitz (Academic, New York), Vol. 14, pp. 1–134.
Reppy, J. D., 1992, "Superfluid helium in porous media," J. Low Temp. Phys. **87**, 205–245.
Rhee, I., D. J. Bishop, A. Petrou, and F. M. Gasparini, 1990, "Si wafers uniformly spaced; bonding and diagnostics," Rev. Sci. Instrum. **61**, 1528–1536.

Rhee, I., F. M. Gasparini, and D. J. Bishop, 1989, "Finite-size scaling of the superfluid density of ^{4}He confined between silicon wafers," Phys. Rev. Lett. **63**, 410–413.

Roth, J. A., G. J. Jelatis, and J. D. Maynard, 1980, "Third-sound velocity and onset on grafoil," Phys. Rev. Lett. **44**, 333–337.

Saam, W. F., and M. W. Cole, 1975, "Excitations and thermodynamics for liquid-helium films," Phys. Rev. B **11**, 1086–1105.

Sabisky, E. S., and C. H. Anderson, 1973, "Onset for superfluid flow in ^{4}He films on a variety of substrates," Phys. Rev. Lett. **30**, 1122–1125.

Schmolke, R., A. Wacker, V. Dohm, and D. Frank, 1990, "Specific heat and superfluid density of confined ^{4}He near T_λ," Physica B **165-166**, 575–576.

Scholtz, J. H., E. O. McLean, and I. Rudnick, 1974, "Third sound and the healing length of He II in films as thin as 2.1 atomic layers," Phys. Rev. Lett. **32**, 147–151.

Schubert, P. C., and W. Zimmermann, Jr., 1981, "Measurements of superfluid densities and critical superfluid mass currents of pure ^{4}He and ^{3}He-^{4}He mixtures in Nuclepore near the lambda transition," J. Low Temp. Phys. **41**, 177–207.

Schultka, N., and E. Manousakis, 1995, "Scaling of the specific heat in superfluid films," Phys. Rev. Lett. **75**, 2710–2713.

Schultka, N., and E. Manousakis, 1997, "Boundary effects in superfluid films," J. Low Temp. Phys. **109**, 733–762.

Schultka, N., and E. Manousakis, 1998, "Scaling of the specific heat of superfluids confined in pores," J. Low Temp. Phys. **111**, 783–791.

Selke, W., and L. N. Shchur, 2005, "Critical Binder cumulant in two-dimensional anisotropic Ising models," J. Phys. A **38**, L739.

Sherlock, R. A., and D. O. Edwards, 1970, "Oscillating superleak second sound transducers," Rev. Sci. Instrum. **41**, 1603–1609.

Singsaas, A., and G. Ahlers, 1984, "Universality of static properties near the superfluid transition in ^{4}He," Phys. Rev. B **30**, 5103–5115.

Smith, D. T., K. M. Godshalk, and R. B. Hallock, 1987, "Adsorption and capillary condensation of ^{4}He on Nuclepore: Third-sound and capacitance measurements," Phys. Rev. B **36**, 202–216.

Smith, E. N., 1971, Ph.D. thesis (Cornell University, Ithaca. NY)

Sobnack, M. B., and F. V. Kusmartsev, 2001, "Suppression of superconductivity in mesoscopic superconductors," Phys. Rev. Lett. **86**, 716–719.

Sobnack, M. B., and F. V. Kusmartsev, 2002, "Phase transitions driven by single-vortex excitations in confined geometries," J. Low Temp. Phys. **126**, 517–526.

Sobyanin, A. A., 1972, Zh. Eksp. Teor. Fiz. **63**, 1780 [Sov. Phys. JETP **36**, 941 (1973)].

Steele, L. M., C. J. Yeager, and D. Finotello, 1993, "Precision specific-heat studies of thin superfluid films," Phys. Rev. Lett. **71**, 3673–3676.

Sullivan, P. F., and G. Seidel, 1968, "Steady-state, ac-temperature calorimetry," Phys. Rev. **173**, 679–685.

Sutter, P., and V. Dohm, 1994, "Specific heat of confined ^{4}He near T_λ in 3 dimensions," Physica B **613**, 194–196.

Suzuki, M., 1977, "Static and dynamic finite-size scaling theory based on the renormalization group approach," Prog. Theor. Phys. **58**, 1142–1150.

Symonds, A. J., 1965, Ph.D. thesis (University of Sussex, Brighton, UK).

Takada, T., and T. Watanabe, 1980, "Specific heat near the lambda point in ^{4}He and ^{3}He mixtures: Test of universality of the critical exponent and the amplitude ratio, and observation of the critical-tricritical crossover effect," J. Low Temp. Phys. **41**, 221.

Tam, W. Y., and G. Ahlers, 1985, "Thermal conductivity of ^{4}He I from near T_λ to 3.6 K and vapor pressure to 30 bars," Phys. Rev. B **32**, 5932–5958.

Tam, W. Y., and G. Ahlers, 1986, "Thermal conductivity of ^{4}He I near T_λ from vapor pressure to 28 bars: Comparison of experiment and theory," Phys. Rev. B **33**, 183–196.

Teitel, S., 1982, "Third sound and thermal conduction in thin ^{4}He films," J. Low Temp. Phys. **46**, 77–96.

Terui, G., and A. Ikushima, 1972, "Superfluid density near the lambda point in ^{4}He under pressure," Phys. Lett. **31A**, 161.

Thomlinson, W. C., G. G. Ihas, and F. Pobell, 1973, "Finite-geometry effects and onset of superfluidity in ^{3}He-^{4}He mixtures near T_λ," Phys. Rev. Lett. **31**, 1284–1287.

Thomlinson, W. C., G. G. Ihas, and F. Pobell, 1975, "Finite-geometry effects, superfluid density, and universality in ^{3}He-^{4}He mixtures near the superfluid transition," Phys. Rev. B **11**, 4292–4303.

Tong, Q.-Y., G. Cha, R. Gafiteanu, and U. Gösele, 1994, "Low temperature wafer direct bonding," J. Microelectromech. Syst. **3**, 29–35.

Tong, Q.-Y., W. J. Kim, T.-H. Lee, and U. Gösele, 1998, "Low vacuum wafer bonding," Electrochem. Solid-State Lett. **1**, 52–53.

Töpler, M., and V. Dohm, 2003, "*Finite-size effects on the thermal conductivity of ^{4}He near T_λ*," Proceedings of the 23rd International Conference on Low Temperature Physics [Physica B **329-333**, 200–201].

Tyson, J. A., and D. H. Douglass, 1966, "Superfluid density and scaling laws for liquid helium near T_λ," Phys. Rev. Lett. **17**, 472–474.

Tyson, J. A., and D. H. Douglass, 1968, "Critical-region second-sound velocity in He II," Phys. Rev. Lett. **21**, 1308–1310.

Umicore, Substrate Division, 12 Channel Street 702, Boston, MA 02210.

van de Laar, R. W. A., 1994, Ph.D. thesis (Leiden University, Leiden, The Netherlands).

van de Laar, R. W. A., A. van der Hock, and H. van Beelen, 1995, "Two-dimensional behaviour of very thin ^{4}He films on glass," Physica B **216**, 24–36.

Vasilyev, D., A. Gambassi, A. Maciolek, and S. Dietrich, 2007, "Monte Carlo simulation results for critical Casimir forces," Europhys. Lett. **80**, 60009.

Wang, T. G., M. M. Saffren, E. E. Olli, and D. D. Elleman, 1974, "Onset phenomena in superfluid helium," Phys. Rev. Lett. **33**, 1132–1135.

Wang, X., and F. M. Gasparini, 1988, "Near-monolayer ^{3}He-^{4}He films: Two superfluid transitions and the ^{3}He effective mass and binding energy," Phys. Rev. B **38**, 11245–11258.

Wang, X. F., I. Rhee, and F. M. Gasparini, 1990, "Calculation of van der Waals effects on correlation-length scaling near T_λ," Physica B **165-166**, 503.

Widom, B., 1965, "Surface tension and molecular correlations near the critical point," J. Chem. Phys. **43**, 3892–3897.

Williams, G. A., 2006, "Anisotropic Kosterlitz-Thouless transition induced by hard-wall boundaries," Phys. Rev. B **73**,

214531.
Williams, R., S. E. A. Beaver, J. Fraser, R. S. Kagiwada, and I. Rudnick, 1969, "The velocity of second sound near T_λ," Phys. Lett. **29A**, 279–280.
Wilson, K. G., 1971a, "Renormalization group and critical phenomena. I. Renormalization group and the Kadanoff scaling picture," Phys. Rev. B **4**, 3174–3183.
Wilson, K. G., 1971b, "Renormalization group and critical phenomena. II. Phase-space cell analysis of critical behavior," Phys. Rev. B **4**, 3184–3205.
Yu, Y. Y., D. Finotello, and F. M. Gasparini, 1989, "Finite-size scaling and the convective conductance and specific heat of planar helium films near the superfluid transition," Phys. Rev. B **39**, 6519–6526.
Yuyama, J., and T. Watanabe, 1982, "Superfluid transition of ^{4}He films adsorbed on graphite substrates: A calorimetric study in connection with third-sound observations," J. Low Temp. Phys. **48**, 331–348.
Zhang, C., K. Nho, and D. P. Landau, 2006, "Finite-size effects on the thermal resistivity of ^{4}He in the quasi-two-dimensional geometry," Phys. Rev. B **73**, 174508.